ABSTRACT

Title of Document: INVESTIGATION OF WEAR CHARACTERISTICS OF CONICAL DELRIN THRUST BEARINGS

Seyed Ehsan Mirbagheri, Master of Science, 2012

Directed By: Professor Abhijit Dasgupta, Department of Mechanical Engineering

This study focuses on the wear rate in conical thrust bearings, which is responsible for field failures of stepper motors in optical disk drives (ODD). These bearings support the stepper motor worm shaft and consist of a steel ball supported in a polymer conical bearing cup. The tribological behaviors of polymers used in bearing application has been addressed by using Archard's wear model, a well known classical model for fretting wear in the literature. However, these studies were for planar bearing surfaces and other geometries, not for the conical geometry addressed in this study.

Tests were designed and implemented to study the wear rate of the conical bearing cups at with different load levels. The tribological behavior of Delrin in conical thrust bearing applications has been characterized, by quantifying the wear factors used in the modified Archard's model. Distinct reduction of wear rate is observed due to formation of a polymer transfer film on the steel ball. The variability

of the wear properties is explored through replication of the test conditions. Destructive physical analysis is conducted to gain insight into the fundamental wear mechanisms as a part of this study. The results of the wear tests are used to develop a life model of the stepper motor as a case study, to demonstrate an application of this approach. The life model is used to study the effect of variability in the initial axial bearing preload (due to manufacturing tolerances), on the wear rate and life of the stepper motor.

INVESTIGATION OF WEAR CHARACTERISTICS OF CONICAL DELRIN THRUST BEARINGS

By

Seyed Ehsan Mirbagheri

Thesis submitted to the Faculty of the Graduate School of the
University of Maryland, College Park, in partial fulfillment
of the requirements for the degree of
Master of Science
2012

Advisory Committee:

Professor Abhijit Dasgupta, Chair
Professor Hugh Bruck
Professor Bongtae Han

Dedication

To my beloved guru, family and friends.

Acknowledgements

I owe my deepest gratitude to all people who helped me to learn and gain better knowledge and insight in all aspects of my life.

I am heartily thankful to my advisor, Professor Abhijit Dasgupta, whose encouragement, guidance and support from the initial to the final level enabled me to be at this point in my life. I always admire his kindness, wisdom, brilliance and enthusiasm to help other people. It is an honor for me to be one of his students.

As an international student I owe my achievements to my family and friends who always supported me whenever I needed. I am indebted to many of my colleagues and friends Dr. Moustafa Al-Bassyiouni, Majid, Sandip, Sharon, Koustav, Cholmin, Subhasis, Jingshi, Ehsan, Ranjith, Josh, Jaemi, David, Matt, Julian, Micheal and all other German interns.

Table of Contents

List of Tables

List of Figures

1. Introduction

The main purpose of this chapter is to provide the problem statement and the motivation behind this study. The published studies related to our topic are discussed to provide a framework and rationale for this thesis. In the end of this chapter, the steps to solve the problem are briefly discussed.

1.1- Background and motivation

The use of polymers for bearings in low power industrial applications is continuously increasing because of their suitable properties such as low friction factor, high wear resistance, light weight and low manufacturing cost. Polymer bearings are often used in electro-mechanical devices where high wear resistance and low friction is highly desirable. Typically, failure of these devices is due to wear out of the polymer bearings that are subjected to simultaneous sliding and compressive loads. Therefore, understanding the wear process and wear behavior of polymers is vital for the design of reliable products that can last sufficiently long under typical usage cycles. The focus of this study is on the wear of polymer bearing cups used in stepper motors, a typical dominant failure mode of optical disk drives. This study investigates the wear process of conical thrust bearings and the wear behavior of the bearing material, Delrin, under different load and sliding distances.

1.2- Optical disk drive (ODD) and failure analysis of stepper motor

Optical disk drives are common opto-electro-mechanical devices used as a data storage/recovery media in most modern computing and gaming products. One of the dominant failure modes of these devices is failure of the stepper motor to

properly “home” the optical head, resulting in failure of the device to read the data in a typical ODD. The optical head and stepper motor can be seen in Figure 1-1.

Stepper motor is used in this application because of its precise control of the angle of rotation provides accurate displacement of the optical head inside the ODD. These types of electronic motors convert the digital data generated by the controller into rotation of the worm shaft and consequent sliding of the optical sled attached to the worm shaft. The stepper motor divides each revolution of the worm shaft into a large number of discrete rotation steps, so that they have a better precision compared to other types of motors.

Figure 1-1: Optical disk drive, optical head, and stepper motor

If for any reason the motor misses any step or fails to rotate precisely the same angle with each pulse, the optical head fails to read the data from the optical media and the entire system fails to function. The worm shaft in the stepper motor is supported between two pre-loaded plastic thrust bearings: the pivot bearing (at the pivot end); and the motor bearing (inside the motor housing), as seen in Figure 1-2.

The worm shaft and both bearings are pre-loaded with a compressed leaf spring between the motor bearing and the motor housing. It is necessary to have this pre-loaded leaf spring in the motor housing: (a) to preserve the load-train alignment for varying dimensional tolerances in the motor assembly; and (b) to preserve the alignment in the motor assembly as the dimension of bearing cups change throughout the life of the stepper motor due to mechanical wear.

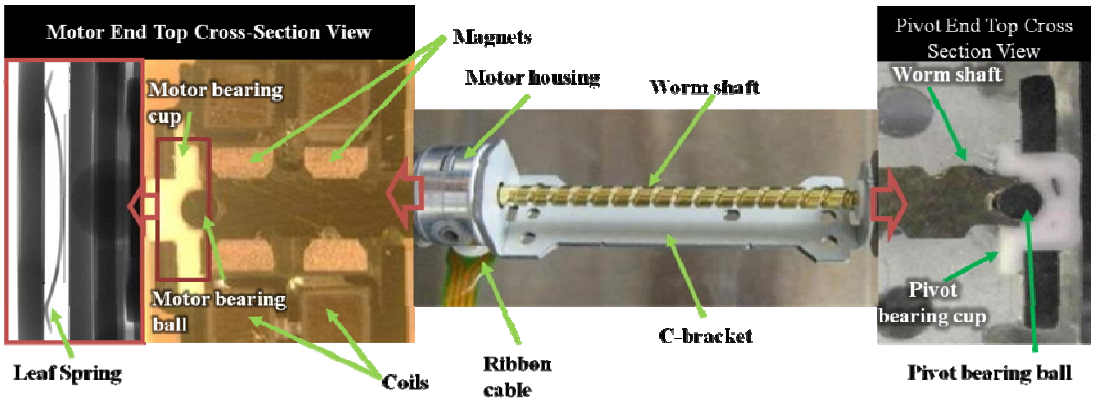

Figure 1-2: Stepper motor structure

Wear out of the plastic bearing cups is the main known cause leading to stepper motor failure. The plastic bearing cup is simultaneously subjected to both sliding motion and pressure, caused by the compressed leaf spring throughout the stepper motor's life.

Failure analysis has been conducted on the stepper motors that have failed in typical field applications, to assess the failure mechanism and failure site. The inner surface of the motor housing as well as the motor magnets was observed to have eroded. This observation led to understanding that the magnets had rubbed against the inner surface of the motor housing. The next cause for this wear is that the worm shaft becomes loose due to the reduction of the leaf spring compression load and lateral force caused by displacement of the optical head. The leaf spring continuously

lowers its compressive force load as the bearings wear out. The loss of axial compressive load allows lateral displacement of the worm shaft during the operation of the stepper motor. Several experiments (Appendix VI) have confirmed that lateral displacement of worm shaft increases throughout the wear process of the motors as bearing wears out. As a result of this lateral displacement, the worm shaft moves off center and the magnetic forces further exacerbate the lateral misalignment. Therefore, the attached magnets to the worm shaft gradually start rubbing against the motor housing, as seen in Figure- 1-3.

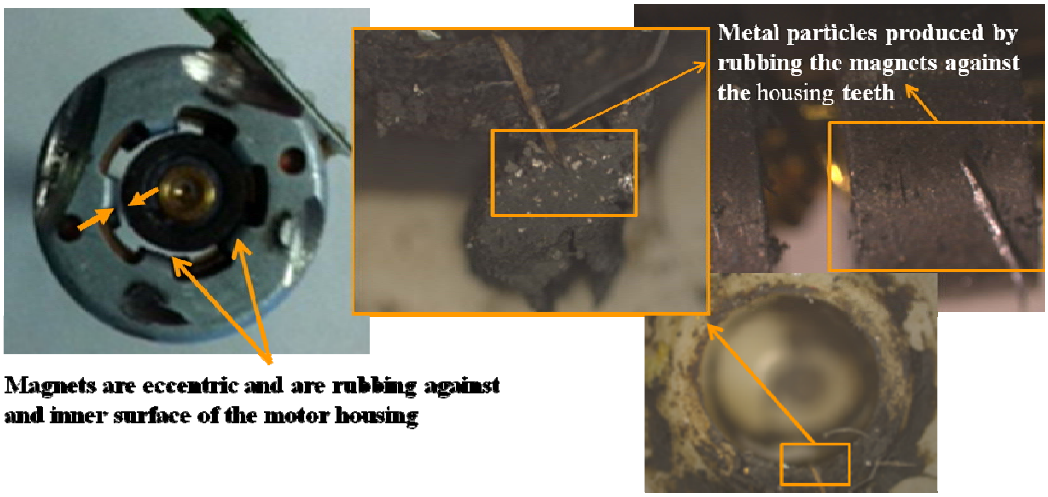

Figure 1-3: Worm shaft misalignment and the consequences

This phenomenon affects functionality of the stepper motor in two ways:

[1] the off-centered magnets do not receive equal amounts of magnetic power from the stepper motor's coils, and

[2] the resistance frictional torque gradually increases due to friction between the magnets and the inner surface of motor housing.

The above reasons cause the stepper motor to start missing steps and degradation of precision of the stepper motor increases to a level at which the optical head cannot read data from the optical media, leading to failure in operation of the optical disk drive. Wear out of the bearing cup is the main reason for this phenomenon. This study focuses on gaining insight into the wear process of the conical Delrin thrust bearing used in stepper motor by using Archard's wear model [1], and on calibrating the model with the results of designed experiments.

1.3- Literature review

In the next few sections, the literature related to stepper motor failure, wear models and polymer behavior is briefly reviewed. More references are provided in subsequent chapters, where required.

1.3-1. Stepper motor failure

Taft and Gauthier [1] discussed the cases where stepper motors fail to function. Their paper provides insights into why and how stepper motors miss steps as well as the behavior of stepper motors under different load conditions. However, they did not provide any information about the degradation of stepper motors over a certain period of usage or possible reasons that lead the stepper motor to fail under a specific use condition.

1.3-2. Wear models

One of the most persistent aspirations of engineers is to develop a mathematical model or relationships between variables and parameters of a system to describe and predict its behavior. These models are essentially crucial for designing

efficient and reliable systems. Similarly, in tribology, it is essentially important to understand the relationship between system parameters and wear rate. There are more than 300 wear and friction models available in the literature [3]. Evolution of wear modeling approaches followed the same path as any other technological field. The advancement of wear equations can be divided to three overlapping stages [4]:

1) Prior to 1970, most of equations were developed empirically using data driven approaches. Barwell [5] proposed that wear of materials follows three curves:

a) $v = \frac{\beta}{\alpha}\{1 - e^{-\alpha t}\}$ **(1)**

b) $= \alpha t$ **(2)**, and

c) $v = \beta e^{\alpha t}$ **(3)**

where v is worn out volume , α is constant , t is time and β was not identified clearly. Another famous model that predicts the wear between polymers and metals has been developed by Rhee [6].

$$W = KF^a V^b t^c \quad \textbf{(4)}$$

Where W is weight of worn-out material, F is load, V is speed, t is time and K, a, b and c are empirical constants.

2) Between 1940 to 1970, wear models were developed by assuming simple analytical relationships and they were physics-based to some extent. They were mostly developed based on contact-mechanics and material properties such hardness H. Archard's and Holm's [7] models are well-known examples of these models. Archard's wear model will be explained

in detail in the following section. Table of most common analytical wear models [8] can be found in Appendix I.

3) Models in last 30 years are mostly based on material failure mechanisms [4]. Tribology scientists started focusing on quantities relating to material flow, fracture toughness, etc. instead of distinguishing the wear resistance as an inherent property of materials. The earliest studies conducted focusing on dislocation mechanics, fatigue properties, brittle fracture properties and shear failure defined by slip line analysis. Equations and derivation are excessively complicated and typically do not provide a simple physics-based analytical model to predict the wear.

Numerous mechanisms such as adhesion, abrasion, fatigue and so on contribute on the wear process. Many aspects of these mechanisms are not fully explored and understood quantitatively yet; hence the general picture of wear incorporated by these mechanisms is still missing [8].

Archard's wear model is used in this study for the following three reasons:

a) Archard's wear model is physics based to some extent and it has less reliance on wear conditions than empirical models,

b) it is feasible to calibrate Archard's wear model using a limited number of test specimens, since it has only one variable, wear factor (K), and

c) simple analytical models are much more preferable by the design engineers in industry. Therefore, the result of this study can be very beneficial to industrial designers.

1.3-3. Archard's Wear Model

Archard's wear model, is a well-known model to predict the worn out volume from one or both contact surfaces based on: **(a)** the constant normal load; **(b)** the wear factor (a dimensionless constant); **(c)** the hardness of the softer of the two materials in contact; and **(d)** the relative sliding distance between the two surfaces. Archard published his model in 1953. He believed the physical phenomenon that occurs in the contact zone of two objects such as mechanical wear is dependent on the actual contact area that is, in general, less than the apparent area due to surface asperities. The actual contact area is a combination of multiple individual contact spots of different sizes and distances of separation. He tried to explain the load proportionality of wear rate by assuming that the volume removal at the contact zone is a result of plastic deformation of the asperities at the contact region. He developed his model in two steps. In the first step, the contact zone consists of one perfectly flat nondeformable surface and a deformable spherical surface. He showed that the actual contact area would be proportional to the applied load by a power law relationship, $A \propto F^{1/p}$, where F is applied load and p depends on the deformation mechanism (i.e., for perfectly plastic deformation p is one). In the second step, he assumed that there are multiple areas of contact; the contact zone consists of one perfectly flat nondeformable surface and a deformable surface with a large number of equal spherical (same radius) asperities. In this step he again showed that the actual contact

area is linearly proportional to the applied load for plastic deformation. Archard used Holm's [7] work where he assumed that the actual contact area is caused by plastic deformation of contacting asperities. Based on Archard's wear model, the worn out volume is dependent on load and sliding distance and it is independent of sliding speed and contact area.

$$\boldsymbol{v = kL\frac{F}{H}} \qquad (\mathbf{5})$$

Where $\boldsymbol{v}$ is worn out volume, $\boldsymbol{F}$ is normal force, $\boldsymbol{L}$ is sliding distance, $\boldsymbol{H}$ is hardness and $\boldsymbol{k}$ is wear factor/coefficient. There are many discussions in the literature about $\boldsymbol{k}$, and it is stated as a constant related to the likelihood of two asperities in contact to produce a wear particle. $\boldsymbol{k}$ also can be seen as a probability that a separated particle leaves the system and does not reattach to the sliding pairs [4]. Thus, geometry might play a role in the wear factor.

Archard validated his model through sets of experiments, except for the fact that, he could not find any evidence to confirm that worn out volume is independent of sliding speed as his model implies (sliding speed has a clear effect on wear rate).

Archard's wear model was widely used in literature to study the wear behavior of surfaces in contact [9]-[11].

1.3-4. Polymers wear properties

Nowadays usage of polymers in electro-mechanical devices is common because of their appropriate wear properties. The fact that engineering

thermoplastics such as Ertacetal (POM-Delrin) do not need additional lubricants also increases their usage in bearing and sliding applications.

Many experimental studies [12] and [23] were conducted to examine the tribological behavior of different polymers. In the study by Feyzollahoglu et al. [13] the friction and wear properties of Ertacetal (POM-Delrin), Ertalyte (PETP), Ertalon and Devateks plastics were examined. This study showed that higher sliding speed causes an increase in the friction coefficient, possibly due to the higher temperature generated by the higher sliding speed. Also, in this study it was shown that the wear rate of polymers is more sensitive to changes of speed than to changes of load. The presented experimental results also showed that weight loss rate of Ertacetal (POM-Delrin) in journal bearing is initially high and eventually decreases as sliding distance increases. In another study by Tevruz et al. [14]-[15], the effect of sliding distance and bearing pressure on wear and frictional behavior of the PTFE bearing was investigated. According to their study the wear rates are initially high and they gradually decrease as the sliding distance increases. Wear rate has been shown to increase as bearing pressure increases, according to a power law correlation.

Some studies have focused on wear and friction of the polymer-metal sliding process in dry conditions [18]. Most engineering polymers are known as self-lubricants, they have superior tribological properties due to formation of the transfer film that can act as a lubricant throughout the sliding process. Transfer film is the best known explanation for the gradual transition of wear behavior from transient to steady state in polymer-metal sliding contacts [18]. The development of transfer film on the metal counterface, which changes the friction and wear behavior of sliding

pairs, is a complex process that depends on many factors such as: metal counterface roughness, temperature, contact pressure, sliding speed and filler or additive materials.

In another study [9], authors used a combination of the finite element method and numerical simulation method based on Archard's wear model, to accurately predict the changes of geometry of a spherical plain bearing with a self-lubricating material due to wear out. They accounted for changes of surface geometry due to material removal by the boundary displacement method (BDM) in their finite element analysis. In this study, the wear rate of woven fabric as input of their simulation was quantified by the pin-on-disk experiment. Turvus et al. [15] studied the wear rate of PTFE in journal bearing (a metal shaft sliding inside a polymer housing). Rolling of metal ball on a flat polymer surface was studied by Harras et al. [24]. Olofsson et al. [21] explored wear of polymer housing washer with metal roller in roller thrust bearings. Pin-on-disk test to measure and to compare wear of different polymers was used in many studies such as [29] &[32]. Most of these studies have presented wear rate of polymers and they experimentally studied the effect of different parameter such as sliding velocity and contact pressure in wear of polymers.

1.3-5. Gap in the literature

Tribology behavior of polymers has already been examined in different geometries such as pin-on-disk, metal shaft in polymer housing (journal bearing), metal ball on flat polymer surface, etc. Wear behavior of self-lubricating polymers in

conical thrust bearing application (sphere metal ball inside conical polymer cup) has not been adequately explored. Most of the earlier studies have tried to avoid geometric complexities by using flat contact surfaces to enable better focus on comparing the wear behavior of different polymers or different sliding parameters such as: sliding velocity, temperature, etc.

In reality, the wear behavior of polymers in non-planar geometries is more significantly complex than that of a planar sliding pair. Formation of a transfer film and presence of trapped debris between the sliding pair (steel metal counterface and Delrin polymers surface in this study), can cause significant random variabilities in complex geometry geometries. Simple contact geometries such as pin-on-disk are not fully capable of capturing those effects. For instance, the separated wear particles can leave the contact zone much easier in the pin-on-disk geometry, compared to the conical thrust bearing geometry. Therefore, to understand the wear behavior of polymers in an application with complex geometry we need to conduct wear test using a geometry that is similar to the intended application.

According to Archard's model, wear rate of a sliding surface has an inverse correlation with the hardness of the softer surface in contact. No insight in changes of hardness in contact surface of polymer during the wear process and its effect(s) in transition of wear behavior of polymer in polymer-metal bearings is available.

The wear behavior of a self-lubricating polymer, Delrin (POM), in conical thrust bearing geometry (more complex non-planar) is explored in this study. The possible variability in wear behavior of the conical Delrin thrust bearing is explored.

1.4- Approach and thesis layout

This document is written in multiple chapters, with each chapter building on the former chapter(s).

The second chapter of this thesis is dedicated to the design and implementation of the wear test. The result of wear test is later used to extract the wear factor and calibrate the wear model that has been used in the third chapter. Several parameters were monitored during the wear test that will be comprehensively explained in the second chapter.

Chapter two of this thesis is dedicated to Archard's wear model that is used in this study and detailed approach to extracting the wear factor of conical Delrin thrust bearing. Furthermore, a detailed finite element model is developed and presented in 4^{th} Chapter, to account for elasto-plastic deformation of plastic bearing cups. This deformation affects the contact area and axial penetration of the bearing ball which are needed to precisely calculate the wear factor and to accurately calibrate the wear model using the wear test results.

The hardness of Delrin cups is measured and discussed in Chapter 5. Moreover, life model of conical thrust bearing is presented as a case study to demonstrate an application of this study.

2. Wear Test

In this chapter the fabrication and implementation of the wear test that was used to study tribological behavior of conical Delrin thrust bearings will be explained in detail.

2.1- Introduction and design of wear test

Delrin is one of the most common engineering thermo plastics and its wear properties have been already explored through different studies [24], [25]. One might raise a question of why it is necessary to conduct more experimental study to understand the wear behavior of Delrin. To answer this question, we should mention some studies such as [14] and [15] (journal bearings) that show wear behavior of polymers is dependent on many environmental factors such as sliding speed and contact pressure. Also, there is no clear insight into the effect of geometry on wear rate of polymers, available in the literature. Therefore, in order to get insights into wear behavior of materials in a particular application, it is necessary to study tribological behavior of those materials using wear tests that covers the range of conditions (contact zone geometry, counterface roughness, sliding velocity, temperature and the contact force) expected in the desired operational and environmental application.

The wear test experiments were designed to enable us to monitor required parameters to calibrate the model and so to extract the wear factor for the conical thrust bearing geometry (a spherical steel bearing ball inside a conical Delrin bearing cup) at the required condition. In the wear model section, different parameters that

are necessary to modify the model and extract the wear factor (**k**) that affects the wear rate of bearing such as, normal force ($\mathbf{F_N}$), and angular velocity of worm shaft/bearing ball ($\boldsymbol{\omega}$), will be discussed in detail.

2.2- Life- cycle load condition

Stepper motors experience complicated loading conditions in the use environment. As bearings wear out, the axial leaf spring expands to compensate for the gap caused by material removal of the plastic bearing cup. Figure 2-1 and 2-2 provide visualization of how and why the bearing geometry and contact zone change with bearing wear, and with resulting axial displacement of the bearing ball relative to the bearing cup.

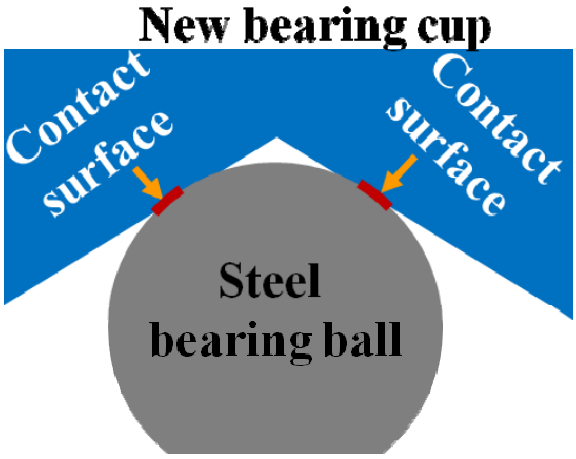

Figure 2-1: New bearing: Contact surface area is small because steel bearing ball has not penetrated into bearing cup yet.

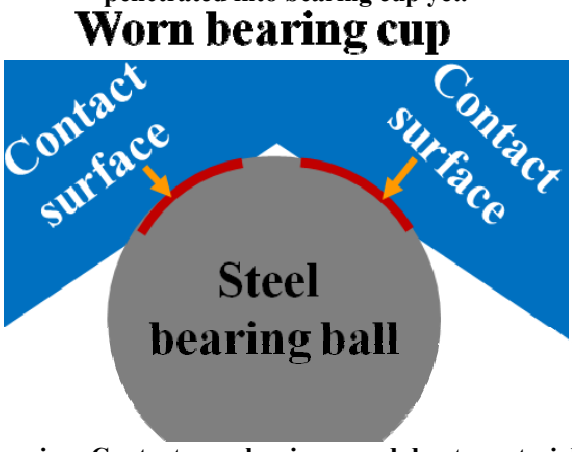

Figure 2-2: Worn out bearing: Contact area has increased due to material removal and resulting axial penetration of bearing ball into bearing cup.

As the leaf spring expands (relaxes) the axial compressive preload exerted by that leaf spring, which lowers the wear rate of the bearing. The leaf spring is not the only source of load on the bearings in a typical use environment (e.g. in an optical disk drive). While the stepper motor moves the optical head in an ODD; there is an axial and lateral reduction force on the bearing cups. The directions of force caused by the optical head sled, the leaf spring and reaction force on the pivot cup can be seen in Figure 2-3.

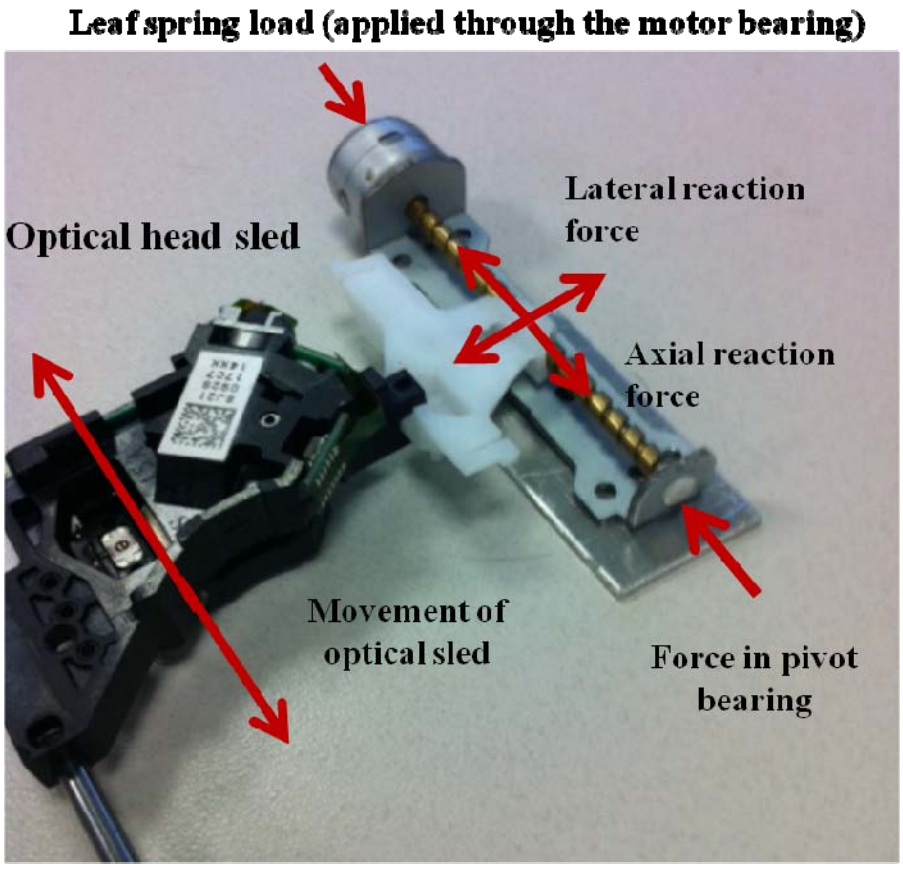

Figure 2-3: The loads applied on the worm shaft, leaf spring and optical sled of the stepper motors

The direction and amplitude of the sled load depend on direction of optical head movement and on the position of the sled on the worm shaft. In addition to mechanical loads, temperature of environment also affects the wear rate of bearings which is not constant all through the usage cycles. Therefore, stepper motor experiences complicated loading history in the field and this complexity of loading condition gets further exacerbated by manufacturing variability. Consequently, it is almost impossible to replicate the field loading conditions in the wear test. It is more feasible to try to understand the effect of each load on the wear process (main failure mechanism) of the conical Delrin thrust bearing separately, by designing and

implementing tests and modeling, to target a particular load in the field. In this study we intended to study the effect of axial load and sliding distance on the wear factor and on the wear rate of bearing cups at, 25˚C ambient temperature.

2.3- Wear test set up

The wear tests were conducted in two different phases:

a. ***Phase I***: Study the variability of wear resistivity and wear rate of four stepper motors with conical Delrin thrust bearing cups (motor bearing cup in the motor end and pivot bearing cup in the pivot end of the stepper motor) under 300g load (typical load that a stepper motor experiences in the field) over 170Km of sliding distance (54 Million cycles of bearing).

b. ***Phase II***: Study the effect of load magnitude on wear behavior of four stepper motors with conical thrust Delrin bearing cups under different loads close to the load that the stepper motor experiences in its use condition over 170 Km of sliding distance (54 Million cycles of bearing).

The tests are conducted on identical stepper motors with thrust bearings consisting of steel bearing ball in a conical polymer bearing cup. The tests are conducted at 25˚C ambient temperature and at a constant sliding speed of 47mm/s.

2.3-1. Fabrication of wear test set up

The test set up fixture consists of Plexiglass parts that were machined and fabricated using a milling machine. The fixture consists of multiple parts such as:

base, weight holder rack, aluminum joints, individual fixtures and the aluminum tubes to hold the IR sensors. The test frame has a modular design with each motor on a separate platform to facilitate periodic off-line characterization of each motor.

Solid Works drawings of main fixture parts including their details and dimensions can be found in Appendix II. The cylindrical dead weights are made of brass. The weights are used to apply a constant axial load and they are held and guided with four aluminum tubes with inner diameter of 1.45 in attached to the weight holder rack on top of the stepper motors, as seen in Figure 2-6. The frequency of the stepper motors are controlled by a code written in LabVIEW8.6 and it is fixed at 250 PPS. Four RB Spa-494 SFE "easydriver" bipolar stepper motor drivers are used to run the motors (transferring the power and controlling signal to stepper motor). The photograph of the driver used in the wear test can be seen in Appendix II. The power of stepper motors and IR sensors are provided by a HP 6236B Triple output power supply. The voltage of stepper motors was fixed at 4.5V (the voltage was fixed at 4.8V at the power supply due to 0.3V drops in the connector cables) and 5V voltage was applied to the Honeywell-HOA1404-002 IR sensors.

2.3-2. Wear test setup

The schematic of the test set-up can be seen in Figures 2-4 – 2-6. In this test, dead weights are used to apply constant axial loads to the bearing while motors are running at a constant angular velocity. The wear out occurs in the contact zone of the bearing ball and cup, where the cup is subjected to compressive pressure and sliding simultaneously. It is necessary to be careful and patient during starting and stopping of the test. The loads were gently inserted in the aluminum tubes while the motors

are running, to avoid any shock and sudden mechanical force that might cause permanent deformation in the motor assembly, especially in the plastic bearing cups.

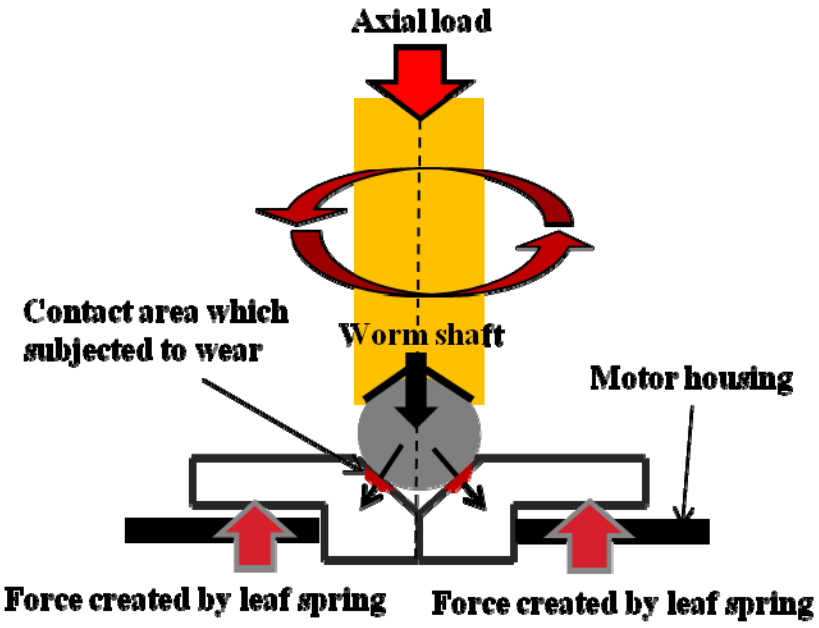

Figure 2-4: A constant axial load is applied to the bearing while the motor was running.

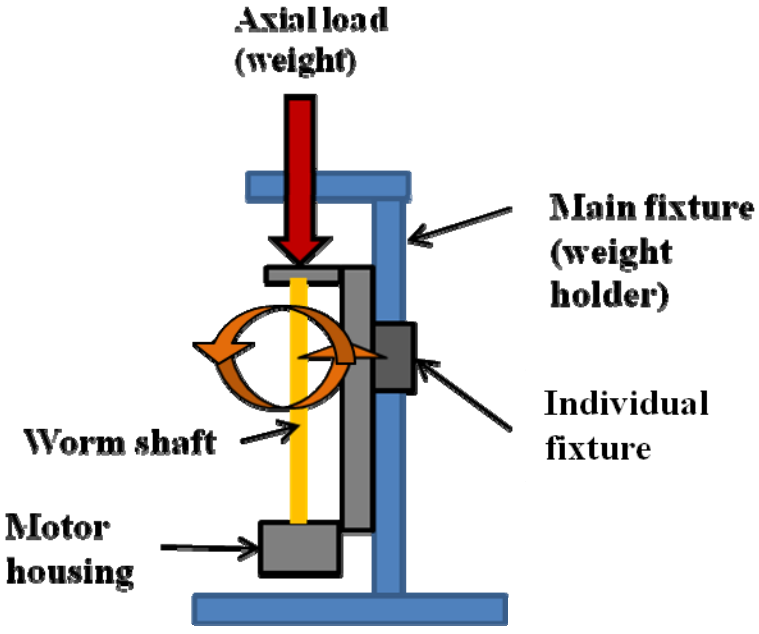

Figure 2-5: Motor mounted on the fixture

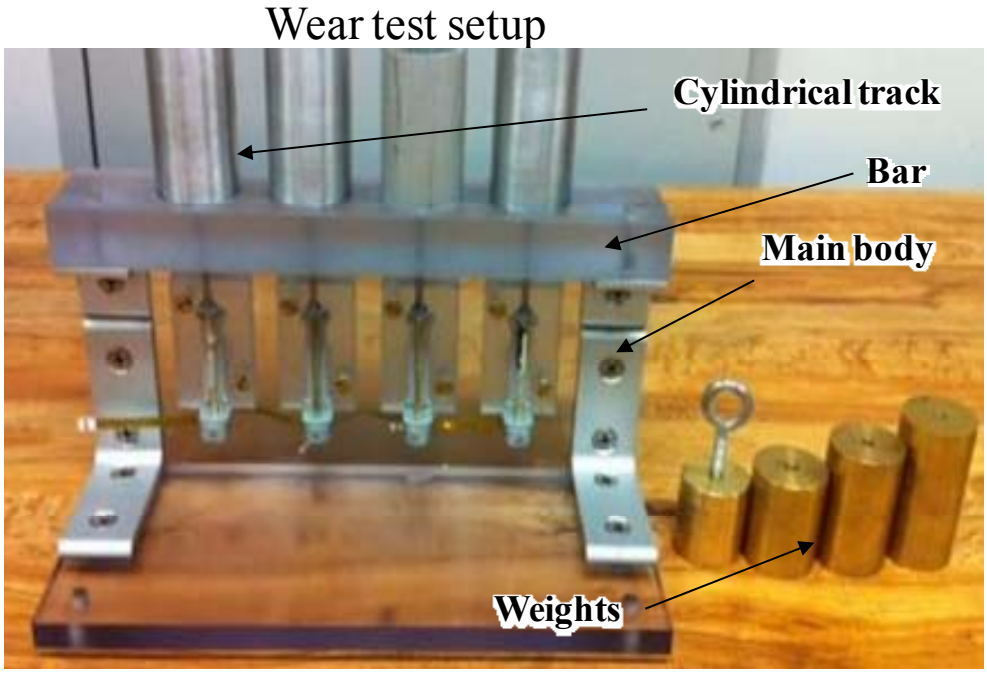

Figure 2-6: Wear test setup (modular fixture)

In this test, each motor was operated at a constant angular velocity under a constant (Phase I) and different (Phase II) axial loads. The parameters are monitored during the tests to identify the model constants and to study the degradation of the motors are:

- Wear depth of bearing cups using optical microscope enhanced with image processing tool at periodic intervals during the tests
- Continuous in situ measurements of angular velocity of worm shaft using IR sensors
- Lateral displacement of worm shaft, measured off-line at periodic intervals
- Required torque to rotate the worm shaft (detent torque), measured off-line at periodic intervals

The first two parameters are necessary to extract the wear model constants and they will be explained in detail in the following sections. The last two parameters (lateral displacement of worm shaft and detent torque) were observed to understand the degradation of the stepper motor as bearing wear progresses. These parameters are not in the scope of this thesis and they are not discussed in detail in this document.

2.3-3. Bearing cup wear

Measuring the volume removal rate of the bearing cups was one of the most challenging tasks in this experiment. Since it is not feasible to disassemble the bearings to measure the instantaneous wear depth during the test, the axial displacement of the motor bearing cup relative to the motor housing was periodically measured throughout the test using an optical microscope coupled with an image processing tool, and used to infer the total axial wear depth of the bearing cups. Each motor was periodically dismounted from the test platform for this measurement. The axial displacement of the motor bearing cup relative to the motor housing was measured by monitoring height of the cup bottom which sticks out of the motor housing, as seen in Figure 2-7. As bearings wear out, the leaf spring expands, which leads the motor bearing cup to move while the pivot bearing cup is fixed against the C-bracket. Therefore, the axial displacement of the motor bearing cup represents the summation of axial wear depth of both bearing cups. The initial height of this step (between housing surface and bearing cup bottom surface) was measured on each motor before starting the wear test and was used as a reference. The changes of the bearing button height relative to the reference show the history of the total axial wear

depth of the bearing cups. Attempts were made also to measure the wear depth rate of pivot cup separately, but this was almost impossible due to inaccuracy of measurement method at the pivot bearing. The limitation of this approach to measure the wear depth of bearings will be explained in detail separately at the end of this document. The worn out motors were destroyed at the end of the wear tests, to conduct failure analysis and to measure the actual wear depth.

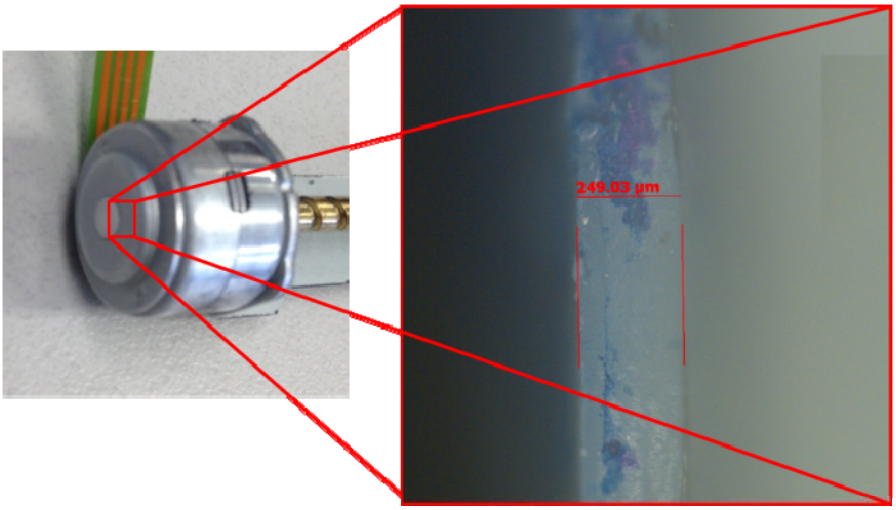

Figure 2-7: Optical measurement of the total bearing wear depth

2.3-4. Angular velocity of the worm shaft

The sliding distance between the bearing ball and bearing cup surfaces is an essential parameter in Archard's wear model for predicting the worn out volume. In order to measure the sliding distance of the bearing ball, the total number of rotations of the worm shaft were counted during the wear test using an IR encoder, as described below. Four Honeywell infrared reflective sensors (HOA1404-002) were used as counters to detect each rotation of the worm shaft of each of four stepper motors in the tests. The output voltage of the sensor is a constant value until the emitted radiation from the sensor reflects back to it; then, the output voltage

drops to a lesser value. Reflective shiny sheets were attached on the worm shafts at a certain distance from the IR sensor. Therefore, the emitted radiation reflects back to the sensor once a cycle and that causes a drop in the output voltage of the IR sensor during each cycle of worm shaft. These changes of output voltage make it possible to count the number of rotations of the worm shafts using the LabVIEW code. The output voltage of the IR sensors was measured by a National Instruments data acquisition card (PCI 6024E) through a National Instruments connection block (CB-68LP). The IR sensors were mounted 3.8mm away from the worm shafts for the best performance of the IR sensors. The output voltage drops when the reflective sheet attached to the worm shaft passes in front of the sensor, as seen in Figure 2-8.

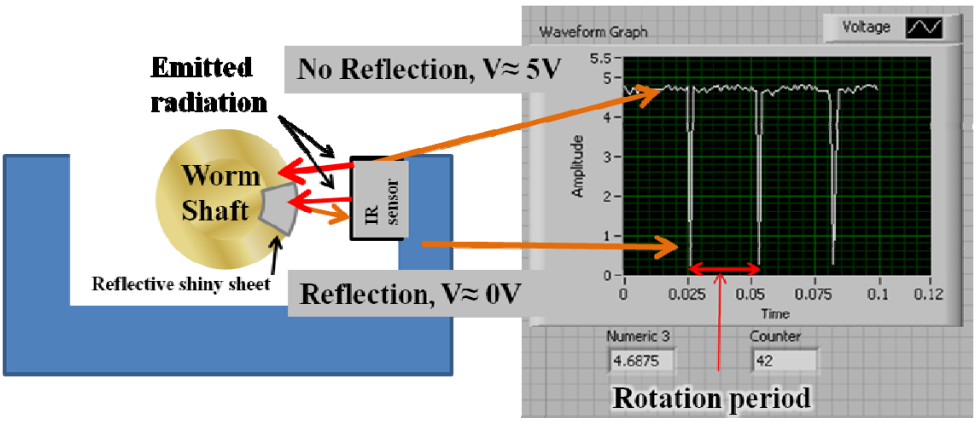

Figure 2-8: The output voltage of IR sensor

3. Wear Test results

The results of Phase I and Phase II of the wear test will be explained and presented in this chapter. Two wear depth measurement techniques, namely, optical and epoxy replicate based techniques were employed in this study. Each technique has its own weaknesses and strengths. Thus, combining the knowledge from both techniques enables us to obtain the most realistic wear depth estimation. The optical measurement technique was modified using the measurements obtained in the epoxy replicate technique. The approach to modify the optical measurements using the epoxy replicate and results from both the techniques will be comprehensively explained in this chapter. The formation of polymer transfer film on steel bearing balls during the wear test and its effects are discussed at the end of this chapter.

3.1- Wear depth measurements using optical microscope

The wear depths of the bearing cups under different loads were measured over 1,000 hours of tests. This corresponds to 170 Km of sliding distance and 54 Million rotational cycles of the bearings and motors. The optical wear depth measurements of five samples obtained from Phase I (Samples 1-4) and Phase II (Sample 5) measurements with 300 g load are depicted in Figure 3-1. These measurements were conducted in a daily basis. These plots are estimates of total wear depth of the stepper motors (wear depth of ***pivot cup*** + wear depth of ***motor cup***) using the optical measurement method described in Section 2.3-3. The total axial wear depth of the motors and the pivot bearing cups were measured by monitoring the displacement of the motor bearing cup relative to the motor housing. Minimize the error of this

measurement method is tried by choosing the most distinct line or sign on the motor bearing cup and motor housing as reference throughout the test period. In order to increase the accuracy of this method, five optical measurements were conducted each time and the average value has been used for estimating the wear rate (each data point in Figure 3-1 is average of five measurements). The range of values is about 10 µm at the worst case of these readings.

One of the important points to get correct results from the wear test of the stepper motor is to select the motors with preloads less than the applied axial load to make sure that the wear process is governed by the applied axial load, not with the stepper motors' preload. The preload of the stepper motors were measured to confirm that their preloads are less than the axial loads.

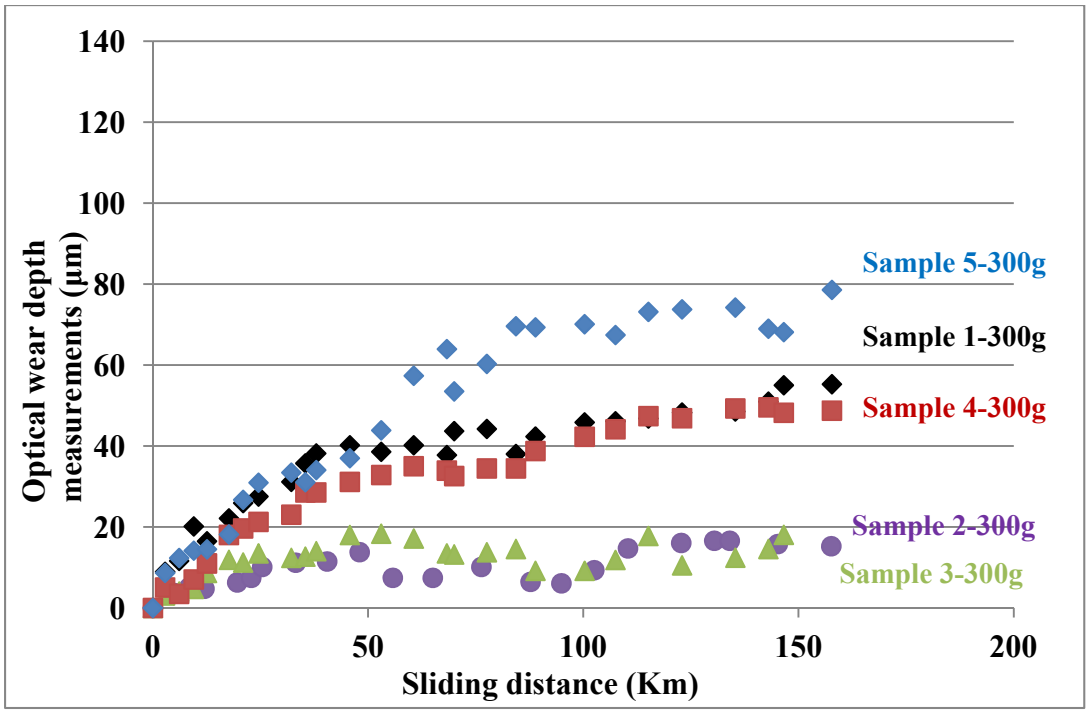

Figure 3-1: Optical wear depth measurements of five motors under 300g load

3.1-1. Error in optical wear depth measurement

As shown in Figure 3-1, there is a significant variation in the wear test results of the stepper motors. Furthermore, the wear depth history obtained from this technique shows a decrease of wear depth at multiple points, i.e., the wear depth trend of Sample 2 in Figure 3-1 shows decrease of wear depth after 90 Km of sliding distance, while it is expected that wear depth should monotonically increase during the wear process.

There are two main reasons for such erroneous measurements:

1. A layer of polymer (eroded debris and transfer film) forms on the bearing ball throughout the wear tests. The thickness of the polymer layer increases over the course of time, but the rate of increase has a somewhat random trend. Therefore, the axial distance between the bearing ball and the cup can increase (negative wear depth based on optical measurement) at some point due to a locking of debris and polymer transfer film between the bearing balls and the cups. Figure 3-2 and 3-3 shows the random formation of the polymer transfer film on the bearing ball surfaces.

2. Although the variation of optical measurements due to human error was carefully controlled, up to a 10 μm variation in five replicates of the same measurement has been observed in a few cases.

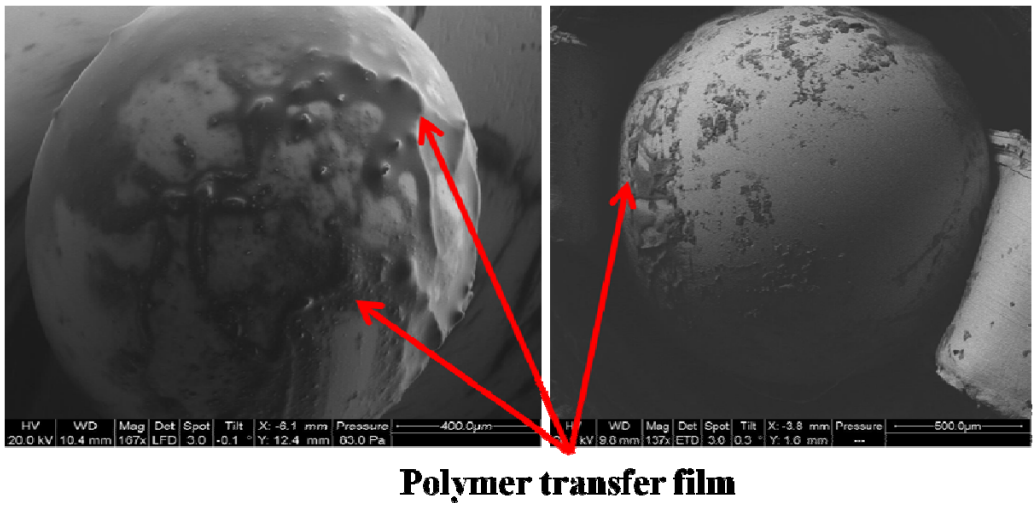

Figure 3-2 – 3-3: SEM picture from transfer film on bearing ball surface

The piece-to-piece variation and error in optical measurements are the two difficulties and limitations in this study. The problem is even further exacerbated by random behavior of the polymer transfer film on the steel bearing balls which will be explained in the rest of this chapter. The details of measurements of axial wear depth obtained by both techniques are listed in Table 3-1. The preload of all five motors were measured before Phase I and Phase II of the wear tests to make sure that the motors' preload are less than the applied axial load and the wear of bearings are governed by the applied loads not with the leaf spring loads. This observation were confirmed before starting the test by observing separation of pivot cup from the C-bracket after exerting the load which means the leaf spring is compressed more and the pivot cup and worm shaft move toward the motor end. Thus, the applied axial load is greater than the leaf spring compressive load.

5 samples at 300g axial load	Pivot Cup(µm)	Motor Cup (µm)	Total wear (µm)		Difference (µm)	P_{ratio} (Pivot/total)	M_{ratio} (Motor/total)
	Epoxy replicate	Epoxy replicate	Epoxy replicate	Optical measurement			
Sample 1 (QX1)	48	31	79	53	26	0.61	0.39
Sample 2 (QX2)	17	24	41	17	24	0.41	0.59
Sample 3 (QX3)	51	16.5	67.5	20	47.5	0.76	0.24
Sample 4 (QX4)	43	90	133	47	86	0.32	0.68
Sample 5 (SS1)	71	45	116	77	39	0.61	0.39
Average	46	41.3	87.3	42.8	44.5		

Table 3-1: Wear depth measurements of five samples under 300g (Phase I wear test)

The optical wear measurements of five samples are mainly from Phase I of the wear test that have been already presented in Figure 3-1. The optical wear depth measurements of three samples from Phase II of the wear test (this wear test was designed to study the effect of load on the wear factor and the wear behavior of the bearings) are shown in Figure 3-4. Also, the results of both measurement methods (optical and epoxy replicate) are shown in Table 3-2. As shown, the percentage contribution of motor cup and pivot cup wear to the total wear depth of the stepper motor varies for each stepper motor and it is believed that this variation is mainly due to random formation and removal of the polymer transfer film on the bearing balls and the manufacturing process. These results are obtained using the optical measurement method. The motor with 600 g load shows intrinsically different behavior than the motors with different loads. It is possible that the wear mechanism that governed the wear of motor with 600 g load is different than that of other motors with smaller loads. The epoxy replicate method was also employed to measure the total wear depth and used to calibrate the optical measurements. The approach to

calibrate the optical measurements using the total wear depth value will be explained in the following section.

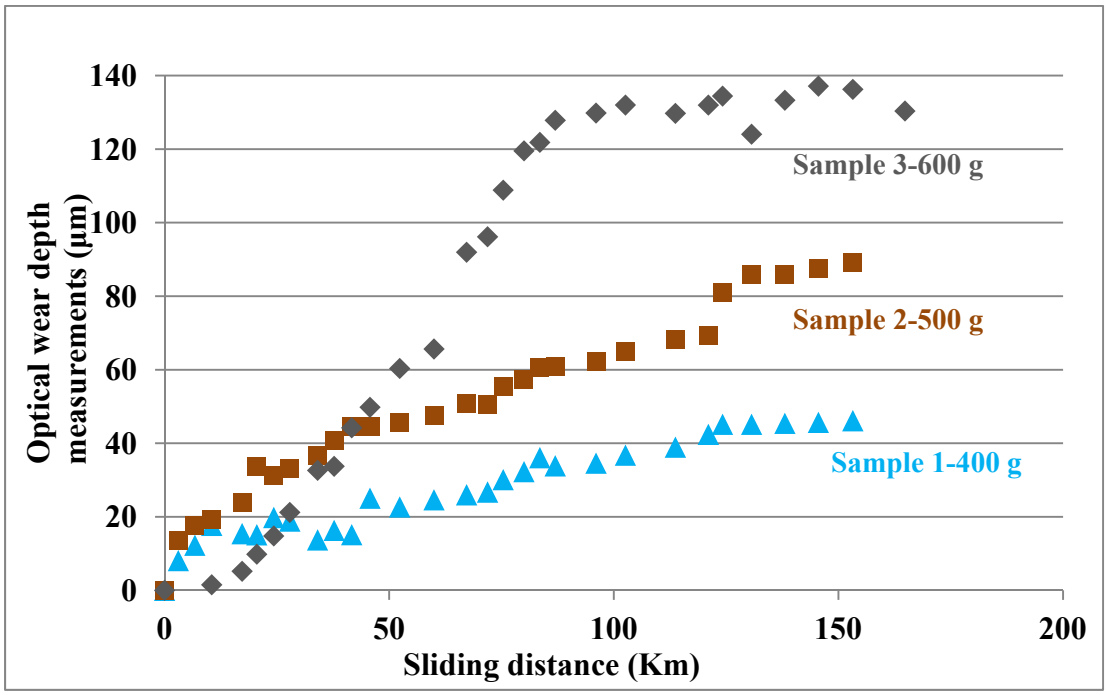

Figure 3-4: Optical wear depth measurement of three motors under 400 g, 500 g and 600 g

	Pivot cup (µm)	Motor Cup(µm)	Total wear(µm)		Difference (µm)	P_{ratio} (pivot/total)	M_{ratio} (Motor/total)
	Epoxy replicate	Epoxy replicate	Epoxy replicate	Optical measurement			
400 g	21	26	47	47	0	0.45	0.55
500 g	38	60	98	85	13	0.39	0.61
600 g	57	117.5	174.5	141.5	33	0.33	0.67

Table 3-2: Wear depth measurements of three motor under different loads (400 g, 500 g and 600 g)

3.2- Actual wear depth of bearing cup using epoxy replicate

The presented results in Figures 3-1 and 3-4 are only estimates of total wear depth obtained from the optical measurement method during the test. Since it was not possible to open the bearings to measure the actual wear depth, the optical wear depth

measurement is the only source of knowledge about the wear depth history of the bearings during the tests. There is uncertainty in the optical wear depth measurements for reasons listed above in Sec 3.1-1 and it is necessary to calibrate the results with the actual value of wear depth for each bearing cup. Due to the randomness in the thickness of transfer film the optical measurement method loses its accuracy as the wear progresses. The top views of new and worn out bearing cup are shown in Figure 3-5. The black debris can be seen on the worn out bearing cup. To better visualize the shape of the bearing cone, the side view of the epoxy replicates is shown in Figure 3-6.

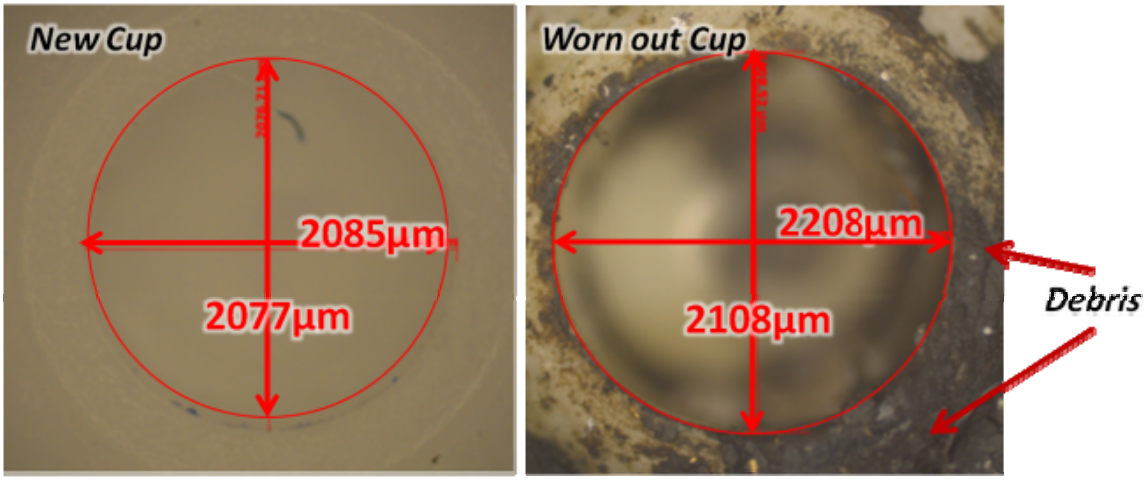

Figure 3-5: Top view of new and worn out bearing cups

The advantage of using epoxy replicate to measure wear depth is that it gives more accurate results than the optical measurement method, because it is not affected by the transfer film and the debris in this technique. The disadvantage of replicates is that it is a destructive method as it requires disassembling of the motors. Hence, it can be performed only once, at the end of the test. Thus, this method does not provide any information about the history of the wear depth evolution during the wear test.

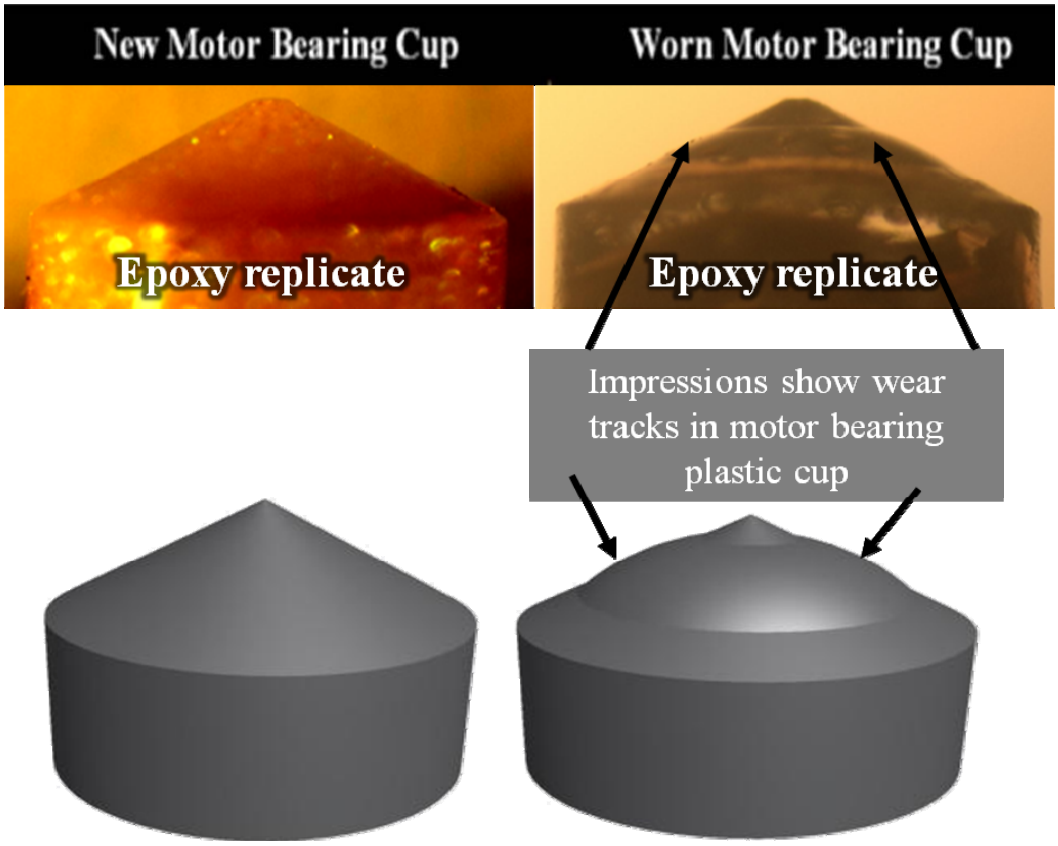

Figure 3-6: Side view of epoxy replicate of new and worn out bearing cup

The wear depth of each bearing was measured by analyzing the images captured using a high resolution microscope during the test as shown in Figure 3-5. Epoxy replicates also confirmed the observed variation in total wear depth of bearings using the optical measurement technique (Figures 3-1 and 3-4). The epoxy replicates of Samples 1 to 4 are shown in Figures 3-8 – 3-11.

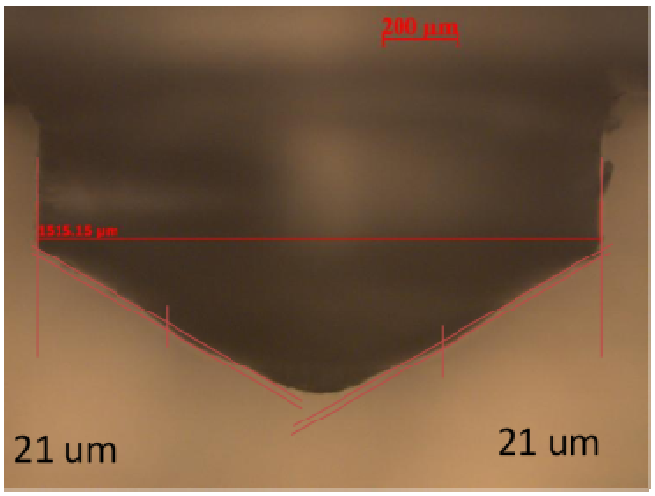

Figure 3-7: Measuring wear depth using epoxy replicates

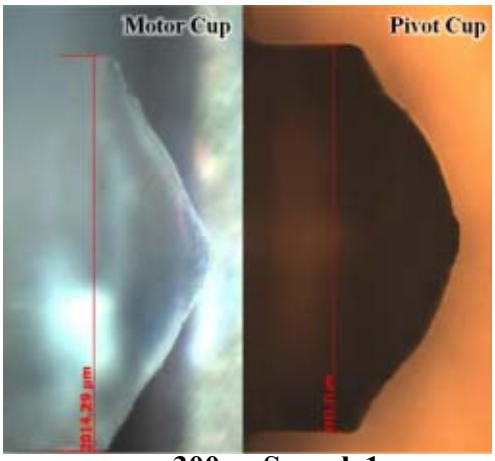

300 g- Sample1

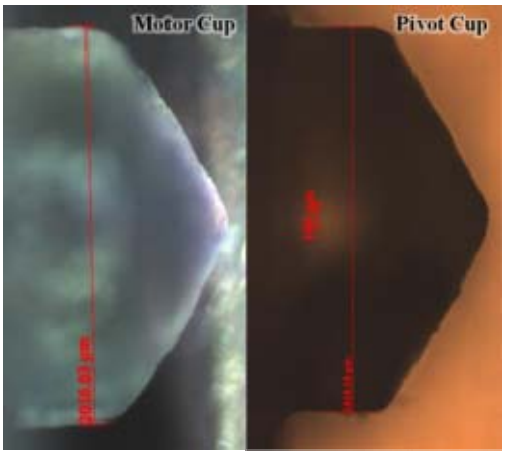

300 g- Sample2

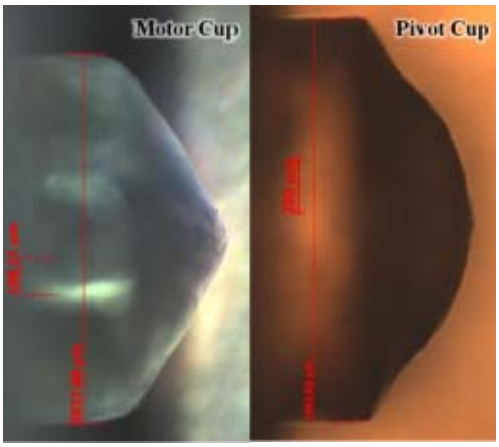

300 g- Sample3

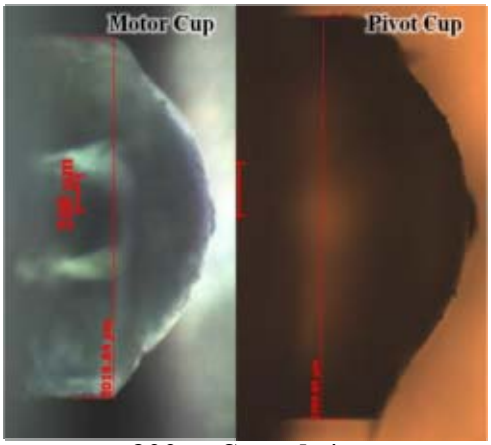

300 g- Sample4

Figures 3-8 – 3-11: Side view of epoxy replicates for four motors under same load (significant variation in final wear depth of motors can be observed from the epoxy replicates)

3.3- Wear depth results and variability in wear depth measurements

As was discussed and presented quantitatively in Tables 3-1 and 3-2, there is a significant difference between two wear depth measurement techniques: the optical measurement method and the epoxy replicate measurement method. The most reasonable hypothesis to explain this variation is formation of the transfer film on the bearing ball and Delrin debris trapped in the conical cup due to abrasion of the cup by the steel bearing ball. The final wear depth values for five samples under the same load, 300 g from both techniques were measured, compared and presented in Figure 3-12.

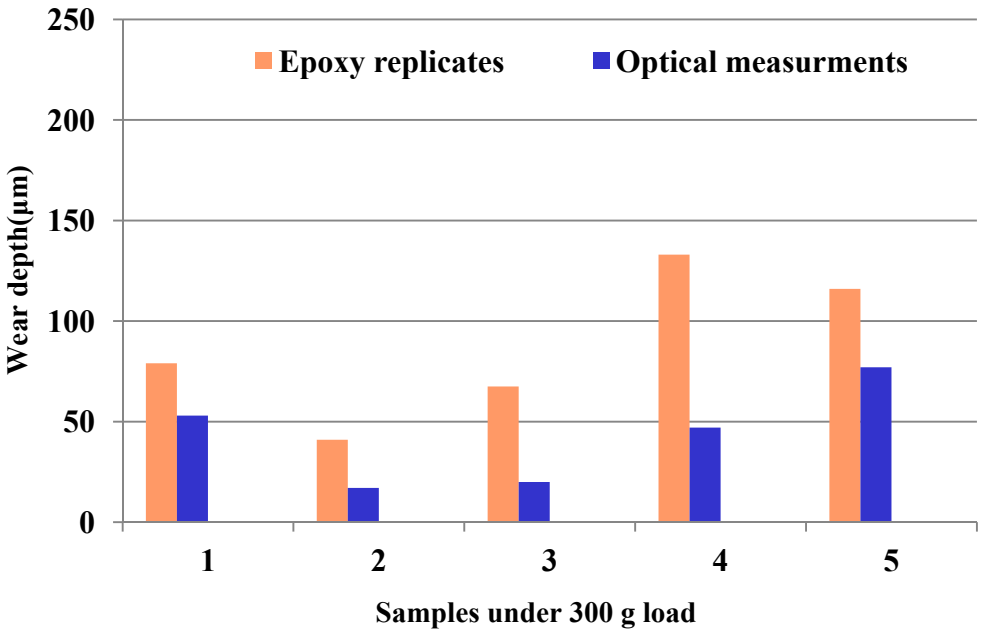

Figure 3-12: Comparison of wear depth measurement by Optical and epoxy replicate technique at the end of wear test

In contrary, optical measurements provide the history of wear depth while its accuracy decreases during the progression of wear. Epoxy replicates provide more reliable value of final wear depth, but they do not provide any information about the

history of wear depth evolution. Therefore, it is necessary to use the combined knowledge from both techniques. Thus, the optical measurements are calibrated using epoxy replicates to get the most realistic estimates of wear rate of the bearing cups. In order to do so, thickness of transfer film is assumed to start zero at the beginning of the test and linearly increase with the sliding distance. It can also be noted that the total wear depth of motors (sum of motor cup and bearing cup) at 300 g load for 1000 hrs of test (170 km of sliding distance) varies between 40 μm and 130 μm, which is a significant variation. There is no clear explanation for this behavior and it is believed that this variation is caused by a combination of random behavior of debris in the bearing which affects the sliding of the ball inside the cup and the random behavior of the polymer transfer film on the bearing ball surfaces.

3.4- Formation of transfer film on steel bearing ball

Transfer of polymer materials to the metal surface during the sliding process is a common phenomenon during the sliding process between polymers and metals. Formation of polymer transfer film on the metal counterface is governed by sliding pairs' material and counterface roughness [19] & [18]. Polymer transfer film has a great impact on tribology behavior of sliding pairs by reducing friction and wear between them. Harrass et al. [24] have studied the volume loss rate of polyamide (PA) in linear ball-on-plate test (Appendix VIII), shown that the volume loss rate decreased throughout the tests, as seen in Figure 3-13. The transfer film is believed to be responsible for such behavior.

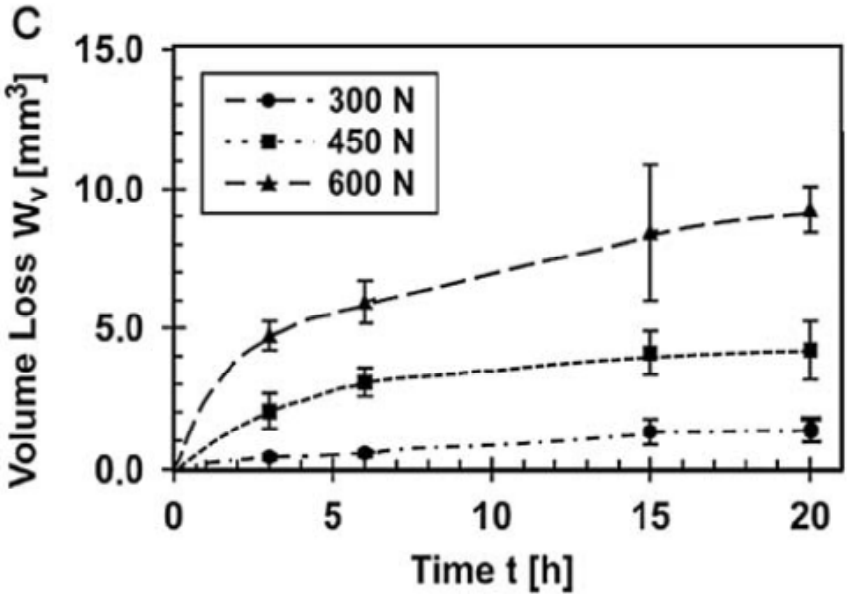

Figure 3-13: Volume loss over testing duration as measure for PA rubbing against steel under different normal loads [Harrass et al (1998)]

In both Phase I and Phase II of the wear test, the wear depth rate was observed to be initially high and to decrease throughout the progression of wear. The geometry analysis for calculating the worn out volume confirmed that the volume removal rate decreases as the sliding distance increases. The volume removal rate of motors in both wear tests will be discussed in detail later in Section 4.1. The existence of transfer film on steel bearing balls of tested motors was qualitatively investigated using optical microscope and SEM. The pictures clearly confirmed the existence of the transfer film on the steel bearing balls surface. Figures 3-14 – 3-15 were taken from optical microscope and Figures 3-2 – 3-3 were taken using SEM.

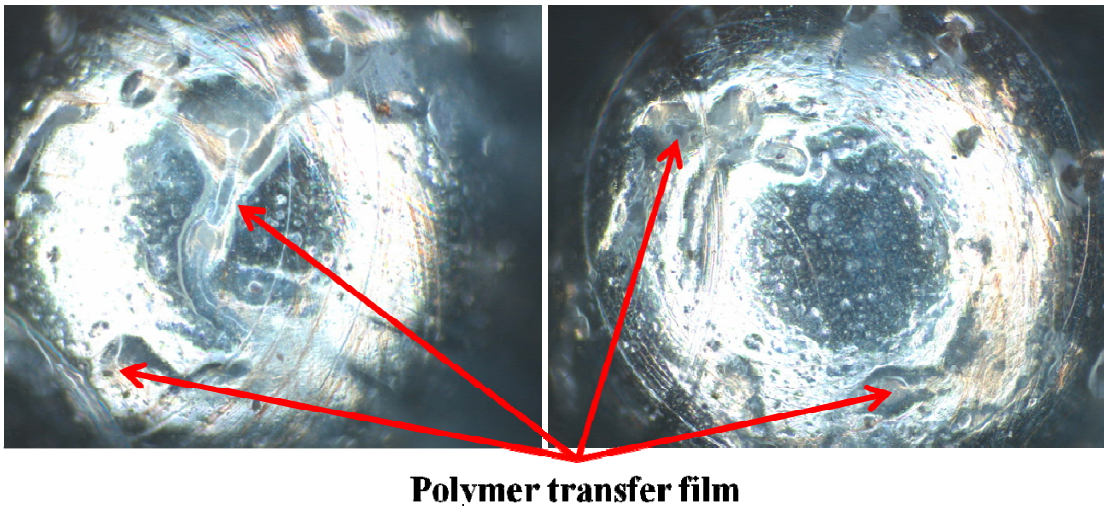

Figure 3-14 – 3-15: Polymer transfer film on bearing ball surface (optical microscope pictures)

3.5- Conclusion

The results of Phase I and Phase II of the wear tests were explained in detail in the previous sections. Two techniques, optical measurements and analysis of epoxy replicates, were used to measure the axial wear depth of the bearing cups in each motor. The optical measurement technique provides the wear rate history of the bearing cups, but its accuracy decreases due to eroded debris and formation of the polymer transfer film on the steel bearing ball throughout the wear process of the bearings. The analysis of epoxy replicates provides reliable estimation of the total wear depth of bearings, while it cannot provide any information about the history of the wear depth. In this study we have tried to combine the information from both techniques, for obtaining the most realistic estimate of wear rate of the bearings. The estimated wear rate values are used in the following chapter to calibrate Archard's wear model by characterizing the wear factor of Delrin in the conical thrust bearing

application at **25˚C ambient temperature**, force range of **300 g to 600 g** and sliding velocity of **47 mm/s.**

4. Modeling the wear rate of the bearings

The process of wear can be considered as a dynamic process that depends on multiple parameters like contact normal force and sliding distance. Archard's wear model has been already discussed in earlier chapters. Archard's wear model states that the worn out volume from one or both of the contact surface varies linearly with the constant normal load and the relative sliding distance between the two surfaces. The proportionality constant is a property and is the ratio of a dimensionless wear constant and the hardness ***(H)*** of the softer of the two materials in contact. The constant ***k*** is a function of temperature and sliding velocity. ASTM D3702 provides a method to estimate the wear factor of plastic in specific condition. In this study we are intended for finding these constant for non-planar bearing geometries, especially for steel bearing ball in conical polymer bearing cup. The worn out volume ***(v)*** during a sliding process based on Archard's model for two sliding planes in contact is given by:

$$\boldsymbol{v = kL\frac{F}{H}} \qquad (\mathbf{5})$$

where ***F*** is normal force, ***L*** is sliding distance, ***H*** is hardness of the softer material and ***k*** is wear factor/coefficient and it is specific to the contact pair. In the rest of this thesis, instead of $\boldsymbol{\frac{k}{H}}$ we use ***K*** (mm^3/Km.N) for more convenience. The volume of removed material from the bearing cups was calculated by geometric analysis of worn out cups. The approach to calibrate Archard's wear model by characterizing the wear rate (***K)*** of Delrin in the conical thrust bearing application at room temperature will be explained in detail in this chapter. Detailed finite element analysis is employed to

refine the wear model by accounting for the effect of elasto-plastic deformation of the bearing cups or the contact surface area and axial movement.

4.1- Geometry analysis of worn out cups

The first step to obtain wear rate (***K)*** for conical bearing, based on the wear test, is to compute the worn out volume of the bearing cups. Obtaining the worn out volume or removed-material is a challenging step for this complex geometries, while the sliding distance and applied load during the test were comparatively easier to determine. The volume of removed material was computed using the geometric analysis of the worn out-bearings. The schematic of the worn out bearing is shown in Figure 4-1.

Figure 4-1: Schematic of worn out-bearing

The pivot bearing and motor bearing have exactly the same shape (sphere steel ball in Delrin conical cup) and the only difference is their dimensions. The

bearing ball is 2 mm and 1.5 mm in diameter (***2R***) in the motor and pivot, respectively, and the cone angle (***2α***) of both the bearing cups is about 120˚. More details of bearing geometry before and after wear out have been shown in Figure 4-2.

The changes of bearing cup geometry, from initial stage (no wear) to final stage (after axial penetration of the ball) are depicted in Figure 4-2. The axial penetration of the bearing ball is ***y*** . ***R*** is the radius of the ball (1 mm for motor cup and 0.75 mm for pivot cup), ***α*** is the half of the bearing cup cone angle (60˚), ***β*** is the half of the angle of the arc that represents the contact zone angle, ***β*** is initially zero and it increases as the wear depth increases. r_{in} and r_{out} are the inner and the outer radii of the contact zone. The worn out volume is demonstrated in Figure 4-3. This volume is calculated by subtracting the volume of the conical frustum from the spherical segment.

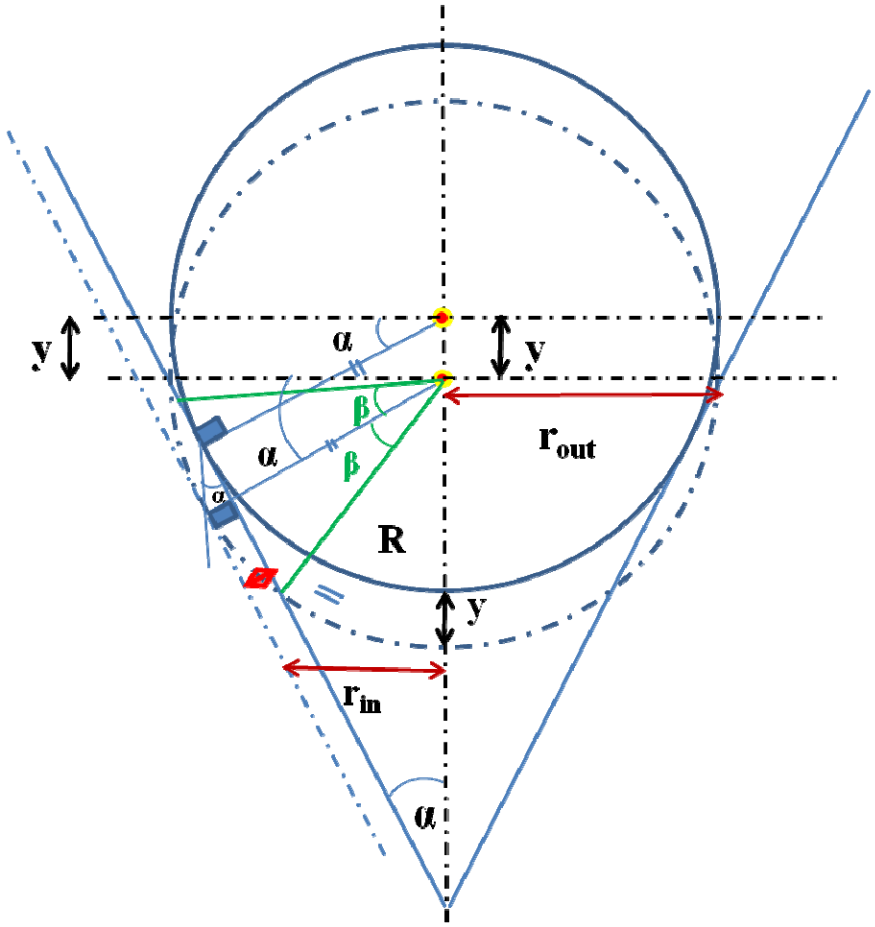

Figure 4-2: Detailed-geometry of bearing

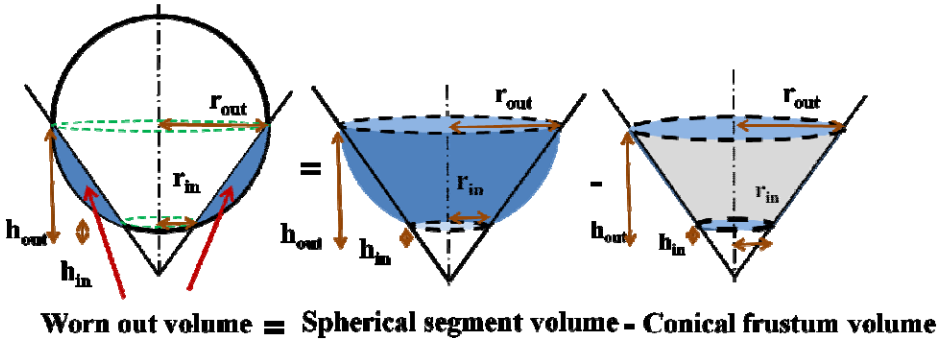

Figure 4-3: Geometry of worn out volume

The volume of the spherical segment is given by:

$$v_{spherical\ segment} = \frac{1}{6} \cdot [3 \cdot {r_{out}}^2 + 3 \cdot {r_{in}}^2 + h^2] \quad (6)$$

The volume of the conical frustum is given by:

$$\boldsymbol{v_{conical\ frustum} = \frac{\pi \cdot h}{3} \cdot [r_{out}{}^2 + r_{out} \cdot r_{in} + r_{in}{}^2]} \quad (7)$$

Therefore, the worn out volume is computed by:

$$\boldsymbol{v_{worn\ out\ volume} = v_{\text{spherical segment}} - v_{\text{conical frustum}}} \quad (8)$$

All the parameters of these equations are calculated by using the axial wear depth (y) of the bearing cups that has been presented in the previous chapter. The equations of these parameters are:

$$\boldsymbol{\beta = Cos^{-1} \cdot \left(\frac{r - y \cdot Sin(\alpha)}{r}\right)}, (9)$$

$$\boldsymbol{r_{out} = r \cdot Cos(\alpha + \beta)}, (10)$$

$$\boldsymbol{r_{in} = r \cdot Cos(\alpha - \beta)}, (11)$$

$$\boldsymbol{h_{in} = r \cdot \left(1 - Sin(\alpha - \beta)\right)}, (12) \textbf{ and}$$

$$\boldsymbol{h_{out} = r \cdot \left(1 - Sin(\alpha + \beta)\right)}. (13)$$

The computation of the worn out volume from the measured axial wear depths is more complex in reality. The measured axial displacement/penetration of the bearing balls are not solely because of removing the material from the cups. The axial load on the bearing balls also causes elasto-plastic deformation of the conical Delrin bearing cup, and this deformation contributes to the measured axial penetration of the bearing balls. Therefore, to rigorously analyze the removed material, it is necessary to investigate the contribution of the elasto-plastic deformation and axial penetration of the bearing ball. Elastic –plastic finite element analysis is conducted to estimate this contribution as discussed below .

4.2- Elastic-Plastic deformation of contact interface

In this study, Finite element analysis (FEA) has been used to develop a more accurate wear model by accounting for elasto-plastic deformation of the bearing cup contact interface.

4.2-1. FEA model of contact geometry

The result of Archard's wear model depends on the worn out volume of the conical Delrin bearing during the wear process. Therefore, to accurately predict the wear rate, it is necessary to use the exact axial penetration of the bearings to compute the worn out volume in the wear model, as the analytical model is not capable of calculating it due to the elasto-plastic deformation of the bearing cup. In this study, commercially available finite element software, ***ABAQUS 6.9***, was used to compute the elasto-plastic deformation of the bearing cup. An axisymmetric deformable model was used to model the conical Delrin bearing cup. Since deformation of the steel bearing ball is negligible, an axisymmetric analytical rigid wire was used to model the steel bearing ball to save computational time. Due to the quasi-static nature of the problem, General/implicit type of steps was selected to run the simulation. Four-node axisymmetric continuum elements with reduced integration were used in this study. The FEA model of this study is basically a contact problem. Therefore, it is necessary to apply the contact properties properly in the FEA model. A coefficient of friction of 0.2 [26] was applied to the contact zone. The mechanical properties of Delrin, such as stress-strain curve that are obtained and published by the manufacturer company [27], were used in the FEA analysis of this study. To facilitate parametric study using the FEA model, it was highly preferable to reduce the computational time as much as

possible. Thus, a mesh refinement study was conducted on the FEA model to find the most efficient size of the elements to optimize the accuracy and computational time of the analyses (Appendix VII). The size and location of the leaf spring were measured and applied as the boundary condition for the model.

The geometry of the model had been changed to account for the material removal of the bearing cup, and the model was remeshed every time after the change of dimension, and samples of these models are shown in Figure 4-4. The parametric study was conducted on the FEA model to study the effect of different wear depths and axial loads on the axial penetration of the bearing ball due solely to deformation of the conical Delrin bearing cup.

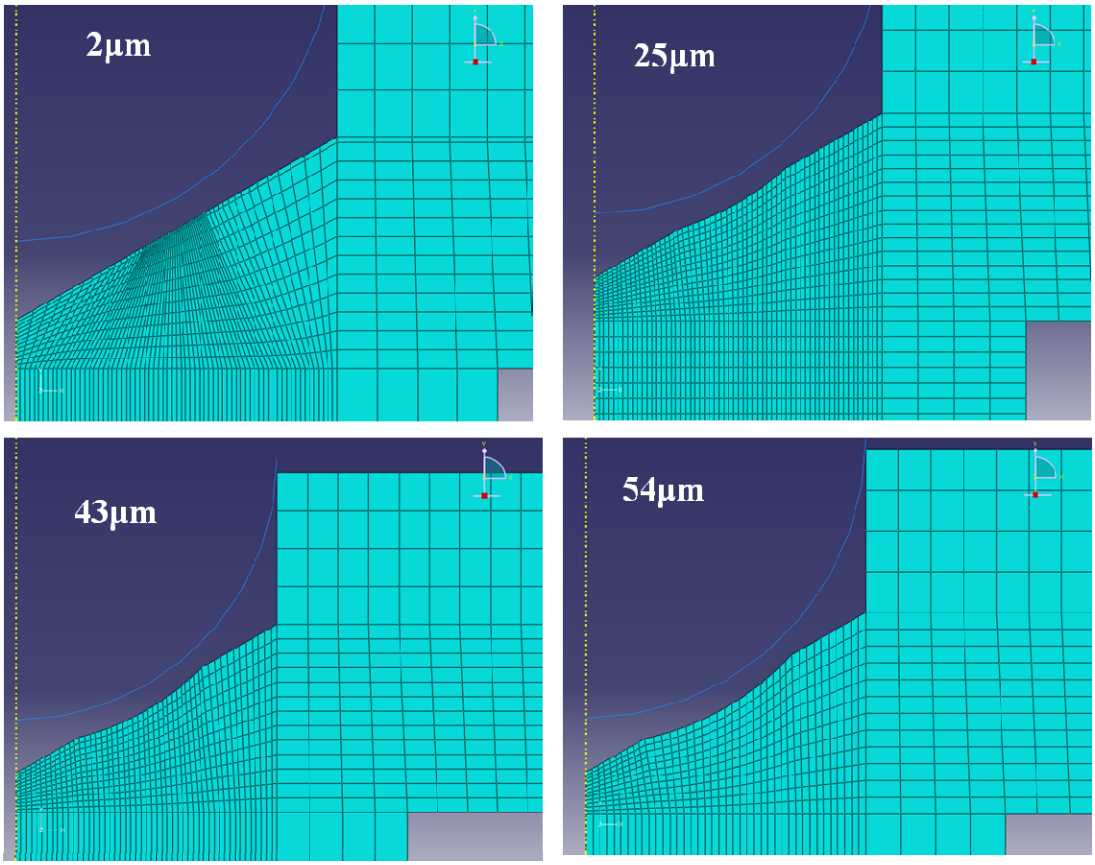

Figure 4-4: FEA model with different wear depths

The FEA model was run in three steps: 1-initial step, the initial boundary conditions and problem at the initial stage were defined in this step; 2-creating contact, the axial displacement was applied as a boundary condition to generate the contact between the bearing ball and cup; and, 3- applying load, the axial load was applied to the center of the bearing ball while the axial displacement of the bearing ball was monitored. The FEA model was also used to investigate whether the applied load caused any plastic deformation in the conical Delrin cup, and no plastic deformation was observed in the load range of this study. It was observed that the implicit approach cannot solve the problem in two steps, and it is necessary to simplify the FEA model by defining the problem in more than two steps. The axial displacement of the bearing ball and the reaction force on the bearing ball were obtained from the output results of the FEA. It was also observed that more complex steps can be solved by the explicit solving approach while the problem has to be simplified by using more steps to be able to use an implicit solving approach.

4.2-2. Results of FEA parametric study

The von-Mises' stress distribution of the model under 600 g load before any wear out is shown in Figure 4-5.

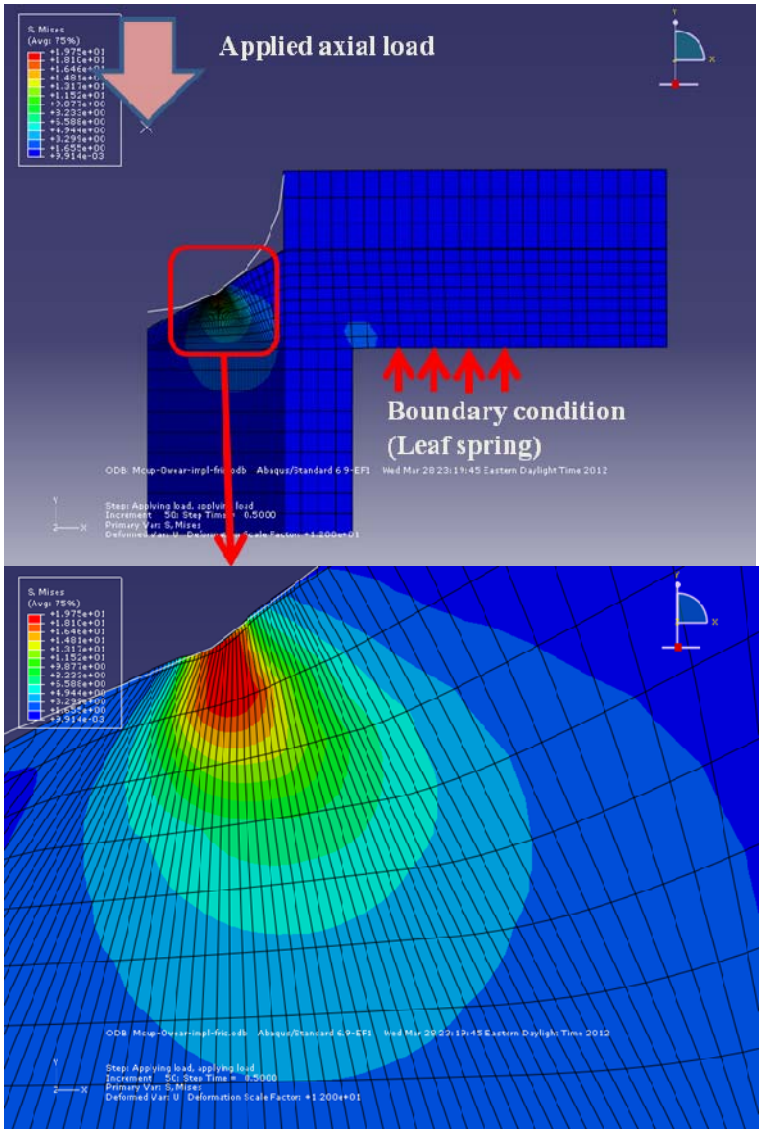

Figure 4-5: von-Misses stress distribution (600 g load and zero wear depth)

The results of the FEA model were assessed for a total of 42 cases: seven wear depths (0, 2, 4, 8, 25, 43, and 54 μm) and six axial loads (1, 2, 3.2, 4, 5, and 6 N). The results of this parametric study are shown in Figure 4-6. The axial penetration of the bearing ball into the conical Delrin bearing cup due to deformation of the cup was

shown in Figure 4-6. The decrease of elastic axial deformation of the bearing cup with increasing wear depth is shown in Figure 4-6. The increase of the wear depth causes the increases of the contact area and consequently a reduction of the axial pressure. Therefore, the axial deformation of the cup reduces as the wear progresses. Similarly, the axial penetration of the bearing ball increases by increasing the axial load.

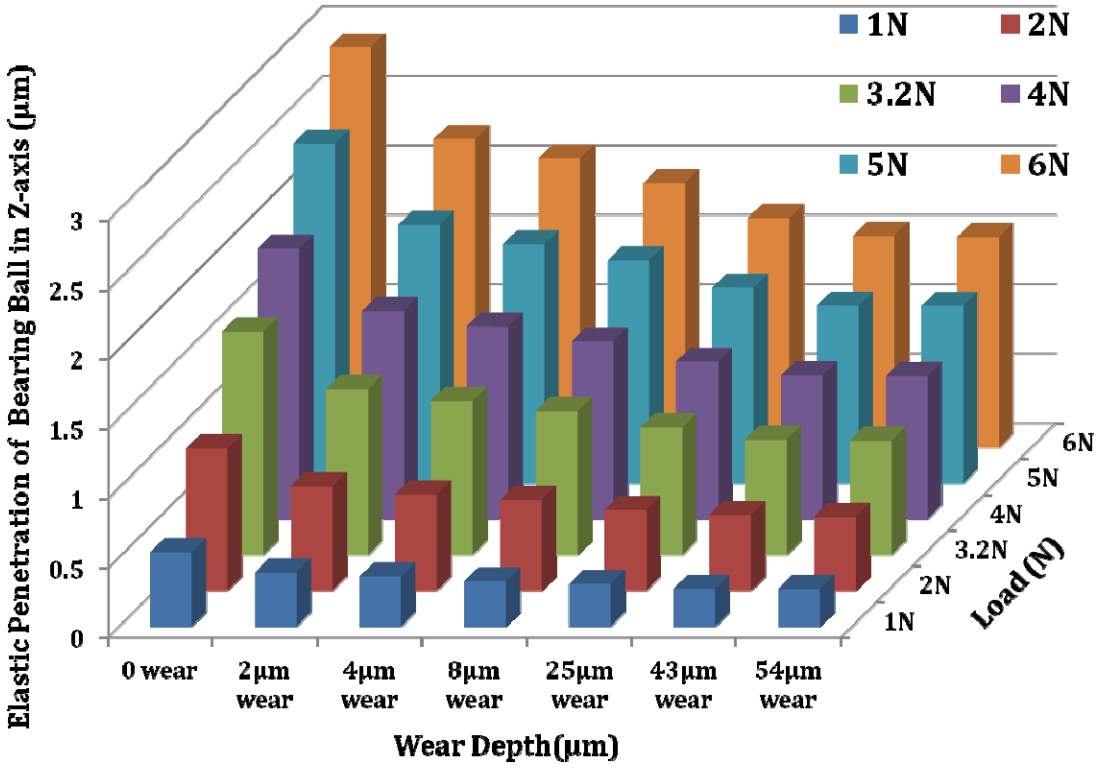

Figure 4-6: Results of parametric study on the FEA model to quantitatively explore the effect of axial load and wear depth of the cup (material removal)

4.2-3. Obtaining the correction factor from the results of FEA parametric study

In this step of the study, we tried to develop an approach to correct and update the results of the wear tests by using the parametric study results.

Since it was not possible to run the parametric study for all the wear depths from the test results, and only limited numbers of parametric results were available, fitting a curve to the obtained results from the parametric study was tried, in order to extract the correction function that can be used to estimate the axial movement of the bearing ball due to deformation for all the measured wear depth from the wear tests. Figure 4-7 shows for calculated axial movement of the ball (the green dots) and the fitted curve.

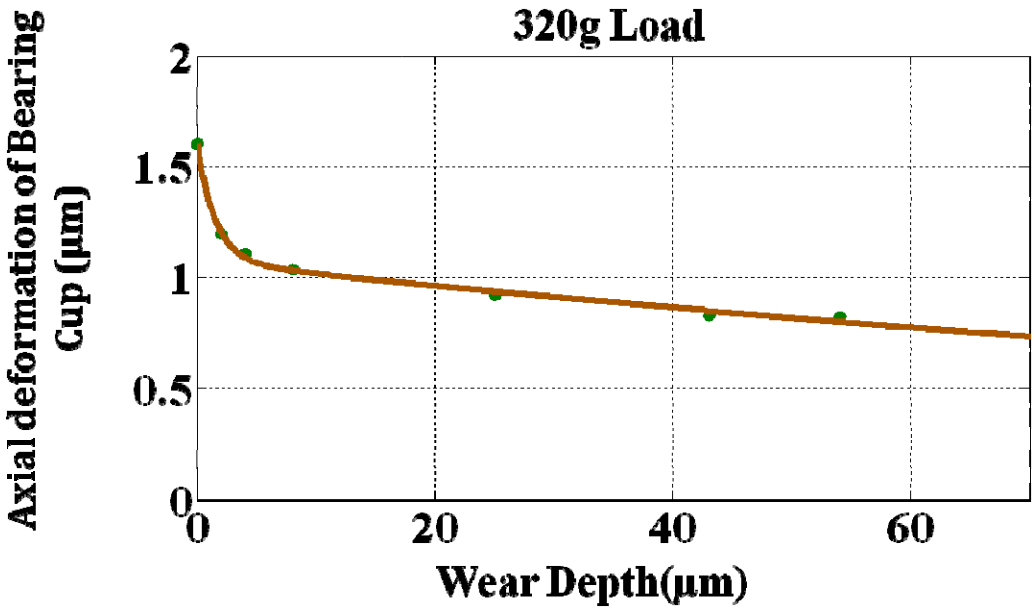

Figure 4-7: Axial penetration of the bearing ball under constant load of 320g and different wear depth of the cups obtained from the FEA model

The following exponential equation (the brown fitted curve) was found to be the best fit (in terms of having least R-square between power law and exponential relations) to the obtained data with R-square of 0.99:

$$L(y) = a \cdot e^{(b \cdot y)} + c \cdot e^{(d \cdot y)} \quad (14)$$

with coefficients being a = 5.32E-4, b = -6.46E-1, c =1.07E-3, and d = -5.44E-3. ***L(y)*** is the axial elastic movement of the ball and y is the actual wear depth of the cup. This fitted equation is used to improve the accuracy of the measured wear depth by eliminating the effect of the deformation of the cup from the measured changes of the heights. Since the motor cup and pivot cup has similar geometry and material, the obtained equation of correction for the motor bearing is used for the pivot bearing, as well. The detail of the approach to predict the actual wear out of the cup by the gained knowledge from the optical measurement, epoxy replicates and FEA analysis will be discussed in detail.

4.3- Estimation of the actual wear depth using the optical measurement, epoxy replicates and FEA analysis

Before discussing the approach to improve the accuracy of the measured wear depth, it would be helpful to review the wear depth measurements one more time. The optical measurements were conducted multiple times during the wear test when the dead weight had been removed (no external load). The height of the bearing cup extended beyond the motor housing was measured while the leaf spring was applying the axial load on the bearing cup. Therefore, penetration of the bearing due to deformation of the conical Delrin bearing cup that has been discussed in the previous section, contributed to the changes of the height of the bearing cup. There are three phenomena contributing to the changes of the height of the cups:

1) the polymer layer, transfer film and eroded debris, between the ball and the cup.

2) wear out of the cups;

3) deformation of the cups; and

The approach to estimate the actual wear depth by accounting for all the above parameters and the available information was developed in three steps:

1) The approach to account for deformation of the conical Delrin bearing cup: In this approach, it is assumed that there is no polymer film between the bearing ball and the conical cup. The following equation can be used to estimate the actual wear depth by assuming the ball is perfectly attached to the cup and there is no gap in between:

$$\Delta \boldsymbol{H_{opt}}(\boldsymbol{n}) = \Delta \boldsymbol{y}(\boldsymbol{n}) + \Delta \boldsymbol{L_{deformation}}(\boldsymbol{y}, \boldsymbol{F}) \ (\mathbf{15})$$

$$\Delta \boldsymbol{L_{deformation}}(\boldsymbol{y}, \boldsymbol{F}) = \boldsymbol{L_{def}}\left(\boldsymbol{y}(\boldsymbol{n}), \boldsymbol{F}(\boldsymbol{n})\right) - \boldsymbol{L_{def}}\left(\boldsymbol{y}(\boldsymbol{n-1}), \boldsymbol{F}(\boldsymbol{n-1})\right) \ (\mathbf{16})$$

where $\boldsymbol{H_{opt}}$ is the measured change of the height of the $\boldsymbol{n^{th}}$ optical measurements ($\Delta\boldsymbol{H}$ is change of the measured height between the $\boldsymbol{n^{th}}$ and $\boldsymbol{n\text{-}1^{th}}$ measurements), $\boldsymbol{y}$ the actual wear depth, and $\boldsymbol{L}$ is the axial movement of the ball due to elastic deformation of the cup. $\boldsymbol{L}$ is a function of the wear depth **(*y*)** and the axial load, as shown in Figure 4-6. The axial penetration **(*L*)** for different wear depths **(*y*)** and loads **(*F*)** has been shown in Figure 4-6. ***(*Δ*L)*** is the changes of the axial penetration between the $\boldsymbol{n^{th}}$ and $\boldsymbol{n\text{-}1^{th}}$ measurements. Moreover, the fitted equation and curve (Figure 4-7) to the computed ***(L)*** from the FEA for the constant load of 320 g was presented in the previous section. This equation was used to estimate the actual wear depth of the bearing cups for each wear depth measurements. Additionally, this approach is simplified, this equation is developed by assuming the constant load of 320 g from the leaf spring, while in reality, the leaf spring force decreases as the wear depth

increases, due to the leaf spring expansion. The effect of the changes of the axial load at the higher wear depth is roughly about 1 μm and it has a very minor affect on the final results (the total axial wear depth range of the stepper motors is from 41 μm to 170 μm). Therefore, to avoid further complexity, the constant axial load of 320 g was assumed for the all measurements. 320 g load is the highest preload/initial leaf spring compressing load that had been observed among a large number of samples. Assuming higher load and consequently more deformation will lead us to obtain more wear depth based on the last two equations. Therefore, this assumption predicts slightly more removed material; consequently, the higher wear factor will be obtained, which is to some extent more conservative.

2) The approach to account for the polymer layer thickness between the bearing ball and the conical Delrin cup. The difference between two wear depth measurement techniques, optical measurements and epoxy replicates, were explained in the previous chapters. As was mentioned, the bearing ball is perfectly attached to the cup at the beginning of the test, and as the wear depth increases the thickness of the transfer film and eroded debris between the ball and the cup increases. The thickness of this layer is only available at the end of the test after destructive analysis of the stepper motors, the difference between epoxy replicates and the final optical wear depth measurements. Since there is no information about the history of this layer, it is assumed that the thickness of this layer increases by a linear correlation with the sliding distance (starts from zero and reaches its maximum at the end of the test). Therefore, the following relationship between the actual wear depth, the optical

measurements and the wear depth based on epoxy replicate can be presented by neglecting the deformation of the conical Delrin cup:

$$\Delta \boldsymbol{y}(\boldsymbol{d}) = \Delta \boldsymbol{H_{opt}}(\boldsymbol{d}) + \frac{\boldsymbol{d}}{\boldsymbol{D}} \cdot \left[\boldsymbol{H_{epx}}(\boldsymbol{D}) - \boldsymbol{H_{opt}}(\boldsymbol{D})\right] \quad (\mathbf{17})$$

where ***y(d)*** is the actual wear depth as a function of sliding distance, ***d*** is the instantaneous sliding distance, ***D*** is the final sliding distance at the end of the test, $\boldsymbol{H_{opt}}$ is the optical wear depth measurements after ***d*** sliding distance and $\boldsymbol{H_{epx}}$ is the wear depth based on the epoxy replicate methods after ***D*** sliding distance at the end of the test. As previously mentioned, it was assumed that the wear depth from the epoxy replicate methods is the actual wear depth since the transfer film and debris cannot interfere with its accuracy.

3) The third step: In this step, the approaches in the previous steps are combined to predict the actual wear depth that is used to quantify the worn out volume.

$$\boldsymbol{y}(\boldsymbol{d},\boldsymbol{f}) = \boldsymbol{H_{opt}}(\boldsymbol{d}) + \frac{\boldsymbol{d}}{\boldsymbol{D}} \cdot \left[\boldsymbol{H_{epx}}(\boldsymbol{D}) - \boldsymbol{H_{opt}}(\boldsymbol{D})\right] - \boldsymbol{L_{def}}(\boldsymbol{y}, \boldsymbol{f}(\boldsymbol{y})) + \boldsymbol{L_{def}}(\mathbf{0}, \boldsymbol{F}) - \boldsymbol{L_{def}}(\boldsymbol{Y}, \boldsymbol{f}(\boldsymbol{Y})) \quad (\mathbf{18})$$

Where d is the instantaneous sliding distance, **D** is the final sliding distance, **F** is the leaf spring load before any wear out, **f(Y)** is the leaf spring load at the end of the test and **Y** is the final wear depth. The other parameters have been already introduced earlier. As seen in Figure 4-6, the axial penetration of the ball at the end of the test (the highest wear depth and the lowest axial load), is very small and can be neglected. Also instead of **f(y)**, the leaf spring load at each wear depth, ***F*** is used for simplification of the equation (it has very minor effect in the final results). Since the level of variation of the final results is high, the stated assumption would not decrease

the accuracy of the measurements. Therefore, by implementing all the above assumptions, the following simplified equation can be introduced:

$$\boldsymbol{y(d,f) = H_{opt}(d) + \frac{d}{D} \cdot \left[H_{epx}(D) - H_{opt}(D)\right] - L_{def}(y,F) + L_{def}(0,F)} \quad \textbf{(19)}$$

These simplifications have small effect on the final results and make it more conservative. The consequences of these simplifications will be discussed in the following sections.

4.4- Removed material from the conical Delrin thrust bearing cup (qualitative study of the wear factors)

The geometric analysis to compute the worn out volume from the conical Delrin thrust bearing using the axial wear depth was discussed in Section 4-1. In Section 4-2, the FEA approach was presented to obtain the axial movement of the bearing ball due to elastic deformation of the conical Delrin cup. The details of the approach to obtain the axial wear depth of the cup using the optical wear depth measurements, epoxy replicate measurements, and FEA analysis were explained in Section 4-3. Thus, the worn out volume of the conical Delrin thrust bearing can be computed by plugging the obtained axial wear into the geometric analysis, which is essential for calibrating the wear model and for characterizing the wear behavior of Delrin in the conical thrust bearing.

The computed worn out volume for the motor bearing cup and pivot bearing cup at 300 g load versus the product of sliding distance ***(L)*** and normal load ***(F)*** is shown in Figures 4-8 and 4-9. Also, it has to be mentioned that Archard's wear model is based on the normal load. Therefore, the X-axis of this figure was calculated based

on the normal load (the axial load divided by the half of the cone angle ***(α)*** to obtain the normal force at the contact zone), Figure 4-2 is shown for better visualization. Based on Archard's wear model, wear factor of the conical Delrin thrust bearing can be obtained by extracting the slope of the curves from Figures 4-8 and 4-9.

$$K = \frac{V}{L \cdot F} \quad (19)$$

Therefore, the slope of the presented curve ***(worn out volume vs. Force X sliding distance)*** represents the wear factor of that particular conical Delrin bearing cup. The discussed assumption in section 4-3 regarding the selected preload (320 g) will lead to obtaining a bigger slope in the wear factor curves (worn out volume versus the sliding distance multiplied by the normal force), Figures 4-8 and 4-9; therefore, the obtained wear factor would be slightly higher, and more conservative.

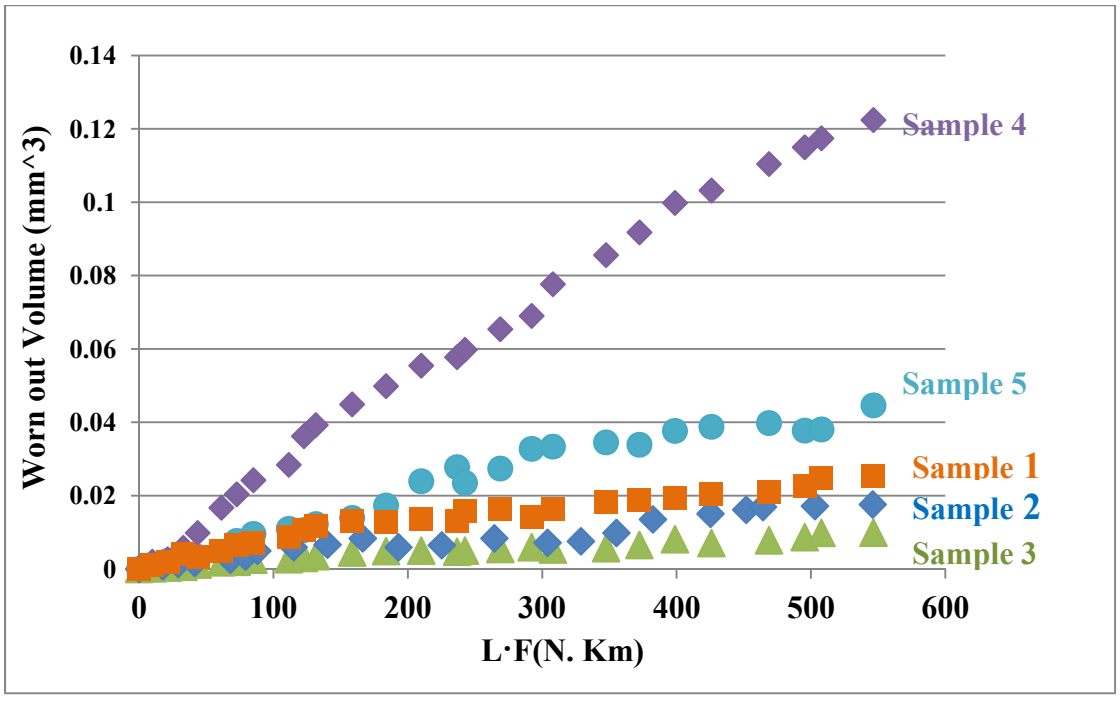

Figure4-8: The worn out volume of the five motor bearing cups under 300g loads VS. Sliding distance times the normal load

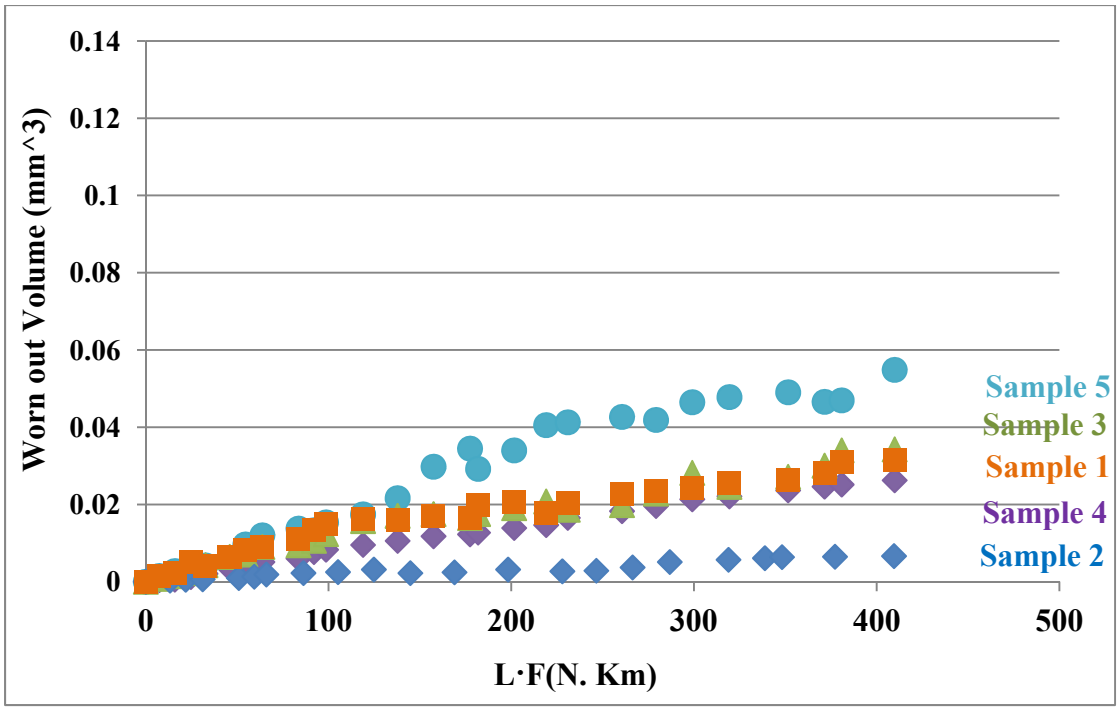

Figure 4-9: The worn out volume of the five pivot bearing cups under 300g loads VS. Sliding distance times the normal load

As expected from the wear depth results, there is a considerable variation between the test results and each motor behaved differently. As is apparent from Figures 4-8 and 4-9, except Sample 4, all of the samples show more than one linear segment in their trend line. It means the wear factor changes as the sliding distance increases; this is a common behavior of polymers against metal counterfaces, Harresi et al. [24] also observed a similar behavior, as was shown earlier in Figure 3-13. The most common explanation for such behavior is formation of the transfer film on the metal counterfaces [18], [19] that has been explained in the literature section. The contact is initially between the metal and the polymer, while gradually by progress of the transfer film on the bearing ball the contact pair becomes more of a polymer to polymer contact rather than a metal to polymer contact and the wear factor changes. The problem becomes even more complicated due to random behavior of the transfer

film on the bearing ball. The formation of the transfer film is a function of many parameters that have not been fully explored yet and shown some randomness. To explore the wear behavior of the bearing in further detail, the presented curves in Figures 4-9 and 4-8 are classified in three different categories:

1) **Constant wear:** The transfer film was not formed on the bearing ball surface; therefore, the wear factor is constant throughout the wear test. An example of such behavior is the motor cup bearing of Sample 4. As can be seen in the Figure 4-10, the worn out volume of the motor bearing cup has a linear correlation with the applied load multiplied by the sliding distance.

$$\boldsymbol{V \propto F \cdot \Delta L} \quad \boldsymbol{(20)}$$

This is fairly rare behavior of the wear factor that has been observed among the eight samples over two wear tests.

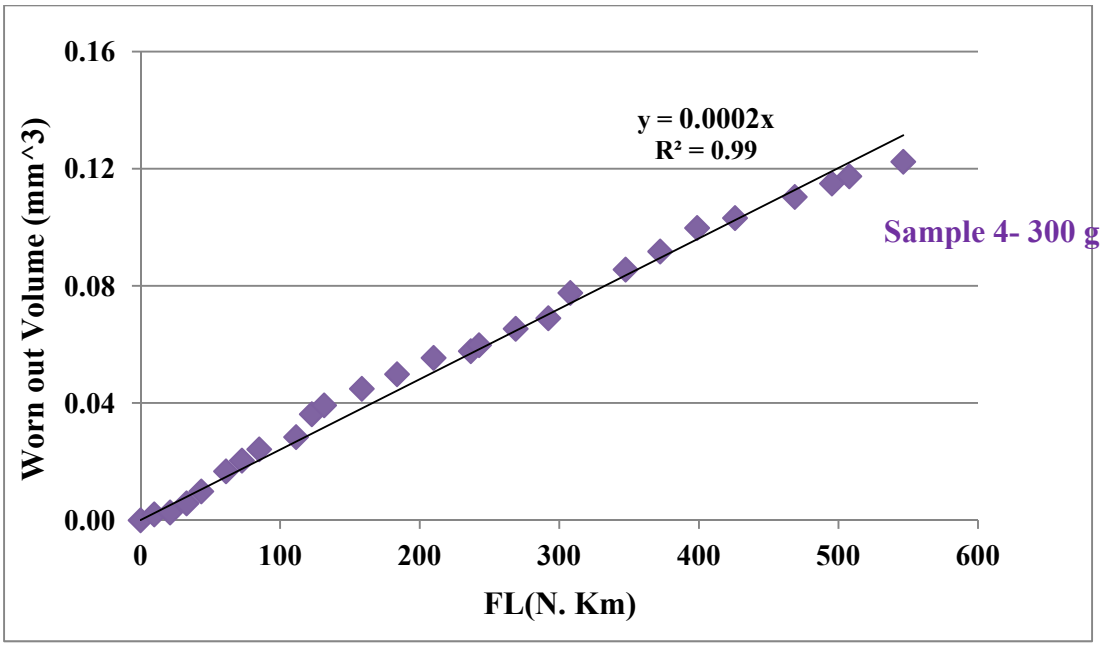

Figure 4-10: Constant wear factor through the wear test (the motor bearing cup)

2) **Two wear regimes:** This is the most common behavior of the bearing wear factor among the eight samples of two wear tests. The pivot cup of samples 1, 3 and 5 are examples of this behavior, as seen in Figure 4-11. The wear factor is initially high (the bigger slope), while the contact was between the Delrin cup and the steel bearing ball. After roughly 50 km of sliding distance for Samples 1 and 3 the transfer film covered the surface of the steel bearing ball and the wear factor decreased to the second smaller slope.

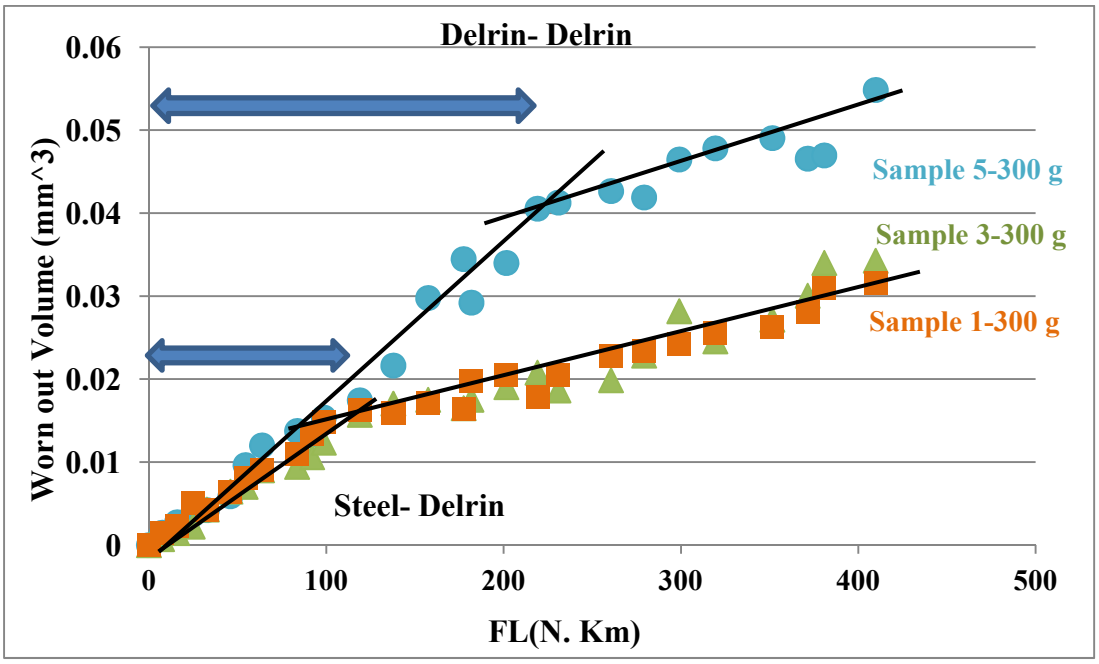

Figure 4-11: Two wear factor for the cup, the contact is initially between polymer and metal and gradually it changes to metal to polymer contact

3) **Multiple wear regimes:** The formation and adhesion of the transfer film on the metal counterface is a function of many factors such as, sliding distance, temperature, contact pressure, sliding velocity geometry of the contact, etc. Most of the studies on transfer film are qualitative and no clear picture of this phenomenon is available yet. Not only, formation of the transfer film is random to

some extent, but it also can be removed from the bearing ball due to environmental condition, such as shear force of friction. The motor bearing cup of Sample 2 is an example of this kind of behavior. As seen in Figure 4-12, Sample 2 had four linear wear regimes. It can also be seen that the first and third trend lines show about the same slope (contact pair: Steel and Delrin), as well as the second and fourth slopes (contact pair: Delrin and Delrin), possibly implying repeated formation and removal of the transfer film. The other possibility is error in the wear depth measurements due to the trapped debris between the ball and the cup.

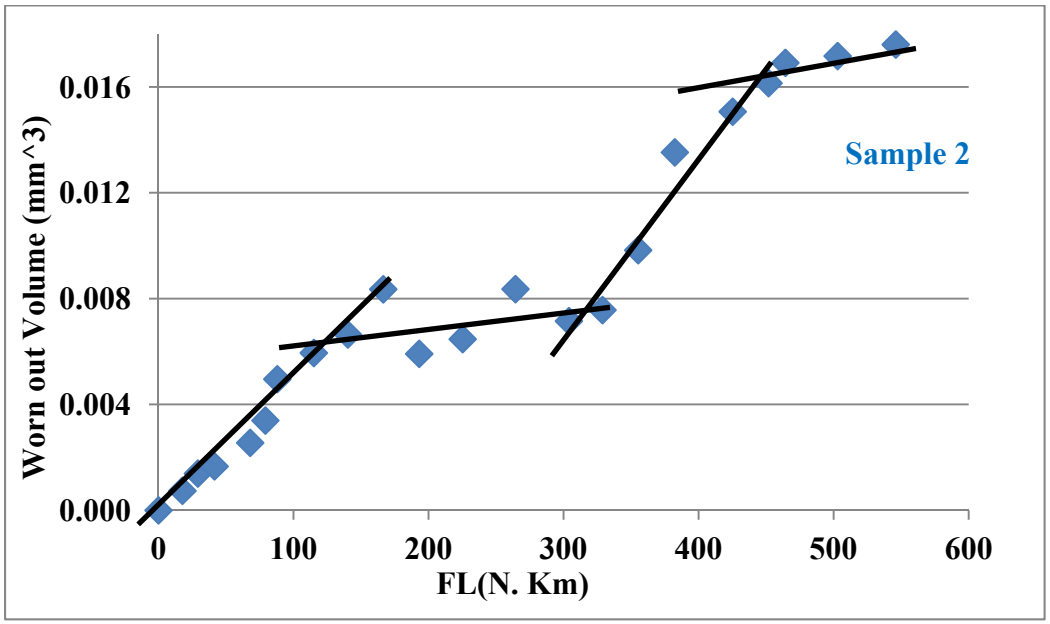

Figure 4-12: Formation and removal of the transfer film during the wear test

The volume removal rate of five stepper motors under 300 g loads (five motor cups, and five pivot cups) was presented in Figures 4-8, and 4-9. The volume removal rate of the other three stepper motors (motor cups and pivot cups) with 400 g, 500 g and 600 g are shown in Figures 4-13, and 4-14.

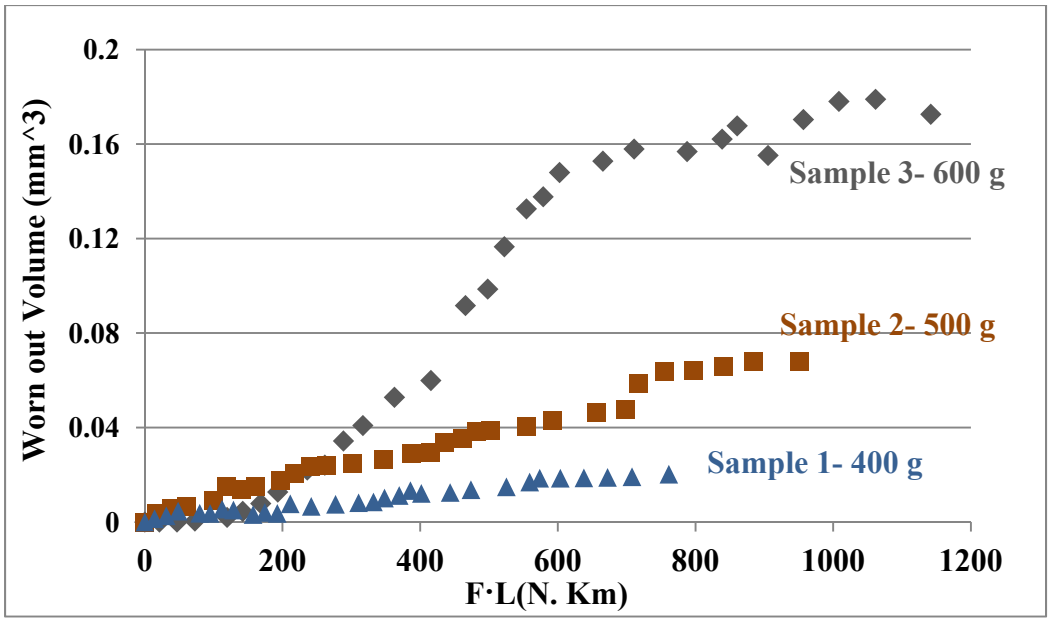

Figure 4-13: The worn out volume of the motor bearing cups under 400, 500, and 600g loads VS. Sliding distance times the normal load

As seen in Figures 4-13 and 4-14, cups with a higher load show a bigger slope, wear factor, than the cups with less load. Considerable variation has been observed in the cups under the same load of 300 g (about an order of magnitude difference in the final worn out volume of the motor cups). Therefore, it is difficult to draw any conclusion about the correlation between the applied load and the wear factor.

The motor under the load of 600 g behaves significantly different from the other motors. It initially had shown lower wear rate, wear factor than other cups and then the wear factor increased drastically to a much higher value than other motors. The wear factor of the bearing cup under 600 g decreased at the end of the test, the same behavior as other cups. It is believed that the wear mechanism of motor at 600 g is different from the other motors and its results are not included in the calculation of confidence bounds. The 600 g load is approximately **100%** higher than the axial load that the stepper motor experiences in the field.

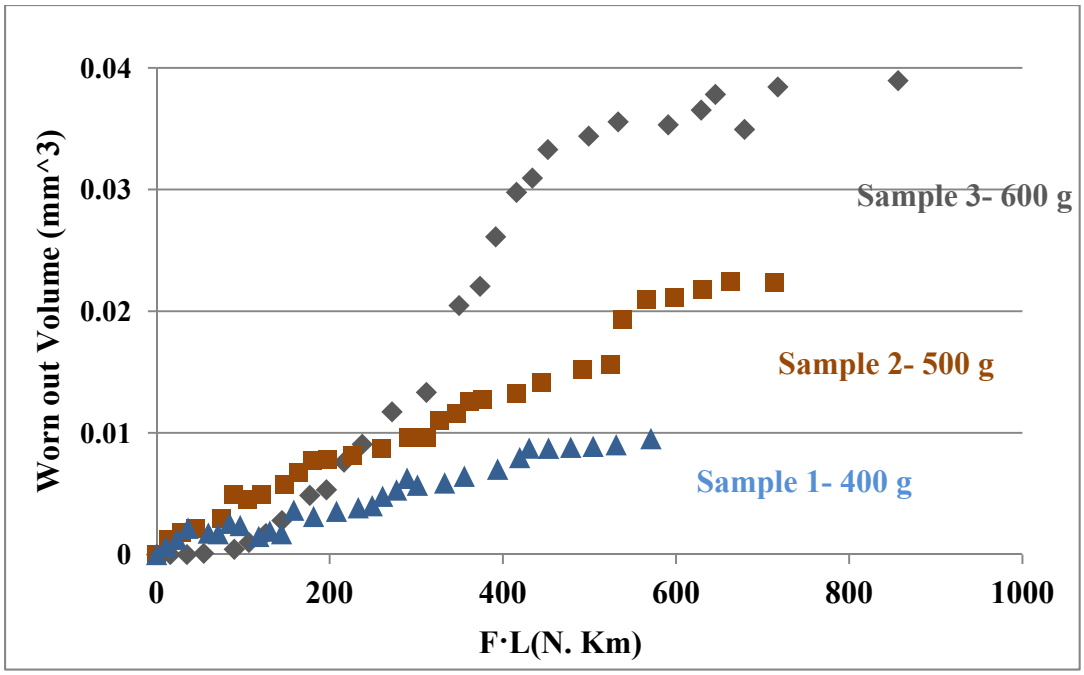

Figure 4-14: The worn out volume of the pivot bearing cups under 400, 500, and 600g loads VS. Sliding distance times the normal load

4.5- Conclusion

The detailed approach to obtaining the axial wear depth, using the two wear depth measurement techniques and FEA analysis to compute the worn out volume from the axial wear depth, have been explained in this chapter.

The wear behavior of the eight samples (eight motor cups and eight pivot cups), five with same load and three with different loads, has been presented and discussed qualitatively in this chapter. The wear factors of the cups will be quantitatively presented in the next chapter, as well as a typical application of this study to predict the life of the bearing based on the obtained wear factor and by assuming the failure criteria.

Three main conclusions that can be drawn from this chapter are:

1. There is fairly high variability in the axial wear depth of the conical Delrin thrust bearings (total axial wear depth of the stepper motors from 41 µm to

131 μm) tested with same loading condition. In the other words, high variability in wear rate of the conical Delrin thrust bearings. The possible reasons for such behavior are: random behavior of trapped debris and random behavior of polymer transfer film on the steel bearing ball.

2. The optical technique is not capable of capturing the actual wear depth, especially at the end of the wear tests. Therefore, the optical measurements have to be calibrated by using the actual wear depth of the conical cups at the end of the wear test (replicate technique).
3. The FEA model exhibited very small amount of axial deformation of conical Delrin cups compared with the wear depth of the cups at the end of the wear tests; therefore, the axial deformation of the conical Delrin cups can be neglected in wear depth calculation. However, it was attempted to bring the effect of increase of wear depth (change of geometry throughout the wear tests) on the axial deformation of the cups into account.

5. The wear factor of the conical Delrin thrust bearing and its application to life prediction

The wear factors of the conical Delrin thrust bearings were qualitatively presented in the last chapter. Two distinct wear factors were found to govern the wear behavior of the bearings (possibly with and without polymer transfer film present on the metal counterface). Also, obtained results showed significant variability (roughly about an order of magnitude difference) in the worn out volume of 10 bearing cups (five motor cups and five pivot cups) with the same axial load of 300 g.

In this chapter, the wear factors will be quantitatively presented and the possible variability in the hardness of conical Delrin cups will be discussed. The wear/life model of the stepper motor will be developed based on the extracted wear factors and transition sliding distance from Phase I and Phase II of the wear tests. The wear/life model will be validated against the experimental results. Furthermore, the 90% confidence intervals for the life of the stepper motor will be presented.

5.1- The wear factors of the conical Delrin thrust bearings

The slope of the worn out volume curves, (Figures 4-8 – 4-14) presented in the last chapter that represents Archard's wear model coefficient, is the wear factor of the conical Delrin thrust bearing cups. As stated in Chapter 3, considerable discrepancy was observed in the acquired wear depth values due to random formation of the transfer film that makes computation of the wear factor more challenging. To obtain the wear factors more accurately, the slope of the linear trend line of each following five data points were calculated. Then, the maximum and minimum values

have been selected to represent the two wear conditions of the conical Delrin thrust bearings: Steel sliding against Delrin and Delrin sliding against Delrin. The maximum wear rates, K_1 (Steel-Delrin, without transfer film) of each bearing cup, are presented in Figure 5-1.

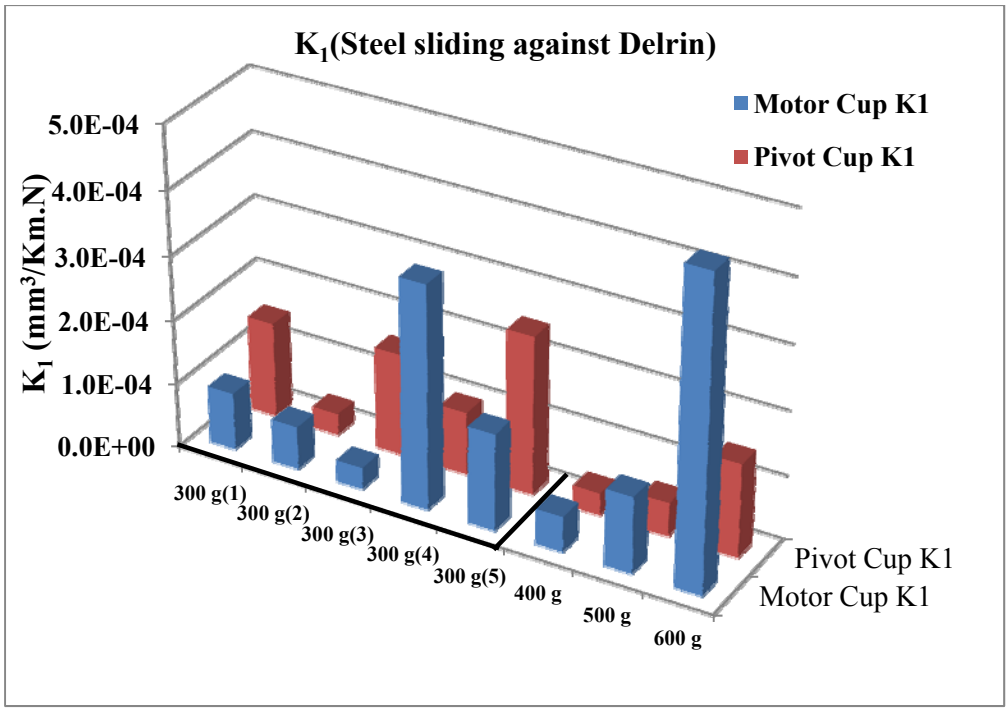

Figure 5-1: The maximum wear rate, K_1 of 10 tested samples (10 motor and pivot bearing cups)

The minimum wear rates, K_2 (Delrin-Delrin, with transfer film) of each bearing cup, are presented in Figure 5-2. The wear rates were calculated for the bearing cups and the stepper motors (the average wear rate for both cups in the stepper motor) using the relation

$$K = \frac{v_{motor\ bearing\ cup} + v_{pivot\ bearing\ cup}}{L_{motor\ bearing} + L_{pivot\ bearing}} \quad (21)$$

The tabular form of the computed wear rates for the motor and pivot cups as well as the total wear rate of the stepper motors is presented in Tables 5-1 and 5-2.

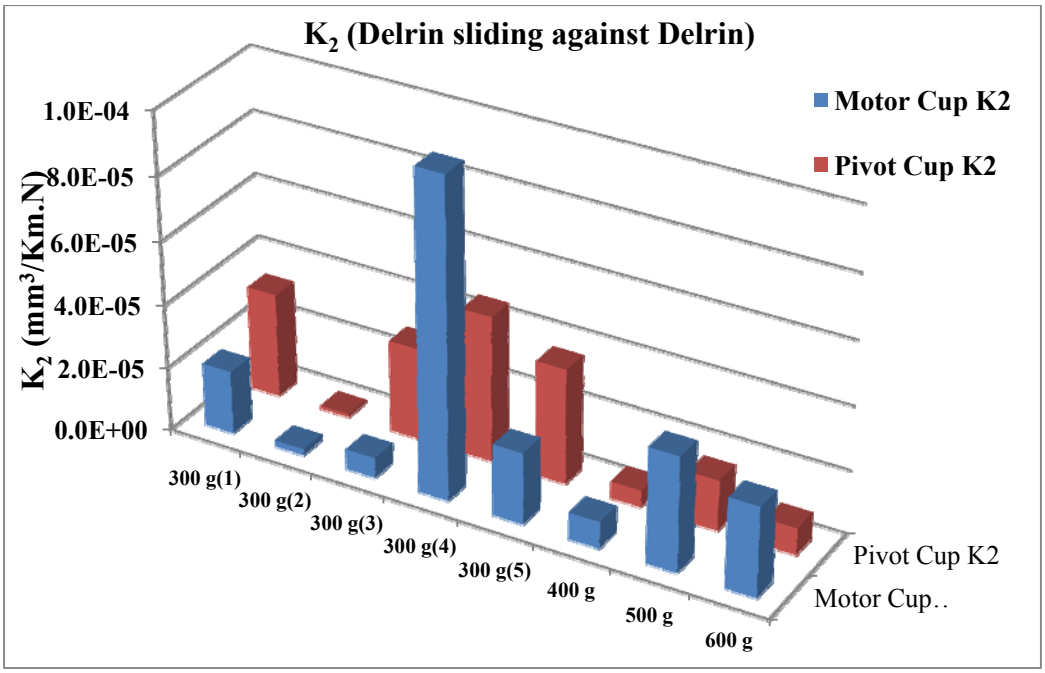

Figure 5-2: The minimum wear rate, K_2 of 10 tested samples (10 motor and pivot bearing cup)

As seen in Tables 5-1 and 5-2, the motor with 600 g load has the highest wear factor. Roughly about an order of magnitude (9.34 times) variation between the maximum wear factors of 18 conical Delrin cups is observed. It should be noted that the maximum wear factor of the motor with 600 g was not included in this variation study. The wear rate of the motor with 600 g axial load is intrinsically different from other motors, the wear rate is initially lower than that of other motors and then it increases to a much higher value as shown in Figure 3-4. Therefore, it is believed that the wear of this motor follows different wear mechanism compared to other motors due to excessive acceleration of loading condition.

xE-5		300 g-1	300 g-2	300 g-3	300 g-4	300 g-5	400 g	500 g	600 g	AVR	STD
Motor Cup	K_1	8.9	6.7	3.4	34.8	15.1	5.5	11.9	48.3	16.8	16.1
Pivot Cup	K_1	14.8	3.4	15.9	9.8	24.8	3.5	5.3	14.6	11.5	7.4
Total	K_1	11.5	5.3	8.8	24.1	19.2	4.6	9.1	33.8	14.5	10.3

Table 5-1: The maximum wear rate, K_1 (mm^3/Km.N)

xE-5		300 g-1	300 g-2	300 g-3	300 g-4	300 g-5	400 g	500 g	600 g	AVR	STD
Motor Cup	K_2	1.99	0.20	0.63	15.8	2.25	0.84	3.62	2.84	3.52	5.11
Pivot Cup	K_2	3.29	0.10	2.90	4.5	3.63	0.53	1.60	0.84	2.18	1.64
Total	K_2	2.54	0.16	1.60	11.0	2.84	0.71	2.75	1.99	2.95	3.40

Table 5-2: The minimum wear rate, K_2 (mm^3/Km.N)

Less than two orders of magnitude (35.5 times) variation between the minimum wear rates of **18** conical Delrin cups is observed. Since the transition of the wear condition did not occur for the ***4th*** Sample with 300 g, the minimum wear factor obtained from this motor was not included in this variation study. By including the minimum wear factor of the ***4th*** Sample, the variation would increase to slightly more than two orders of magnitude (158 times).

Another interesting point about the obtained results is that the conical Delrin bearing cups in the motor housing show about ***53.8%*** higher wear rates (both K_1 and K_2) than the pivot bearing cups on average (10 motor cups and 10 pivot cups). The most reasonable hypothesis for this behavior is the higher temperature inside the motor housing due to energy dissipation of the stepper motor. The earlier experiments showed about ***15 ^oC*** higher temperature of motor housing than the pivot temperature. The motor housing temperature was obtained with a thermocouple at the surface of the motor housing. It is difficult to conclusively assess the effect of temperature on the wear factor of the conical Delrin thrust bearing, due to the high level of variation

in extracted wear factors. The higher temperature can affect the wear behavior in two ways with opposite acceleration effects:

i) Softening the bearing cup material (accelerating the wear process): The bearing cup material, Delrin, becomes softer as a result of the higher temperature and its hardness decreases; therefore, according to the original Archard's wear model:

$$v = F.\frac{k}{H}.L$$

The wear rate, $K\ (\frac{k}{H})$, and the wear factor ***(k)*** increases.

ii) Enhancing the formation of the polymer transfer film (decelerating the wear process): The higher temperature increases the transfer rate of polymer to the metal counterface [28]. The transfer film is formed from a polymer with a lower cohesive energy density on the surface with higher cohesive energy density [18], which higher temperature enhances this phenomenon. The aspects of this phenomenon are not fully explored yet.

In the rest of this chapter, the life model of the steeper motor will be presented to show an application of this study by using the extracted wear factor values.

5.1-1. The hardness of the conical Delrin thrust bearings

According to Archard's wear model, wear rate $K\ (\frac{k}{H})$ has an inverse correlation with the hardness ***(H)*** of the softer surface of sliding pair (polymer's surface in polymer-metal bearings). Thus, to explore the possible reasons for observing: **a)** the high level of variability in the extracted wear rates (approximately

50% coefficient of variation (CV) in K_1 and **39%** CV in K_2), and **b)** transition of wear rate to approximately **47%** of its initial value, the hardness measurement of conical Delrin thrust bearing cups were performed through nanoindentation. Agilent G200 nanoindenter was used to measure the hardness of conical Delrin cups as discussed in Appendix IX. The Delrin cups exhibited the average hardness value of **237 MPa** with **7.3%** CV. Much less variation in hardness of conical Delrin thrust bearing cups was observed compared to the variation in the wear rate of the bearings. The hardness of Delrin cups was measured from the cross section of the cups close to the surface (**3 μm** close to the contact zone) and no significant trend was observed as shown in Appendix IX. There is not adequate evidence available to determine the change in hardness at the contact surface after the wear process.

5.2- The life/wear model of the conical Delrin thrust bearings

In this chapter, the life of the stepper motors will be predicted to demonstrate an application of the present study. The life of the stepper motor will be predicted by assuming a certain axial wear depth of the stepper motor as the failure criterion. All the values used in the life modeling are from the obtained values from the wear tests, excluding the one under load of 600 g, which followed a different wear mechanism due to excessive acceleration.

5.2-1. Failure criterion

One of the limitations of this study was limited access to the field failed motors to obtain the statistical information about the total wear depth of the failed stepper motors. The purpose of this chapter is merely to illustrate a typical application

of this study to predict the life of the stepper motor; therefore, a hypothetical failure criterion, of 125 μm total axial wear depth is assumed. In the other words, it is assumed that after 125 μm of total axial wear depth the stepper motor fails and it cannot home the optical head properly after that much of the axial wear depth. The details of the failure mechanisms and failure mode of the stepper motor have already been discussed in detail in the first chapter.

Since the motor and pivot bearing cups are made of the same material and they experience the same axial load, according to Archard's wear model, the ratio of the removed material from the pivot cup and motor cup is equal to their ratio of the sliding distance. The number of the pivot and motor bearings rotations is the same over the life of the stepper motor; as a result, the ratio between the sliding distances of the motor bearing and pivot bearing is equal to the ratio of the motor and pivot bearing ball radii.

$$\frac{\boldsymbol{V_{pivot\ cup}}}{\boldsymbol{V_{motor\ cup}}} = \frac{\boldsymbol{Pivot\ bearing\ sliding\ distance}}{\boldsymbol{Motor\ bearing\ sliding\ distance}} = \frac{\boldsymbol{R_{pivot\ cup}(0.75mm)}}{\boldsymbol{R_{motor\ cup}(1mm)}} = \boldsymbol{0.75} \quad \boldsymbol{(22)}$$

where $\boldsymbol{V}$ is the worn out volume and $\boldsymbol{R}$ is the bearing ball radius. The total wear depth of bearing cups (125 μm) and the worn out volume ratio constraint are used to calculate the axial wear depth of each motor and pivot bearing cups. The axial wear depth of the motor bearing cup is 59.10 μm and its worn out volume is 0.066 mm^3 and similarly, the axial wear depth of the pivot bearing cup is 65.89 μm and its worn out volume is 0.0495 mm^3. The worn out volume ratio and the total wear depth are inputs to the MATLAB code (Appendix IV) that calculates the axial wear depth of the motor and pivot bearing cup.

5.2-2. Field loading condition

The field loading condition has been comprehensively explained in Chapter 2. It is assumed that the failure of the bearing is only due to the axial wear factor; thus, the lateral force generated by the optical head is neglected in this life prediction. The axial loads on the bearings are shown in Figure 5-3.

5.2-2.1. The axial load on the motor bearing

The applied load on the motor bearing cup, $F_{leaf\ spring}$ is always equal to the generated force by the leaf spring, which decreases as the leaf spring expands due to changes of the bearing cups' geometries. The axial load of the leaf spring has a linear correlation with the total axial wear depth of the stepper motor ($\mathbf{y_{total}}$), which is a combination of the axial wear depth of the motor ($\mathbf{y_{motor\ cup}}$) and the pivot bearing cups ($\mathbf{y_{pivot\ cup}}$).

$$\mathbf{y_{total} = y_{motor\ cup} + y_{pivot\ cup}} \quad (23)$$

$$\mathbf{F_{leafspring} = Preload - K_{leaf\ spring} \cdot y_{total}} \quad (24)$$

where Preload is the initial compressing load of the leaf spring before any wear out and $K_{leaf\ spring}$ is the stiffness of the leaf spring. Therefore, the leaf spring's axial load (the load on the motor cup) is a function of the total wear depth and Preload. The total axial wear depth ($\mathbf{y_{total}}$) has been already discussed in detail in the previous chapters.

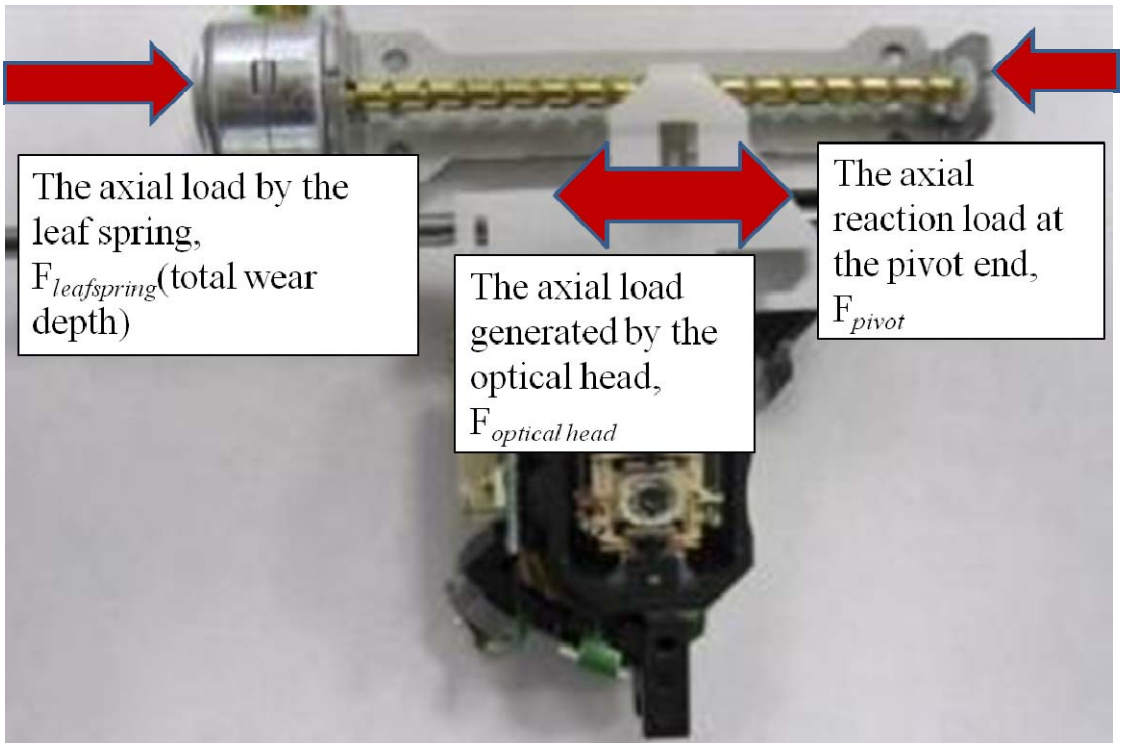

Figure 5-3: The axial loads on the stepper motor's bearings

5.2-2.2. The axial load on the pivot bearing

The applied load on the pivot bearing cup, the reaction force at the pivot end can be calculated from the following relation:

$$\mathbf{F_{pivot}} = \mathbf{F_{leafspring}} + \mathbf{F_{Optical\ head}} \quad (25)$$

$$\mathbf{F_{Optical\ head}} \approx \pm 85\mathbf{g} \quad (26)$$

where F_{pivot} is the reaction force on the pivot cup, $F_{leaf\ spring}$ is the load generated by the leaf spring and $F_{optical\ head}$ is the axial load generated by the leaf spring. $F_{optical\ head}$ was quantified by measuring the additional required torque to move the optical head. The magnitude of the load caused by the optical head is assumed to be constant; however, the direction of the load depends on the direction of the optical head displacement. The optical head can only move along the worm shaft. Therefore, the

optical head moves toward the motor bearing (F_{pivot}= $F_{leafspring}$+85g) half of the stepper motor life and it moves toward the pivot bearing (F_{pivot}= $F_{leafspring}$-85g) in the rest of its life. The direction of the optical head displacement is distributed equally throughout the life of the stepper motor. Since the worn out volume predicted by Archard's wear model has a linear correlation with the applied load, the average force of F_{pivot} can be used in this life model. The average force of F_{pivot} can be calculated from:

$$\boldsymbol{F_{pivot} = \frac{(F_{leafspring} - 85g) + (F_{leafspring} + 85g)}{2} = F_{leafspring}} \quad (27)$$

5.3- Life/wear model of the stepper motor

The failure mechanism of the stepper motor is the wear of the conical Delrin thrust bearing cups. Wear of the conical Delrin bearing cups is governed by different parameters such as: the normal force at the contact zone, wear factor, etc. In order to develop the wear model of the stepper motor, all of the parameters have to be determined as a function of other known parameters. The model is developed in MATLAB (Appendix V), the model is numerically solved in incremental steps. The necessary steps to obtain the required parameters to predict the life of the stepper motor are:

1. **The wear factor**: The most challenging step to predict the removed material from the bearing cup is to obtain the wear factor of the bearing cup. As discussed, the wear factor of a self lubricated polymer is a function of: the sliding speed, the sliding distance, the contact pressure, the counterface material and roughness, the

contact zone geometry and temperature. Eight stepper motors or 16 cups (16 conical Delrin thrust bearing, one of the most common applications of polymers in bearings) were tested to extract the wear factor of Delrin in the conical thrust bearing application. The test condition was selected as close as possible to the field condition. The maximum obtained wear factors for both wear conditions: Steel-Delrin and Delrin-Delrin are used to predict the volume of removed material of the bearing cups during the life of the motor. The wear factors for each motor were extracted based on Archard's wear model. The transition distance for each sample obtained from the test results (the break point that the slop of the wear behavior changes). The average of obtained values for the wear behavior of the 7 samples (stepper motor): K1 (the total wear factor for Steel-Delrin condition), K2 (the total wear factor for Delrin-Delrin condition) and the transition distance (The point that the slope of the worn out volume vs. sliding distance changes) are used as inputs of the wear/life model of the stepper motor.

2. **The normal force**: The normal force is obtained based on the leaf spring load and bearing cup geometry. The detail and the equation to obtain the leaf spring load were discussed earlier. The axial load generated by the leaf spring is obtained by using the results of the previous steps (the total axial wear depth of the motor and pivot bearing cup). The leaf spring load is an input to the model.
3. **The volume of removed material**: Archard's wear model was employed to predict the worn out volume by applying the wear factor, the normal force and the sliding distance of the each step. The worn out volume is calculated based on other inputs of the model.

4. **The wear depth of each bearing cup**: One of the involved steps in developing the wear/life model of the stepper motor was obtaining the wear depth of each bearing cup based on the removed volume, while calculating the volume of the removed material based on the wear depth is much more straightforward.
5. **MATLAB code**: The model for life prediction was implemented in MATLAB. The model is executed until the total wear depth reaches the failure criterion. The model accounted for the change in wear factor after certain sliding distance (accounts for changes of wear condition). As mentioned, the problem was solved by applying a numerical approach; the removed material of each step was calculated based on the constant load of the previous step and the sliding distance of the step. The sliding distance of the steps is an input of the model. Since the numerical approach is used and the sliding distance of steps has to be selected and inserted as an input, it is necessary to study if the solution is convergence and the accumulation of errors does not kill the accuracy of the solution. Therefore, the convergence study of the results was conducted by changing the step size (sliding distance of each step) to find a right step size.

5.3-1. Verification of the life model

The purpose of this section is to verify the wear/life model. In order to do so, model wear properties (K_1, K_2, and transition distance) were extracted based on six samples (The sample with 600 g load was excluded and so was stepper motor 3). The test condition (constant load of 300 g is used for the model) was simulated in the model. To simulate Sample 3 the wear rate was extracted for each wear region/condition. The average wear rates of each wear condition, Steel-Delrin ***(K_1)***

and Delrin-Delrin ***(K_2)*** were extracted from the experimental results and applied to the model. The extracted values from the tested samples that are used in the life/wear model are presented in Tables 5-3. The confidence intervals are calculated based on the t-distribution. Similarly, the transition sliding distance (67 Km) was obtained by averaging the transition sliding distances (Table 5-3) from Phase I and Phase II of the wear tests. The experimental data and the predicted wear depths based on the model were compared in Figure 5-4.

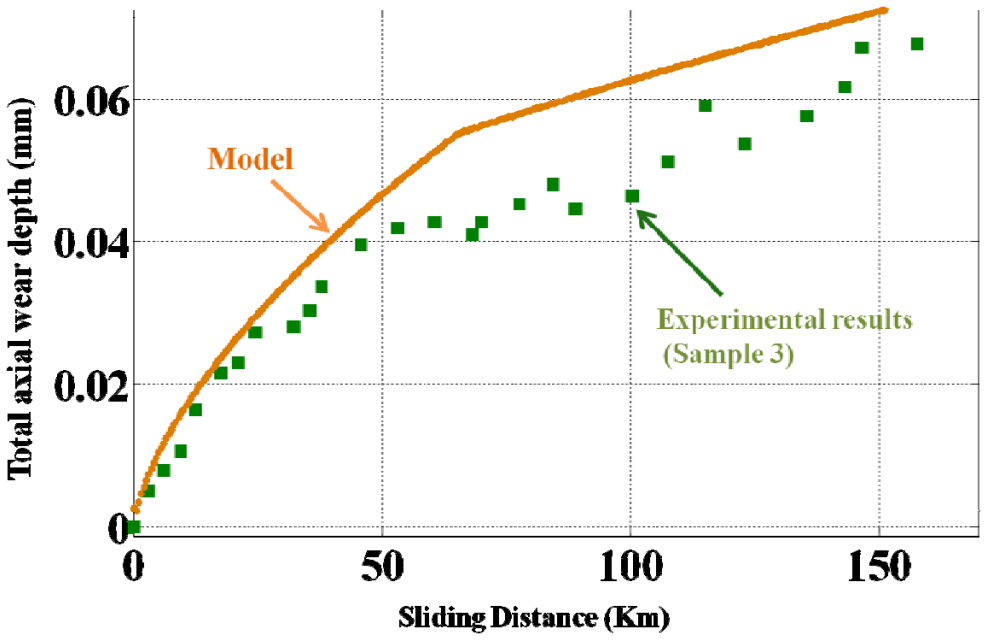

Figure 5-4: The experimental results compared with the total axial wear depth obtained from the model, for Sample 3

5.3-2. Confidence bounds on the life model of the stepper motor

In this section the life of the stepper motor is estimated by using the extracted values from all seven samples tested in the Phase I and II of the wear tests (Sample 6 with 600 g is omitted).

Extracted values from Phase I and II of the wear tests		K1 (mm^3/Km.N)	K2 (mm3/Km.N)	Transition sliding distance (Km)
Sample 1	300 g	**1.06E-04**	**3.85E-05**	**42**
Sample 2	300 g	**4.00E-05**	**2.74E-05**	**48**
Sample 3	300 g	**6.80E-05**	**3.58E-05**	**46**
Sample 4	300 g	**1.61E-04**	**--**	**160**
Sample 5	300 g	**1.40E-04**	**6.39E-05**	**68**
	400 g	**7.78E-05**	**2.27E-05**	**10**
	500 g	**6.61E-05**	**5.49E-05**	**44**
	600 g	**1.78E-04**	**3.84E-05**	**86**
Ave		**9.41E-05**	**4.05E-05**	**63**
STD		**4.72E-05**	**1.59E-05**	**47**
80% (without 600 g)	Upper	**1.23E-04**	**5.01E-05**	**86**
	Lower	**7.04E-05**	**3.09E-05**	**34**
90% (without 600 g)	Upper	**1.26E-04**	**5.37E-05**	**94**
	Lower	**5.39E-05**	**2.74E-05**	**25**
95% (without 600 g)	Upper	**1.34E-04**	**5.73E-05**	**104**
	Lower	**6.22E-05**	**2.38E-05**	**16**

Table 5-3: Extracted values from the wear test that has been use in the wear model

The life of the stepper motor based on 300 g preload and the wear behavior from test results including the 90% confidence intervals are shown in Figure 5-5.

5.4- Study of the effect of Preload on the wear behavior of the stepper motor based on the life/wear model

The wear/life model is also used to study the effect of initial preload by applying the mean values for K_1, K_2 and transition sliding distance to address one of the most common issues in the manufacturing process, the variability in the preload due to assembly tolerances. The life of the stepper motor for 250 g, 300 g and 350 g preload is depicted in Figure 5-6. The variation in preload of the stepper motors is approximately 7% CV.

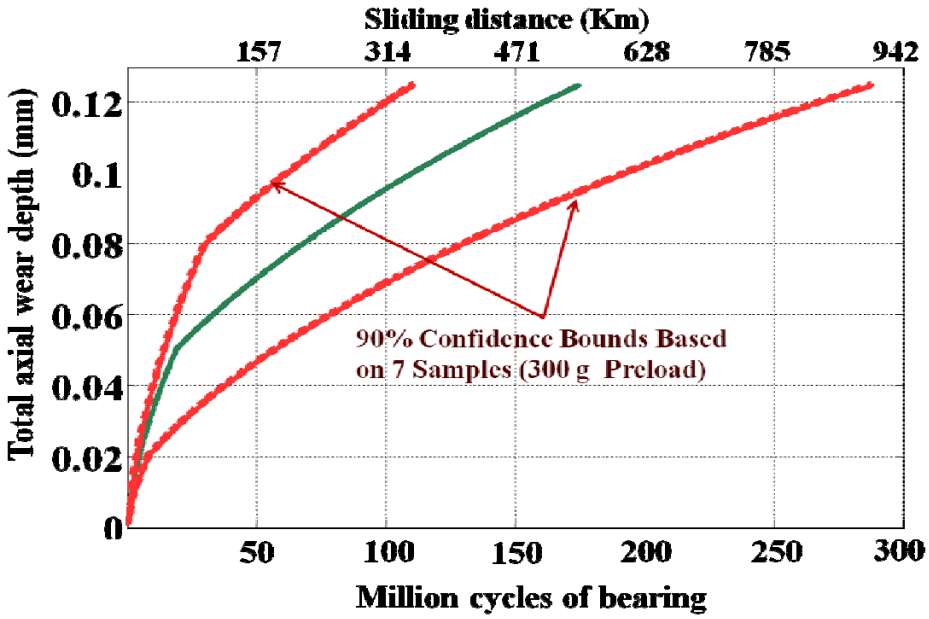

Figure 5-5: The sliding distance and number cycles of stepper motor for the moderate case (125 µm total axial wear depth as the failure criterion and 300 g preload)

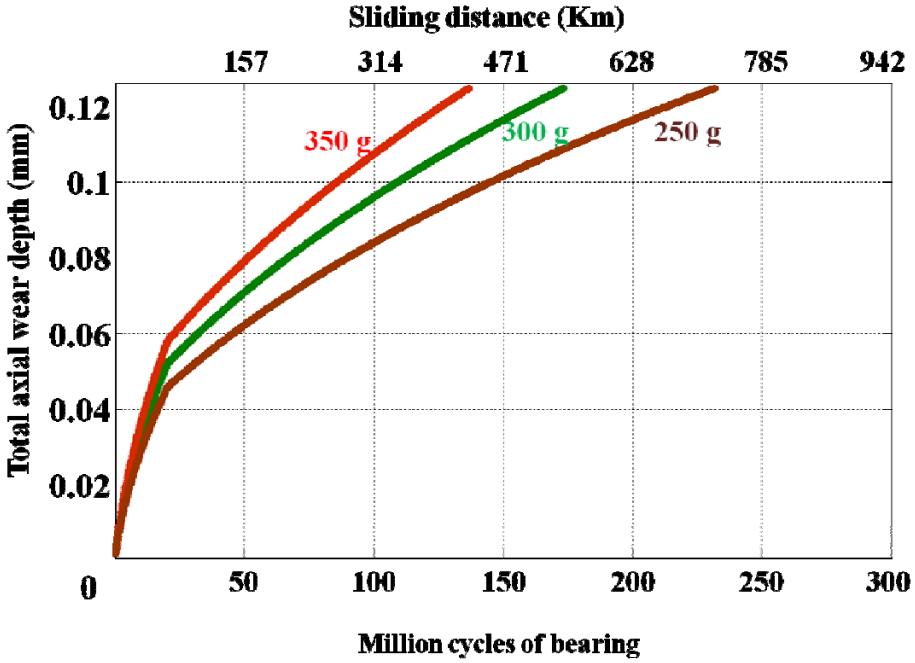

Figure 5-6: Study of the effect of Preload on the life of the stepper motor

5.5- Conclusion

The obtained wear factors of the tested bearing cups are quantitatively presented in this chapter. Considerable variation was observed in the wear rates (approximately **50%** CV in K_1 and **39%** CV in K_2). This observation motivated us to

explore the variability of conical Delrin cups' hardness. The hardness of conical Delrin thrust bearings was determined by nanoindentation and the average hardness of **237 MPa** with **7.3%** CV was observed. It may be noted that the variability in hardness is only about 15% of the observed variability in the measured wear rates, $\boldsymbol{K_1}$. Also, the hardness of new and worn-out cups was measured approximately **3 μm** away from the contact zone and no significant difference was observed. Adequate information about evolution of hardness at the polymer contact surface was not possible to gather to conclude on the contribution of hardness in the drop and variability of the wear rates.

The wear rate of Delrin has been already measured in many studies and a wide range of values have been reported. Pin-on-disk is a popular approach to extract and to compare the wear rate of polymers [Table 5.4]. The reported wear rates available in literature and the average value extracted from the present study are listed in Table 5-4 and graphically presented in Figure 5-7. The wide range of values of wear rates can be attributed to the difference in: roughness of metal counterface, sliding velocity, contact pressure and additives etc.

Wear rate of Delrin							
Material	**Counterface surface roughness, Ra (μm)**	**Load (N)**	**Velocity (m/s)**	**Geometry**	**Source**	**k_1/H_1 (mm^3/km.N)**	**k_2/H_2 (mm^3/km.N)**
Delrin-(POM)	Approximately 0.2	3	0.047	Conical thrust bearnig	Conical thrust bearing (this study)	9.41E-05	4.05E-05
Delrin-170	-	0.87	0.25	Ring against stationary steel washer	ASTMD 3702 [26]	2.82E-06	-
POM-Delrin	-	95	1.57	Steel shaft inside Delrin washer	Journal Bearing [13]	5.24E-02	1.02E-02
POM	-	30	0.88	Pin-on-Disk	Pin-on-Disk [16]	4.46E-02	-
POM	-	30	1.76	Pin-on-Disk	Pin-on-Disk [16]	2.88E-01	-
POM-C	0.1 ± 0.02 (stainless steel)	150	0.05	Pin-on-Disk	Pin-on-Disk [29]	8.90E-03	-
POM-C	0.1 ± 0.02 (stainless steel)	150	0.1	Pin-on-Disk	Pin-on-Disk [29]	1.12E-02	-
Ertacetal-C	0.7-0.9	-	0.33	-	Pin-on-Disk [30]	1.50E-02	-
Ertacetal H-TF	0.7-0.9	-	0.33	-		2.60E-03	-

Table 5-4: Reported wear rates for Delrin with different wear conditions

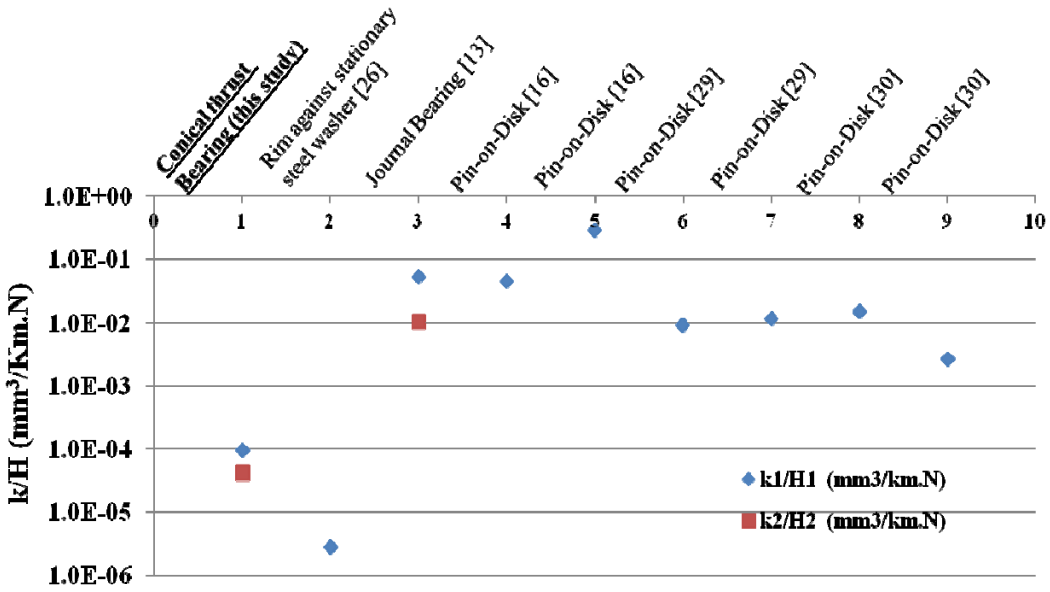

Figure 5-7: Reported wear rate for Delrin in the literature

The approach to develop the life/wear model of the stepper motor was presented. The life/wear model of the stepper motor was verified against the wear depth history of Sample 3 from the wear test. The life model was used to study the

variability of stepper motor life due to: ***a)*** variability in wear behavior of conical Delrin thrust bearings; and, ***b)*** variability in preload due to manufacturing process. The model exhibited that the variability in wear behavior of the Delrin cups has more significant effect on life of the stepper motors compared with preload variability due to manufacturing process.

This life prediction model can be updated for any changes of the stepper motor such as: geometry of the bearing cups, bearing cup material, leaf spring load, etc. There are not enough statistical data available to accurately predict the life of the stepper motors in the field; therefore, the model should be improved by conducting more wear tests for obtaining more realistic wear factors and failure analysis of more failed motors from the field to determine more accurate failure criterion. The life prediction model can be further used for designing more reliable conical polymer thrust bearings.

6. Summary and Conclusion

This study was intended to explore the wear behavior of one of the most common thermoplastics in sliding applications, Delrin (POM) in conical thrust bearing applications, at force range of **300 g** to **600 g**, up to sliding distance of 170 Km (47 mm/s sliding velocity) and at 25˚C ambient temperature.

This study was intended to understand the wear behavior of conical Delrin thrust bearing, one of the most common failure mechanisms of stepper motors. Nine Delrin wear rate values that have been found from the literature are mostly from pin-on-disk and journal bearing geometries. Except the reported value from ASTM standard for Delrin-170, **2.8E-6 mm^3/Km.N**, the other **seven** reported values are in the range of **2.88E-1** to **2.60E-3 mm^3/Km.N**. The average wear rate values of **9.41E-4 mm^3/Km.N** and **4.05E-4 mm^3/Km.N (**before and after the transition of wear behavior) were observed in this study. The extracted values from this study are approximately two orders of magnitude smaller than most of the reported values (7 out of 8) from simpler geometries (mostly pin-on-disk geometry) which might be due to the conical geometry of the bearing in this study. Since most of these studies did not report all the important parameters in the wear behavior, (such as: counterface roughness, additives, contact pressure, hardness of Delrin at the contact surface, etc.) and the sliding conditions (sliding velocity, contact pressure, etc.) were different, it is difficult to make a strong conclusion about the effect of geometry on the wear rate.

High level of variability was observed in wear rate of the conical Delrin thrust bearings, **50%** CV in the wear rates before the transition of wear behavior and **39%** CV in the wear rates after the transition. The possible reasons for such behavior are: **a)**

random formation of polymer transfer film on the steel bearing balls; and, **b)** random behavior of debris in the conical Delrin thrust bearings.

Most of the conical Delrin bearings exhibited two wear slopes, before and after transition of wear behavior. The wear rate of the conical Delrin thrust bearings reduce to around **43%** of their initial value after the transition of the wear behavior. The possible reasons for this behavior are: formation of the transfer film on metal counterface and presence of debris between the contact pair. This is a typical behavior of self-lubricating polymers sliding against metal counterfaces.

The molded conical Delrin cups exhibited the average hardness value of **237 MPa** with **7.3%** CV. No significant change of hardness was observed in new and worn-out cups close to the contact surface (**3 µm** apart from the contact zone) from the cross section of six molded cups. It was not feasible for us to measure the hardness of conical Delrin cup right at the **actual** contact surface.

The life/wear model of the stepper motor was developed as a case study to demonstrate an application of the present study. Furthermore, the effect of variability in the wear rate of conical Delrin thrust bearing (observed based on seven tested samples in this study) and variability in the preload (from measured preloads) on the wear behavior and wear life of the stepper motor were studied. It was observed that the wear life of the stepper is significantly more sensitive to the wear rate variability of the conical Delrin cups rather than preload variability caused by manufacture tolerances.

Detailed FEA was used to account for deformation of the Delrin bearing cups to calculate the wear factors accurately by obtaining the exact worn out volume.

Negligible deformation of Delrin cups (less than **3 μm** axial deformation of the cup at the most extreme case, loading and unloading 600 g load when there is no wear) was obtained from the FEA model. The smallest axial wear depth of the tested cups was about **25 μm** and the highest axial wear depth was about **110 μm** for the bearing with 600 g load. Therefore, the effect of deformation of the conical Delrin cups can be neglected.

The existence of the transfer films on the surface of the bearing balls was confirmed and qualitatively studied using SEM and an optical microscope.

7. Thesis contributions

This study was intended to explore the wear behavior of self-lubricating polymers in conical thrust bearing geometry which has not been comprehensively studied earlier. This study also contributed to developing a systematic approach and experimentation to evaluate the wear behavior of polymers in conical thrust bearings, one of the most common applications of the self-lubricating polymers. The wear behavior of Delrin was studied and extracted in conical thrust bearing application at sliding velocity and load condition close to usage environment of stepper motors in the optical disk drives.

The contributions of each chapter are provided in the list below:

- A detailed experimentation approach to study the wear behavior of conical Delrin thrust bearings:
  - Guidelines for building the test set up to monitor the required parameters to develop the wear model and study the degradation of the stepper motor to the bearing cup wear out (Appendix VI).
- Wear test results
  - Study of the wear rate history of the conical Delrin thrust bearing.
  - Study of the variation of the conical Delrin thrust bearing cup wear resistivity (at 300 g load)
  - Study of the effect of load on wear behavior of the conical Delrin thrust bearing
  - Insight into formation of the transfer film on the surface of the steel bearing balls

- Approach to extract the wear factors of Delrin in conical thrust bearing application
  - Approach to refine the wear depth measurement methods by accounting for the change of the conical Delrin cups deformation due to change of conical Delrin cup geometry (change of axial wear depth) by using the FEA model.
  - Approach to extract the wear factors of conical Delrin thrust bearings using the wear depth, applied load and the sliding distance
  - Estimate of the wear factor of conical Delrin thrust bearings for two conditions: when there is no transfer film on the surface of the bearing ball and after formation of the transfer film on the bearing ball surface
  - Estimate of the sliding distance before transition of the wear condition in conical Delrin thrust bearings
- Wear factors of Delrin in conical thrust bearing and wear/life model to predict the life of the stepper motor
  - Statistical comparisons of eight conical Delrin thrust bearings
  - Illustration of the life/wear model of stepper motor based on the extracted results from the wear tests

8. Limitation and future works

Limitation of the present study and future works are discussed in this chapter.

8.1- Limitations

The limitations of this study are:

- No pin-on-disk test result of Delrin with the exact wear condition of the conical Delrin thrust bearing used in this study (i.e. counterface roughness, sliding velocity, temperature etc.) is available to explore the effect of geometry in wear behavior of self-lubricating polymers.
- The formation of the transfer film has some random behavior and it was not possible to monitor the formation of the transfer film on the steel bearing balls during the wear test.
- It was not possible to measure the hardness of Delrin right at the contact area of new and worn out Delrin cups to directly study the change of polymer hardness at the contact surface because of the wear process.
- There was not enough resource available to quantitatively measure the thickness and area of the transfer film on the surfaces of the bearing balls after destructing failure analysis of the bearing.
- Significant piece to piece variation due to manufacturing process elevated the level of variation of the final results.
- The wear tests were conducted at a typical use condition: a constant velocity, specific loading condition and room temperature, the wear factor of the conical Delrin cup changes if the wear condition changes.

- The failure mechanism and failure mode were comprehensively explored, but the performance threshold at which the stepper motor fails to home the optical head is not yet clear. There was a limited access to the field failed motors, which prevents us from obtaining the exact amount of axial wear depth as the failure criterion.

8.2- Future work

Further research to be conducted to enlighten this area of tribology are:

- The formation of the transfer film through the sliding process can be more explored. A simpler test can be designed to explore on formation of the transfer film more fundamentally for instance, monitoring the thickness of the transfer film and the portion of the sliding contact covered by the transfer film during the sliding process and its effects on the wear factor and friction coefficient of the polymer counter face.
- Simpler test set can be used to study evolution of hardness in polymer contact surface during the wear process and its contribution to the transition of the wear behavior.
- The broader picture of wear behavior of Delrin can be obtained by conducting the wear tests at other environmental conditions such as: running test at elevated temperature, running test at different sliding velocity, and changing the load level.
- The accuracy of the life model presented in this study can be further improved by obtaining more experimental data for wear factors and transition sliding

distance. The failure criterion can be improved by conducting more failure analysis on the field failed motors.

Acknowledgement

The work reported here was sponsored by the members of the Electronic Products and Systems Consortium at the Center for Advanced Life Cycle Engineering (CALCE) at the University of Maryland, College Park.

Appendix I: Analytical wear models [8].

Table 1 Analytical expressions for prediction of wear

Year	Author	Type of wear	Equation of wear
1937	W. Tonn (Germany)	Abrasive	$\epsilon = kH + B$
1940	R. Holm (Germany)	Atomic	$W = kP/H$
1941	M. M. Kruschov, M. A. Babichev (U.S.S.R.)	Microcutting	$\epsilon = kH$
1952	I. T. Burwell, C. D. Strang (U.S.A.)	Adhesive	$W = kP/H$
1953	J. F. Archard (England)		$W = kP/H$
1952	T. L. Oberle (U.S.A.)	—	$W \simeq E/H \cdot 10^6$
1958	I. V. Kragelsky (U.S.S.R.)	Fatigue	$T = \sqrt{\frac{h}{R}} \cdot \frac{P_a}{P_r} \cdot \frac{0.18\,\alpha^*}{n}$ elastic contact: $n = \left(\frac{\sigma_0}{KfP_r}\right)^t;\ P_r = \frac{E^{4/5}\Delta^{2/5}P_c^{\,1/5}}{2}$ plastic contact: $n = \left(\frac{\epsilon_p}{\epsilon_x}\right)^t;\ P_r = H$
		Microcutting	microcutting: $n = 1;\ P_r = H$
1958	G. Yoshimoto, T. Tsukizoe (Japan)	Oxide film	$W = \frac{1}{6}\tan\theta\,(P/H)$
1960	A. Schallamach, D. M. Turner (England)	Abrasive	$W = \frac{1}{2}\gamma S^2 k_1 a^2$
1962	R. G. Bayer, W. C. Clinton, C. W. Nelson R. A. Schumacher (U.S.A.)	Fatigue	$\frac{n_f}{2000} = \left(\frac{\gamma_R T_y}{T_{max}}\right)^9$
1965	E. Rabinowicz (U.S.A.)	Abrasive	$W = P\tan\theta/\pi H$
1972	D. Pavelescu (Rumania)	Universal	$w = A_0 + A_1 H_R + A_2 H_c + A_3 v + A_4 H +$
1974	N. P. Suh (U.S.A.)	Delamination	$W = \left(\frac{B_1 h_1}{d_{c(1)}} + \frac{B_2 h_2}{d_{c(2)}}\right) P/H$

[Bahdur, S. 1978]

Appendix II: Drawing of test set up fixture (all dimensions are in inches).

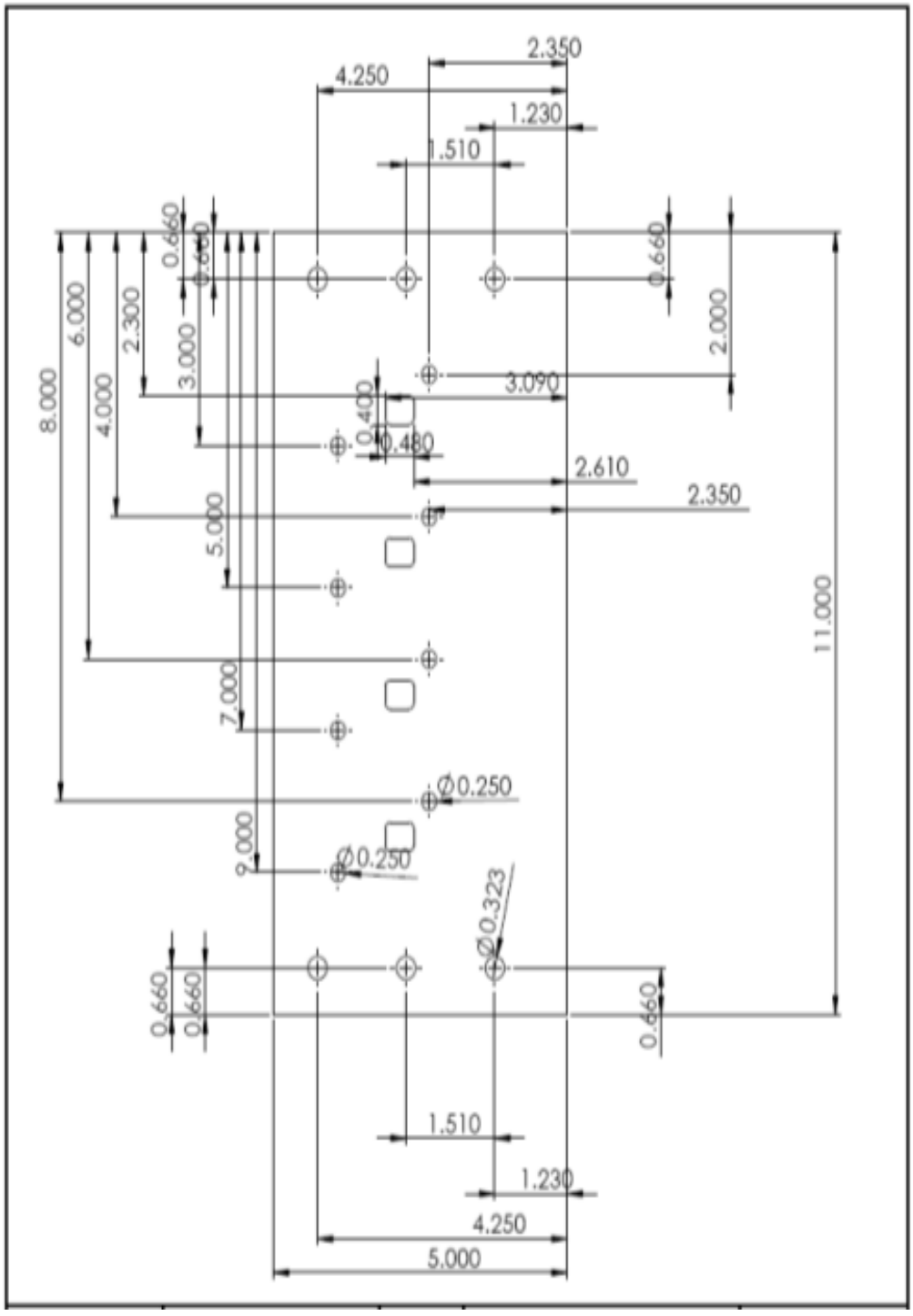

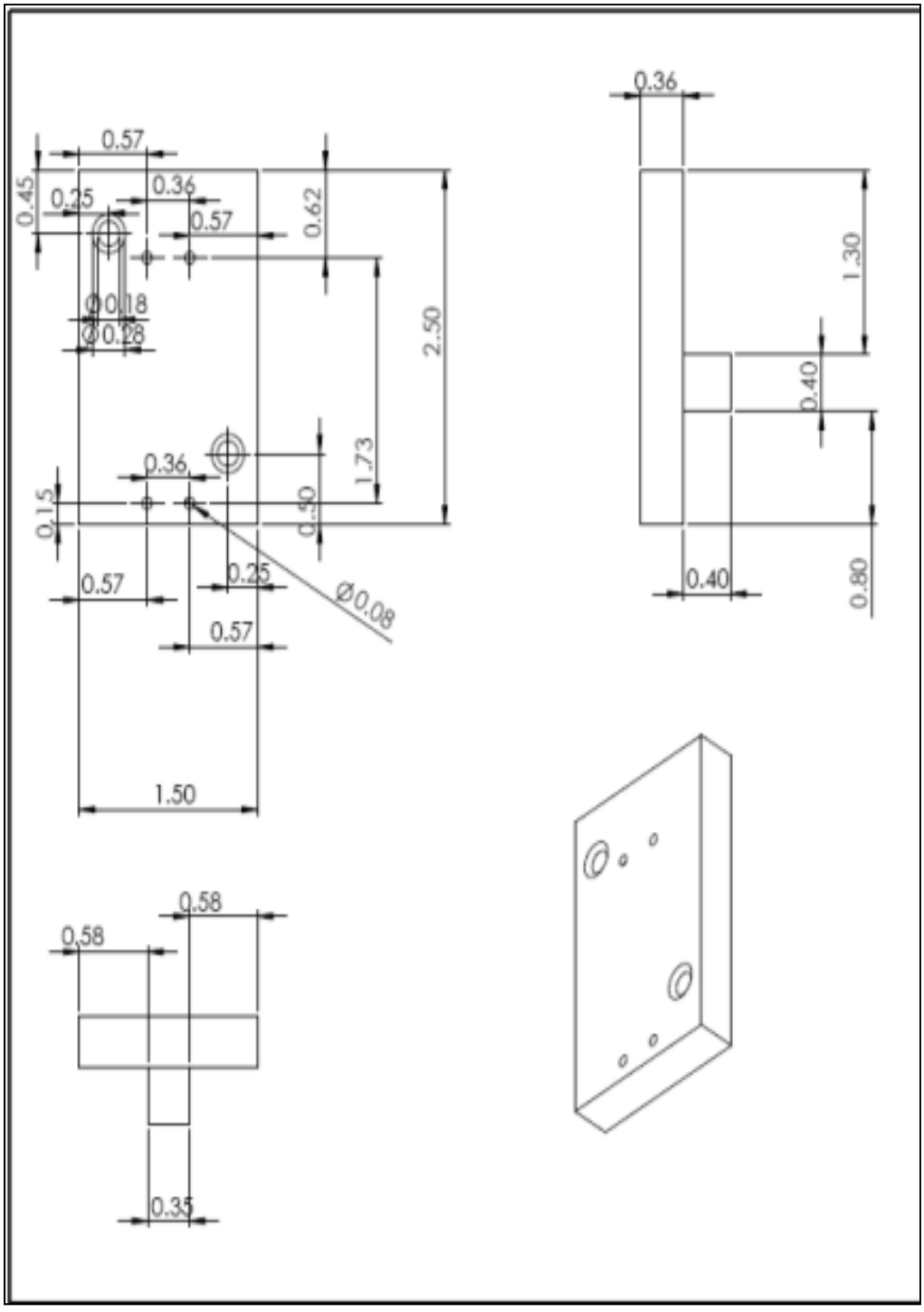
0.57
0.45
0.25
0.36
0.57
0.62
2.50
Ø0.18
Ø0.28
0.36
1.73
0.15
0.50
0.57
0.25
Ø0.08
0.57
1.50
0.58
0.58
0.35
0.36
1.30
0.40
0.40
0.80

Appendix III: SFE EasyDriver.

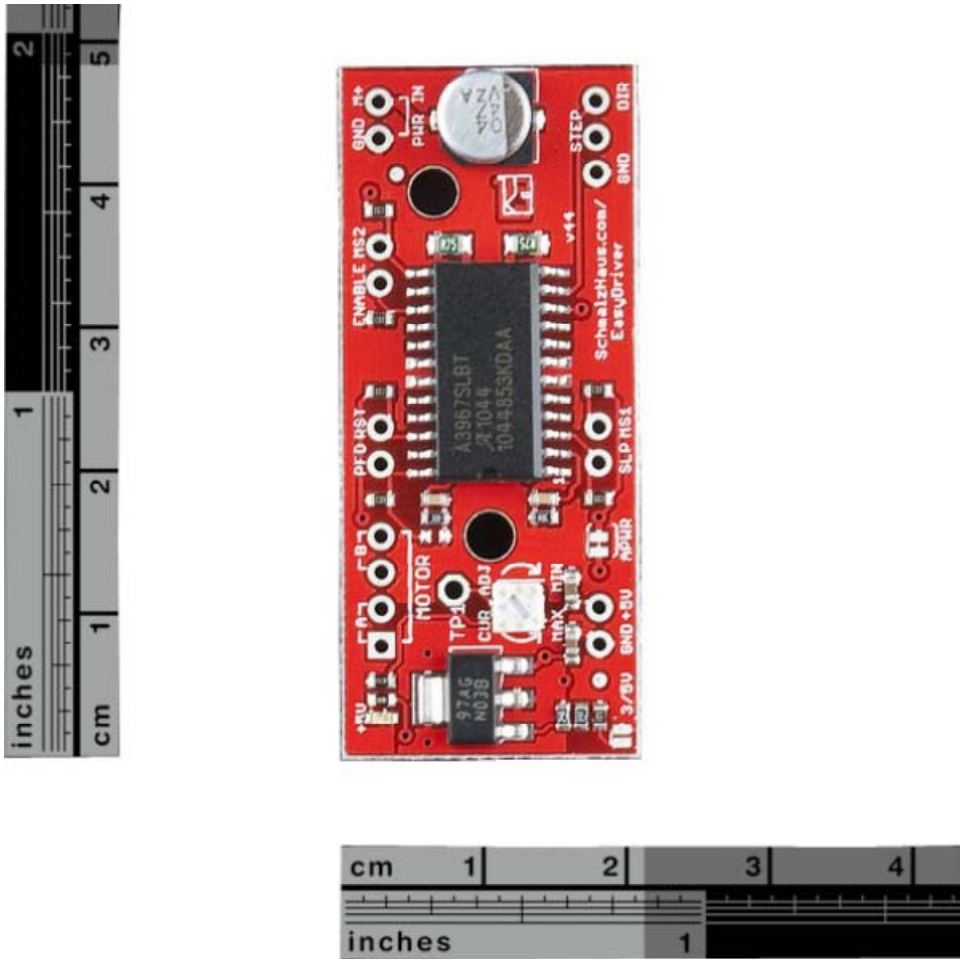

SFE EasyDriver Bipolar Stepper Motor Driver

Appendix IV: The MATLAB code to calculate the axial wear depth of the motor and pivot bearing cup.

```
%finding wear depth of each cup by using the Archad's law %
syms x y
bp=acos((0.75-x*sin(pi/3))/0.75)
bm=acos((1-y*sin(pi/3))/1)
rpo= 0.75*cos ((pi/3)-bp)
rpi= 0.75*cos ((pi/3)+bp)
rmo=1*cos ((pi/3)-bm)
rmi=1*cos ((pi/3)+bm)
hpi=0.75*(1-sin((pi/3)+bp))
hpo=0.75*(1-sin((pi/3)-bp))
hmi=(1-sin((pi/3)+bm))
hmo=(1-sin((pi/3)-bm))
Vm=(pi/6)*((3*hmo*rmo^2+hmo^3)-(3*hmi*rmi^2+hmi^3)-2*(hmo-
hmi)*(rmi^2+rmi*rmo+rmo^2))
Vp=(pi/6)*((3*hpo*rpo^2+hpo^3)-(3*hpi*rpi^2+hpi^3)-2*(hpo-
hpi)*(rpi^2+rpi*rpo+rpo^2))
S=solve (Vm-4/3*Vp, x+y-0.1)
```

Appendix V: Life/wear model MATLAB

```
clear all
close all
global Vwp Vwm
Km1=12E-5; % The initial wear factor/condition (Metal-Delrin Contact),
mm^3/(Km.N)
Km2=7.3E-5
Kp1=12E-5; % The wear factor/condition (Delrin-Delrin Contact)
Kp2=7.3E-5
X(1) = 1.4e-3; % The initial penetration of the bearing ball obtained from FEA
Y(1) = 1.4e-3; % The initial penetration of the bearing ball obtained from FEA
Vwp = 0;
Vwm = 0;

l = 0.5; % The sliding distance increments (Km)
L=1;
while (X(end)+Y(end))<0.125 % (X(end)+Y(end)) is the total wear depth, hear is the
place to define the failure cariterion
   if L*l<56.72
      Km = Km1; % The initial wear factor/condition (Metal-Delrin Contact)
      Kp = Kp1
   else
      Km = Km2;% The initial wear factor/condition (Delrin-Delrin Contact)
```

```
        Kp = Kp2
    end
    F=(3- (X(L)+Y(L))*9.50)/sin (pi/3); % The compresive force by the leaf spring as
a fuction of total wear depth (leaf spring expansion)
    dVwm=F*Km*l; % The removed volume based on Archard's wear model for the
Mcup
    dVwp=F*Kp*l*0.75; % The removed volume based on Archard's wear model for
the Pcup
    Vwp = Vwp+dVwp;
    Vwm = Vwm+dVwm;
    x0 = 1.4e-3;          % Make a starting guess at the solution
    y0 =1.4e-3;
    L=L+1;
    options=optimset('Display','iter');   % Option to display output
    X(L) = fsolve(@myfunP,X(L-1),options); % Call solver
    Y(L) = fsolve(@myfunM,Y(L-1),options);
    grid on
end
%plot((0:L-1)*l,X+Y);
%plot((0:L-1)*l*1e6/pi,X+Y);
x1 = (1:L)*l*1e6/pi;
y1 = X+Y;
y2 = X+Y;
x2 = (0:L-1)*l;
hl1 = line(x1,y1,'Color','b');
% plotyy(x1,y1,x2,y2)
ax1 = gca;
set(ax1,'XColor','b','YColor','b')
ax2 = axes('Position',get(ax1,'Position'), 'XAxisLocation','top', 'YAxisLocation','right',
'XColor','k','YColor','k');
hl2 = line(x2,y2,'Color','k','Parent',ax2);
xlabel('Million cycles')
title('Sliding distance (km)')
l*L(end)
```

myfunP:

```
function F = myfunP(x)
global Vwp
F = 1/6*pi*(9/16*(9/4+9/4*sin(1/3*pi+acos(-1+2/3*x*3^(1/2))))*cos(1/3*pi+acos(-
1+2/3*x*3^(1/2)))^2+(3/4+3/4*sin(1/3*pi+acos(-1+2/3*x*3^(1/2))))^3-
9/16*(9/4+9/4*cos(1/6*pi+acos(-1+2/3*x*3^(1/2))))*sin(1/6*pi+acos(-
1+2/3*x*3^(1/2)))^2-(3/4+3/4*cos(1/6*pi+acos(-1+2/3*x*3^(1/2))))^3-
(3/2*sin(1/3*pi+acos(-1+2/3*x*3^(1/2)))-3/2*cos(1/6*pi+acos(-
1+2/3*x*3^(1/2))))*(9/16*sin(1/6*pi+acos(-
```

```
1+2/3*x*3^(1/2)))^2+9/16*sin(1/6*pi+acos(-1+2/3*x*3^(1/2)))*cos(1/3*pi+acos(-
1+2/3*x*3^(1/2)))+9/16*cos(1/3*pi+acos(-1+2/3*x*3^(1/2)))^2))-Vwp;
```

myfunM:

```
function F = myfunM(y)
global Vwm
F = 1/6*pi*((3+3*sin(1/3*pi+acos(-1+1/2*y*3^(1/2))))*cos(1/3*pi+acos(-
1+1/2*y*3^(1/2)))^2+(1+sin(1/3*pi+acos(-1+1/2*y*3^(1/2))))^3-
(3+3*cos(1/6*pi+acos(-1+1/2*y*3^(1/2))))*sin(1/6*pi+acos(-1+1/2*y*3^(1/2)))^2-
(1+cos(1/6*pi+acos(-1+1/2*y*3^(1/2))))^3-(2*sin(1/3*pi+acos(-1+1/2*y*3^(1/2)))-
2*cos(1/6*pi+acos(-1+1/2*y*3^(1/2))))*(sin(1/6*pi+acos(-
1+1/2*y*3^(1/2)))^2+sin(1/6*pi+acos(-1+1/2*y*3^(1/2)))*cos(1/3*pi+acos(-
1+1/2*y*3^(1/2)))+cos(1/3*pi+acos(-1+1/2*y*3^(1/2)))^2))-Vwm;
```

Appendix VI: Monitoring degradation of the stepper motor

Detent torque –Detent torque of the worm shaft was measured off-line on a RSA III Dynamic Mechanical Analyzer periodically to quantitatively measure the degradation of stepper motor throughout the test as a function of bearing wear and lateral displacement.

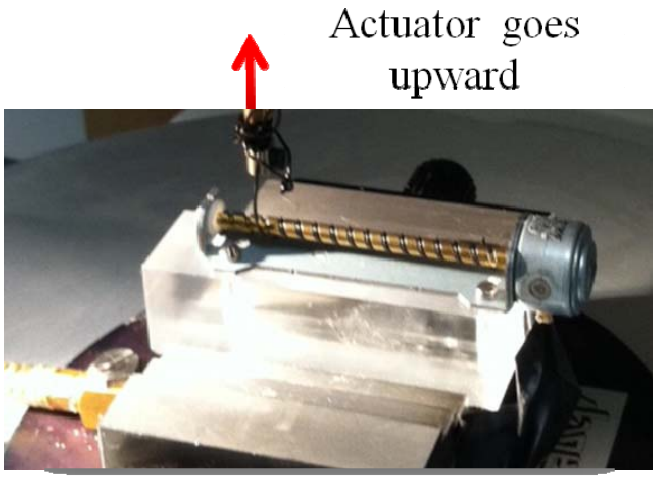

Measuring detent torque

Measuring the required force to pull the fabric (approach to measure the detent torque)

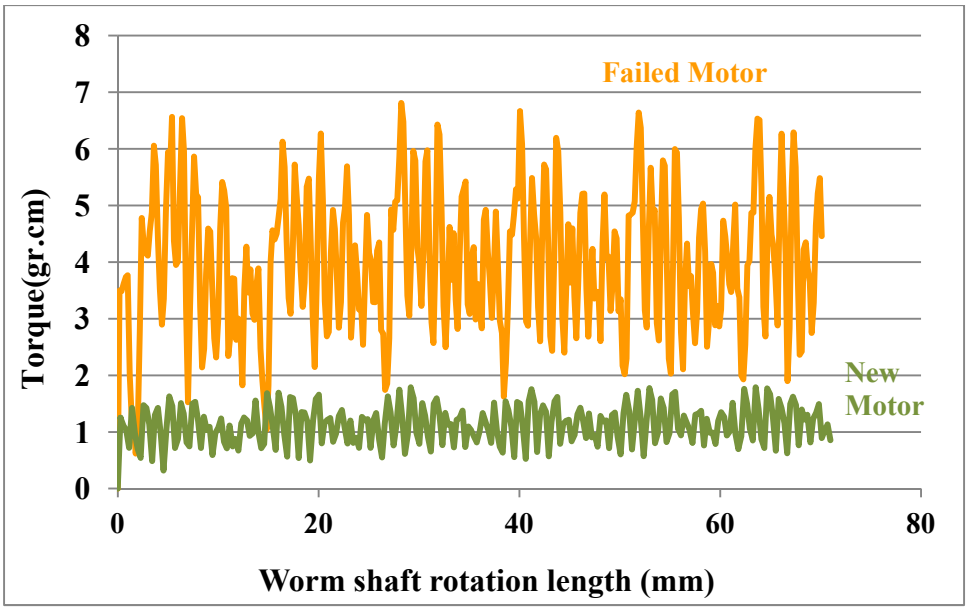

The required torque to rotate the worm shaft increase throughout the life of the stepper motor

Lateral displacement –The lateral displacement of worm shaft is the main reason for failure of the motor, which is caused by wear out of the bearing cup. Therefore, it was of interest to confirm the hypothesis that wear out of the bearing causes increase in lateral displacement of worm shaft. The lateral displacement of worm shaft has been measured by applying certain amount of lateral force both to right and left of the worm shaft while the location of worm shaft was being captured under optical microscopy**.** These measurements have been done off-line periodically throughout of the test.

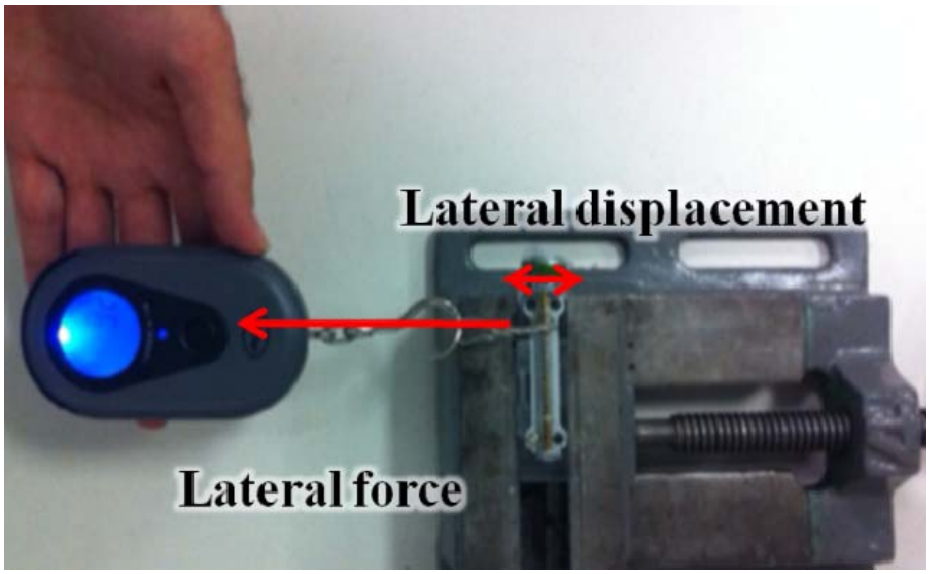

Lateral displacement increases with decrease in compression force on the bearing throughout the wear test.

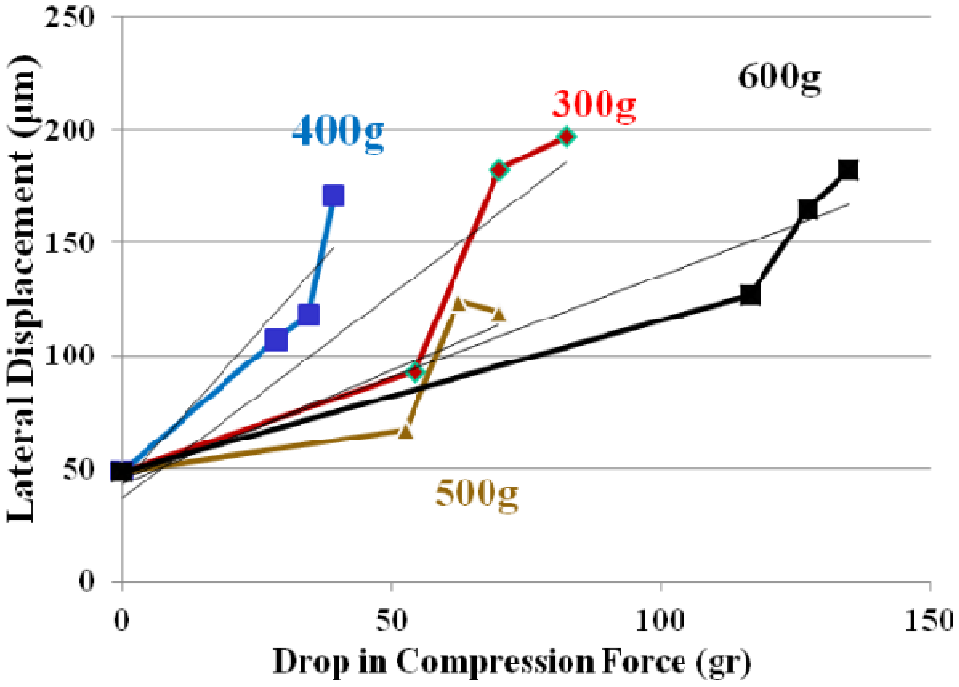

Appendix VII: Mesh refinement study

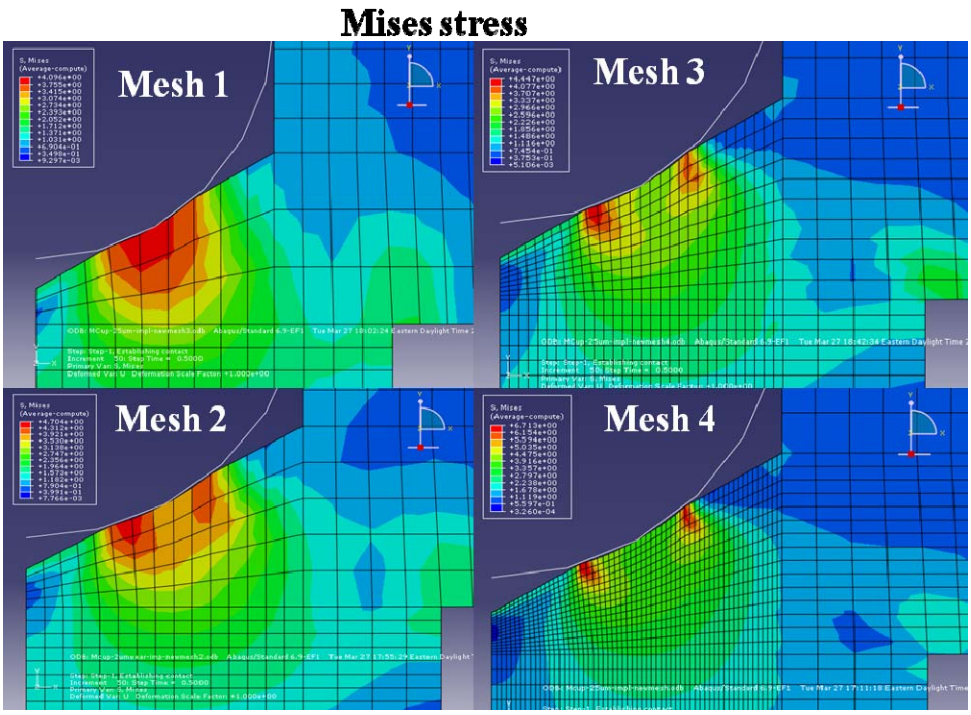

Different mesh density

- Same model has been run at four different mesh refinement levels.
- Same displacement has been applied to the bearing ball as a BC and reaction force has been extracted and presented in the next Figure.

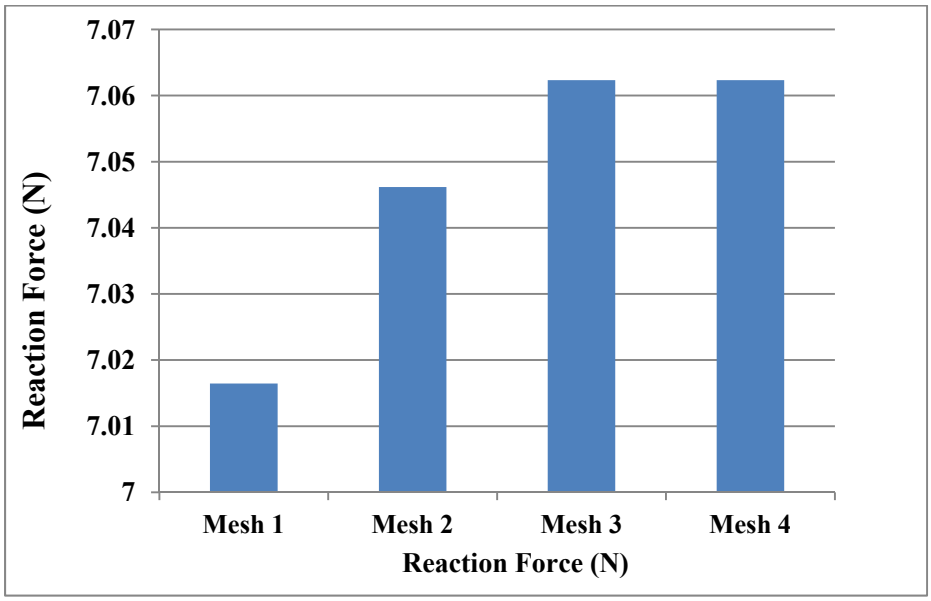

Mesh Refinement Study (Four Levels)

Appendix VIII: Schematic view of wear tests that their results are shown in Figure 3-15 Harrass et al. [24].

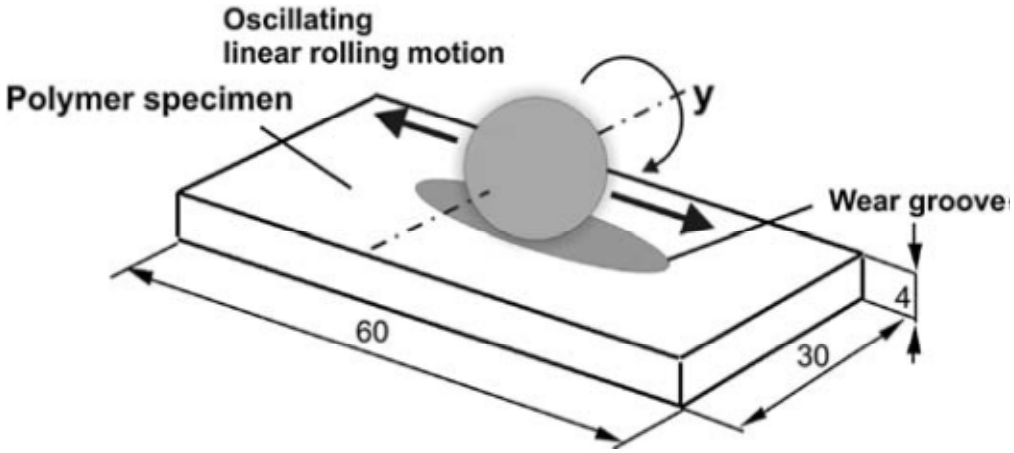

Schematic view of the linear ball-on-plate principle (a) [Harrass et al (1998)]

Appendix IX: The hardness of conical Delrin thrust bearing cups was measured to: a) study the variability of hardness within one sample; and, b) to explore piece-to-piece hardness variability of seven samples. A G200 Agilent nanoindenter with a Berkovich tip was used to measure the hardness. The mean hardness value of **237 MPa** was obtained from 15 measurements per sample across the 7 samples with **7.3%** CV. Indention depth of 1 μm was selected and indentation points were selected 50 μm away from each other, these conditions were selected based on the study by Archodoulaki, et al. [31] to compare the conical Delrin bearing hardness with their reported value. The measured hardness values are fairly close to the one reported in Archodoulaki, et al. [31] as shown in the following Figures.

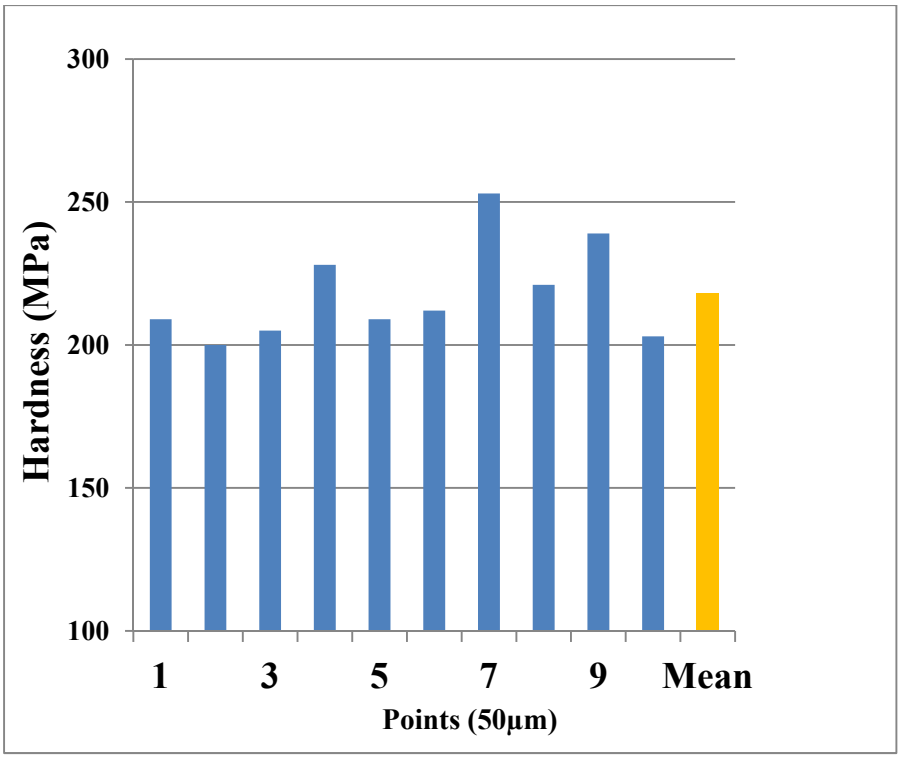

10 indentation points in one conical Delrin cup

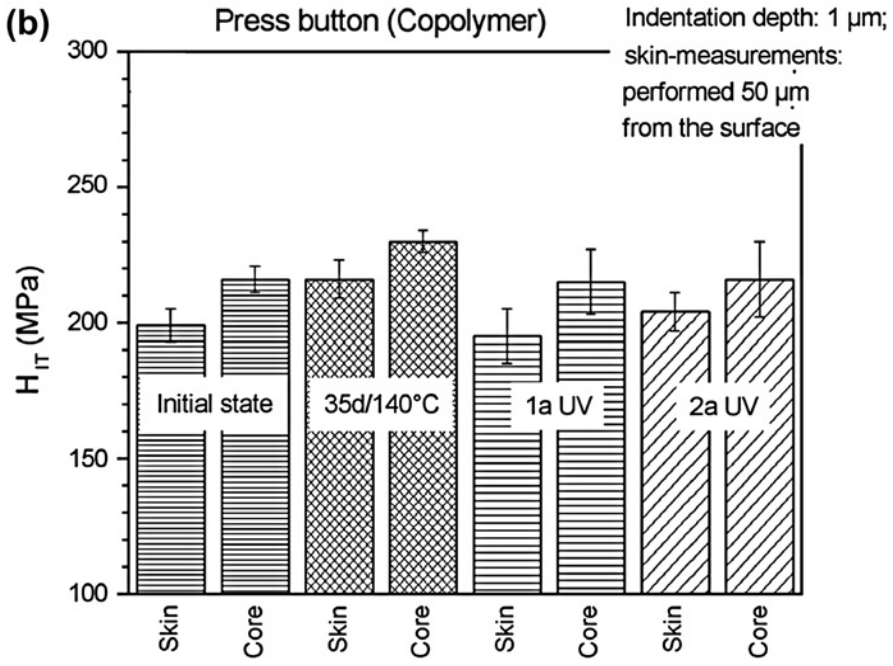

Hardness of Delrin measured by Archodoulaki et al. [31]

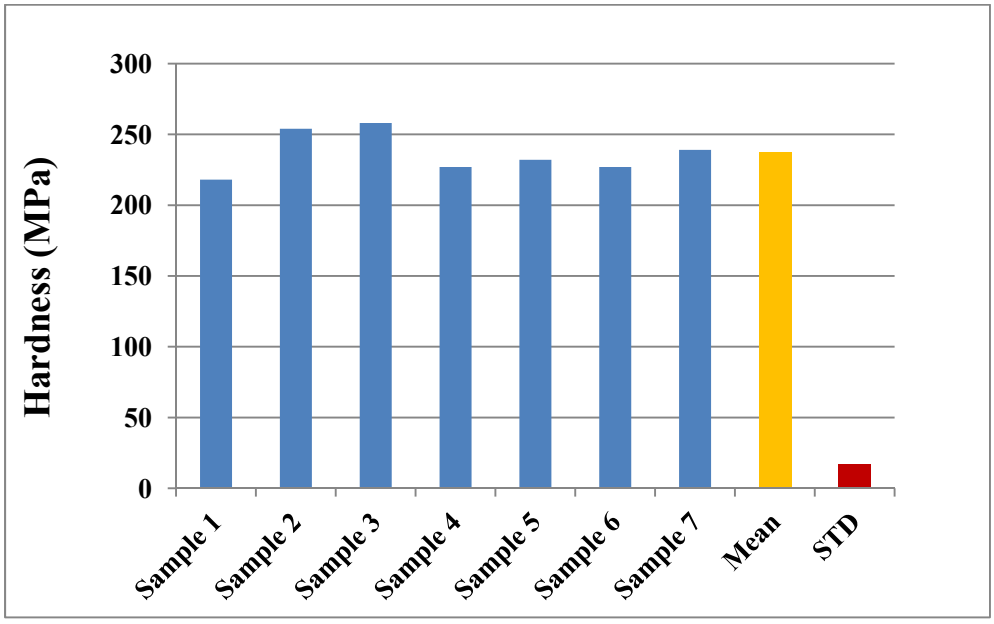

Hardness of seven molded Delrin cups

Also, indentation points were selected close to the contact region (3 µm apart) on both new and worn out cups, as shown in the Figure below.

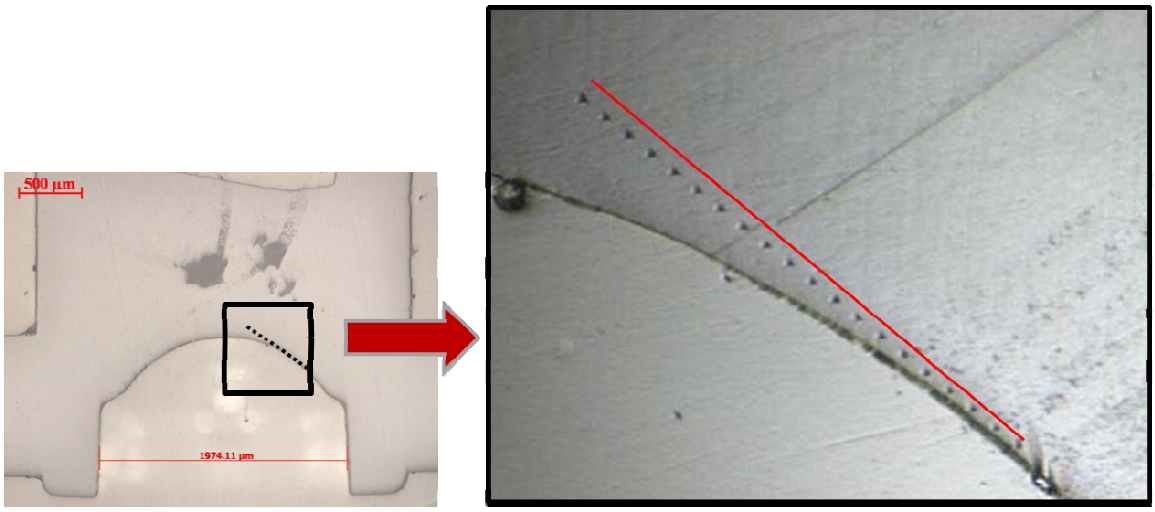

Hardness Delrin close to the contact surface

The hardness values of new and worn out Delrin cups close to contact area are shown in the two following Photographs.

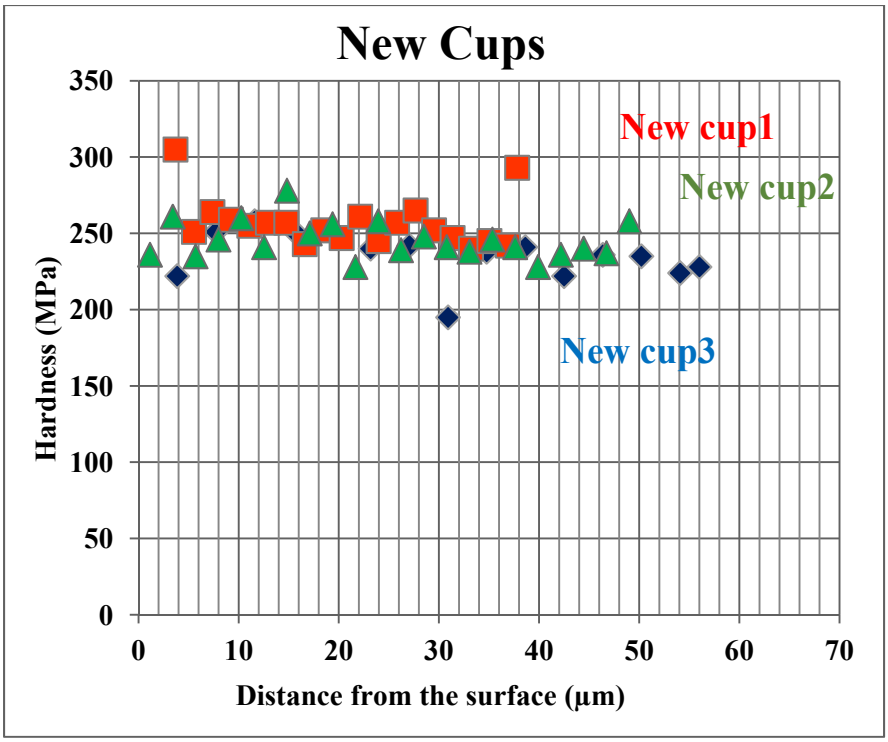

Hardness of new Delrin cups vs. distance from the contact surface

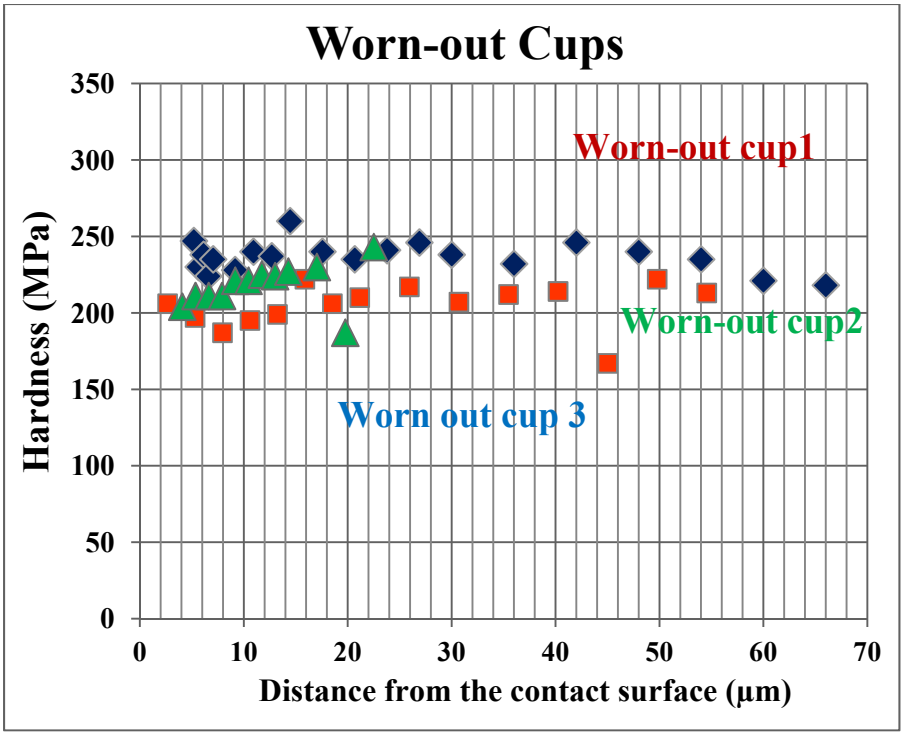

Hardness of worn-out Delrin cups vs. distance from the contact surface

References:

[1] Archard, J. F., Journal of Applied Physics, Vol. 24, 1953, pp. 981-988.

[2] Taft, C. K. and Raymond, G. G, "Stepping Motor Failure Model," Industrial, IEEE Transactions on, 1975, Vol.22, pp.375-385.

[3] Meng, H.C., "Wear molding: evaluation and categorization of wear models", Ph.D. Thesis, 1994, University of Michigan, Ann Arbor.

[4] Meng, H.C. and Ludema, K.C., "Wear models and predictive equations: their form and content", Wear, 1995, 181-183, pp.443-457.

[5] Barwell, F.T., "Wear of metals", *Wear, 1, 1957*, pp. 317-332.

[6] Rhee, S.K., "Wear equation for polymers sliding against metal surfaces", Wear, Vol.16, 1970, 431-445.

[7] Holm, R., Electrical Contacts, 1946.

[8] Bahadur, S.," Wear research and development", ASME, 1978, pp. 449-454.

[9] Lei, X. and Cao, R. L., "Numerical simulation of sliding wear based on Archard model," MACE, 2010, pp. 325-329.

[10] Pietrabissa, R., Raimondi M. and Di Martino. E., "Wear of polyethylene cups in total hip arthroplasty: a parametric mathematical model", Medical Engineering & Physics, Vol. 20, 1998, pp.199–210.

[11] Esoy, K., Nurnberg, G., Golle, M., and Hoffman. H., "Simulation of wear on sheet metal forming tools- An energy approach" Wear, Vol. 265, 2008, pp. 1801–1807.

[12] Stolarski, T. A., "Rolling contact fatigue of polymers and polymer composites". Advances in composite tribology, Chapter 17, 1993. pp. 629–67.

[13] Feyzullahoglu, E. and Saffak, Z., "The tribological behavior of different engineering plastics under dry friction conditions", Materials and Design, Vol. 29, 2008, pp. 205-211.

[14] Tevrüz ,T., "Tribological behaviours of bronze-filled polytetrafluoroethylene dry journal bearings", Wear, Vol. 230, 1999, pp 61-69.

[15] Tevrüz, T., "Tribological behaviours of carbon-filled polytetrafluoroethylene dry journal bearings", Wear, Vol. 221, 1998, pp 61-68.

[16] Unal, H. and Mimaroglu, A., "Friction and wear behavior of unfilled engineering thermoplastics", Materials and Design, Vol. 24, 2003, pp183-187.

[17] Jia, J., Chen, J., Zhou, H., Hu, L. and Chen, L., "Comparative investigation on the wear and transfer behaviors of carbon fiber reinforced polymer composites under dry sliding and water lubrication", Composites Science and Technology, Vol 65, 2005, pp 1139-1147.

[18] Bahadur, S., "The development of transfer layers and their role in polymer tribology", Wear, Vol 245, 2000, pp 92-99.

[19] Jain, V.K. and Bahadur, S., "Material transfer in polymer-polymer sliding", Wear, Vol 46, 1978, pp 177-188.

[20] William, A. B. and Donald, H. B., "Adhesion and friction of PTFE in contact with metals as studied by Auger spectroscopy, field ion and scanning electron microscopy", Wear, Vol 26, 1973, pp 75-93.

[21] Olofsson, U., Andersson, S. and Björklund, S., "Simulation of mild wear in boundary lubricated spherical roller thrust bearings", Wear, Vol 241, 2000, pp 180-185.

[22] Li, C., Zhang, Ye, L. and Friedrich, K., "Tribological properties of epoxy nanocomposites: III. Characteristics of transfer films", Wear, Vol 262, 2007, pp 699-706.

[23] Henrique da Silva, C. and Sinatora, A.," Development of severity parameter for wear study of thermoplastics", Wear, Vol 263, 2007, pp 957-964.

[24] Harras, M., Friedrich, K. and Almajid, A. A. "Tribological behavior of selected engineering polymers under rolling contact" Tribology International, Vol 43, 2010, pp. 635-646.

[25] Zang, S. W. "State of the art of polymer tribology" Tribology International, Vol. 31, 1998, pp 59-60.

[26] "Delrin properties." *modernplastics*. N.p., n.d. Web. 12 Apr 2012. http://modernplastics.com/pdf/Ensinger_Delrin.pdf.

[27] "Design Guide-Module III." *Dupont*. N.p., n.d. Web. 12 Apr 2012. <http://plastics.dupont.com/plastics/pdflit/americas/delrin/230323c.pdf>.

[28] Yang, E-L., Hirvonen, J.-P. and Toivanen, R.O., "Effect of temperature on the transfer film formation in sliding contact of PTFE with stainless steel", Wear, Vol 146, 1991, pp 367-376.

[29] Mergler, Y.J., Schaake, R.P. and Huis, A.J., "Material transfer of POM in sliding contact", Wear, Vol 256, 2004.

[30] "Machinist-Materials, Plastics Comparison Table" Web. May 2012. <http://www.machinist-materials.com/comparison_table_for_plastics.htm>.

[31] Archodoulaki, V., Luftl, S., Koch, T., and Seidler, S., "Property changes in polyoxymethylene (POM) resulting from processing, ageing and recycling", Polymer Degradation and Stability, Vol 92, 2006, pp 2181-2189.

[32] Unal, H. and Mimaroglu, A., "Friction and wear behavior of unfilled engineering thermoplastics", Materials and Design, Vol. 24, 2003, pp183-187.